Durham E-Theses

Electroluminescent devices based on blended polymeric thin films

Widdowson, Nicholas E.

How to cite:

Widdowson, Nicholas E. (2006) *Electroluminescent devices based on blended polymeric thin films*, Durham theses, Durham University. Available at Durham E-Theses Online: http://etheses.dur.ac.uk/2603/

Use policy

The full-text may be used and/or reproduced, and given to third parties in any format or medium, without prior permission or charge, for personal research or study, educational, or not-for-profit purposes provided that:

- a full bibliographic reference is made to the original source
- a link is made to the metadata record in Durham E-Theses
- the full-text is not changed in any way

The full-text must not be sold in any format or medium without the formal permission of the copyright holders.

Please consult the full Durham E-Theses policy for further details.

Academic Support Office, Durham University, University Office, Old Elvet, Durham DH1 3HP
e-mail: e-theses.admin@dur.ac.uk Tel: +44 0191 334 6107
http://etheses.dur.ac.uk

Electroluminescent devices based on blended polymeric thin films

Nicholas E. Widdowson, M.Eng.

St. John's College

The copyright of this thesis rests with the author or the university to which it was submitted. No quotation from it, or information derived from it may be published without the prior written consent of the author or university, and any information derived from it should be acknowledged.

A thesis submitted in partial fulfilment

of the requirements for the degree of Ph.D.

School of Engineering and Centre for Molecular and Nanoscale Electronics

Durham University

29th August 2006

11 JUN 2007

Electroluminescent devices based on blended polymeric thin films

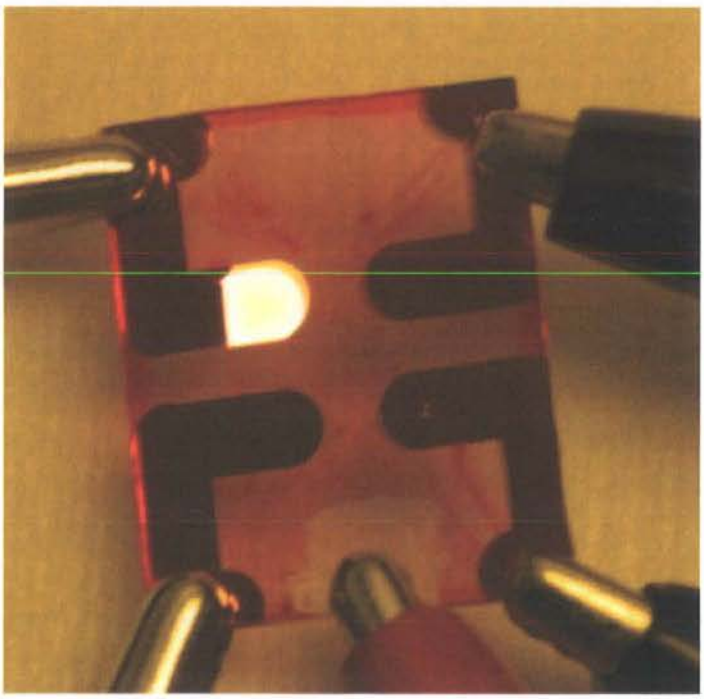

Nicholas E. Widdowson

Copyright © 2006 by Nicholas E. Widdowson

The copyright of this thesis rests with the author. No quotation or reproduction from it should be published without his prior written consent and information derived from it should be acknowledged.

Declaration

I hereby declare that the work carried out in this thesis has not been previously submitted for any degree and is not currently being submitted in candidature for any other degree.

Signed.....N. E. Widder.....

Candidate

The work in this thesis was carried out by the candidate.

Signed.....McPeth.....

Director of Studies

Signed.....N. E. Widder.....

Candidate

For my family

Acknowledgements

Without the generosity of many people this thesis would not have been possible. The encouragement of my supervisor, Professor Michael C. Petty, has been fundamental. I thank Mike for his enthusiasm and insight, and for the times when he has highlighted details that I might otherwise have overlooked. Dr Christopher Pearson has assisted me throughout this research. I am grateful to Chris for training me to use the laboratory apparatus as well as for his resourcefulness and sense of humour.

Most of the organic materials studied as part of this research were synthesised in Durham, and for this I thank Professor Martin R. Bryce, Dr Changsheng Wang and Mr Kiran Kamtekar. I am also grateful to Dr Igor Perepichka who performed the energy level calculations and to Dr Cristina Bertoni and Dr Steve Dunn, both from Cranfield University, for depositing the aluminium-doped zinc oxide films.

For building the measurement apparatus, I thank the Technical Staff in the School of Engineering, including Mr Ian Hutchinson, Mr Colin Dart and Mr Ian Glassford. I am indebted to all my colleagues at the Centre for Molecular and Nanoscale Electronics and the Microsystems Technology Group. In particular, I thank Dr Jin Hyung Ahn and Dr Marco Palumbo for numerous valuable discussions. Marco, for the impromptu Italian lessons, 'grazie tante'.

There are many outside the University who have not only encouraged me in this project, but also helped me to maintain a balance when the thesis threatened to consume my every thought. The support of my friends and my family at Christchurch Durham is gratefully acknowledged.

I am always humbled by the patience and sacrifices of my parents, from whom I have learnt so much. I thank them profoundly for their constant encouragement and unwavering support throughout my education and always. Finally, thank you to my wife, Rachel, for never doubting that I could produce this volume. Rachel has consistently encouraged me to persevere and without her support, friendship and love it may never have become a reality.

Abstract

This thesis is concerned with the characteristics of organic light-emitting devices based on the polymer poly(2-methoxy-5-(5'-ethylhexyloxy)-p-phenylenevinylene) (MEH-PPV).

The emissive layer of each device was formed either from pure MEH-PPV or from a blend of MEH-PPV with an electron-transporting small molecule material. A film of either indium tin oxide (ITO) or aluminium-doped zinc oxide (AZO) on glass was used to provide a transparent anode. The pure or blended emissive material was spin-coated from solution onto the anode. Calcium or aluminium cathodes were deposited by thermal evaporation onto the emissive film.

The current-voltage, light-voltage, quantum efficiency and stability characteristics of the devices were obtained using purpose-designed measurement equipment. These characteristics were influenced, amongst other factors, by the blend composition. The devices with an aluminium cathode and an emissive layer formed from 50 % MEH-PPV and 50 % PDPyDP had among the best characteristics. Compared with the equivalent unblended devices they averaged 40 times greater light emission, 35 times higher efficiency, and they emitted light for more than 18 days in place of tens of minutes. The half life of the most stable devices was 63 h which, though much less than the tens of thousands of hours claimed by commercial developers, represents an increase of 30 times that of an unblended device. The increased light emission and quantum efficiency data resulted from the enhanced carrier injection and transport provided by the electron transport material. It is suggested that the increased stability was caused by the small molecule material performing the role of a nano-encapsulation around each polymer chain. That is to say, the data suggest that each polymer chain was individually protected from the effects of contaminants such as oxygen and water vapour by the small molecule within the film.

The choice of anode material also affected the rate of degradation. The surface morphology of the anode material of devices which had previously been operated for extended periods were analysed using an AFM. Electromigration of ITO anodes to form sharp spikes was not uncommon, particularly in devices with short lifetimes. As-deposited AZO generally had a smoother morphology than as-deposited ITO. Following device operation fewer electromigration spikes were observed in AZO than ITO.

Contents

Nomenclature

AFM	Atomic force microscope
AZO	Aluminium-doped zinc oxide
CRT	Cathode ray tube
DIO	Digital input output
EDAX	Energy-dispersive X-ray spectroscopy
EL	Electroluminescence
ET	Electron transport
ETL	Electron transport layer
GPIB	General purpose interface bus
HOMO	Highest occupied molecular orbital
HT	Hole transport
HTL	Hole transport layer
I-V	Current-voltage
ITO	Indium tin oxide
LCD	Liquid crystal display
LUMO	Lowest unoccupied molecular orbital
MEH-PPV	poly(2-methoxy-5-(5'-ethylhexyloxy)-p-phenylenevinylene)
OLED	Organic light-emitting device
PEDOT:PSS	Poly(3,4-ethylenedioxythiophene) poly(styrenesulfonate) (often further abbreviated to PEDOT)

PLED	Polymer light emitting device
PPV	poly(p-phenylenevinylene)
QE	Quantum efficiency
RGB	Red, green, blue
SEM	Scanning electron microscope
SMOLED	Small molecule light emitting device
SOLED	Stacked organic light emitting device
SOLED	Single layer organic light emitting device
WOLED	White organic light emitting device

Chapter One

Introduction

1.1 Introduction and text organisation

In 2004, the worldwide display market was worth in excess of $79 billion [1] and it continues to grow rapidly. There is constant demand from both industry and consumers for larger displays with enhanced brightness and contrast, and lower power consumption. This has led to significant interest among the research community into new technologies which might, in the future, fulfil some of the demand.

The technology which has developed most rapidly in recent years is the organic light emitting device (OLED), which has potential applications in solid state lighting as well as displays. More than 100 companies and research institutions are working on aspects of the technology [2]. Despite this concentrated research interest there are relatively few commercially available OLEDs. This is because several hurdles remain before they can compete effectively with the more established display technologies. Perhaps the most significant obstacle is that organic emissive materials are relatively unstable, which results in devices degrading with time.

The aim of the research described in this thesis is to investigate the characteristics of OLEDs based on blends of a polymer emissive material with small molecule materials. Particular emphasis is placed on the influence of blends and anode materials on device degradation. Methods of reducing the rate of degradation in OLEDs are investigated.

Chapter 2 begins with a general introduction to electroluminescence in organic materials before discussing the principles of operation in OLEDs. There is a brief review of the latest OLED research, and comparisons are made with other display technologies.

Details of the experimental techniques used during this research are given in Chapter 3. The fabrication of the emissive polymer films from solution and the deposition of metallic cathodes are described. There is also a discussion of the techniques used to characterise the devices and their constituent components. A range of microscopy and spectroscopy techniques are described as well as electrical analysis techniques. Chapter 4 provides a description of the bespoke automated equipment which was designed and produced to measure the electrical and light emission characteristics of batches of up to 24 devices. The variation between identically produced devices is discussed and justification for the batch fabrication and characterisation approach is given. The equipment components are described and details are given of the programming logic.

In Chapter 5, the first results chapter, evidence is provided for the degradation mechanisms associated with the device anode. Two anode materials are compared and the effect of including an additional layer between the anode and the emissive layer is discussed. AFM images of anodes which have been separated from devices after operation are used to verify the high degree of anode damage. Chapters 6 and 7 focus on the influence of blending the emissive polymer with two different small molecule electron transporting materials. The effect on the electrical, light emission and stability characteristics of devices is compared for a variety of blend ratios. In Chapter 8, the results for a third electron transport material are given and there is a brief discussion of macro approaches to encapsulation.

Chapter 9 offers conclusions drawn from the research reported in the thesis and some suggestions for further work.

1.2 References

1 J.G. Eden, *Information display early in the 21st century: Overview of selected emissive display technologies.* Proceedings of the IEEE 94, 567 (2006).

2 D.E. Mentley, *State of flat-panel display technology and future trends.* Proceedings of the IEEE, 90, 453 (2002).

Chapter Two

Introduction to organic light emitting devices

2.1 Introduction

Interest in organic electroluminescence (EL) has expanded rapidly in the past twenty years. Recent devices bear little resemblance to those first demonstrated half a century ago. In this chapter, Section 2.2 records some of the milestones in the history of research into organic electroluminescence and the reasons why there has been so much interest in this topic. The essential structure of organic light emitting devices and the principles of their operation are described in Section 2.3, while Section 2.4 provides further information on carrier injection and transport in organic devices. Options for producing full colour and white light devices are identified in Section 2.5, and Section 2.6 provides a discussion of the issues which influence the current focus of research both in the academic and commercial environments.

2.2 History of research into electroluminescence in organic materials

2.2.1 Origins and progress

The first example of electroluminescence in an organic material was demonstrated by Bernanose [1] in 1953, by applying a high voltage a.c. field to crystalline films of acridine orange and quinacrine. This was followed in 1963 by the first observation of electroluminescence in the d.c. mode as demonstrated by Pope *et al.* [2] using single crystals of anthracene. Hartman *et al.* observed the first electroluminescence from an emissive polymer in the a.c. mode in 1967 [3]. These initial demonstrations of electroluminescence in organic materials required material thicknesses of the order of tens of microns and greater, and voltages in excess of 100 V.

Electroluminescence in inorganic semiconductors based on aluminium gallium arsenide was first observed in the 1950s and the research developed quickly. This led to the first commercial examples in the 1960s. For this reason, development of organic light emitters was not explored in further detail for two decades.

Subsequent research in organic electroluminescence has focused on two categories of organic material. The first category to become popular is that of small molecule organic materials, often deposited by vapour deposition. One of the main catalysts for research in this area was the 1987 publication by Tang and Van Slyke [4] in which these workers demonstrated electroluminescence in thermally evaporated 8-hydroxyquinoline aluminium

(Alq_3) (Figure 2.1) at a voltage of 2.5 V d.c.. The low voltage operation was achieved in part by using a second non-emissive thermally evaporated organic layer in addition to the Alq_3 to control the flow of charge carriers.

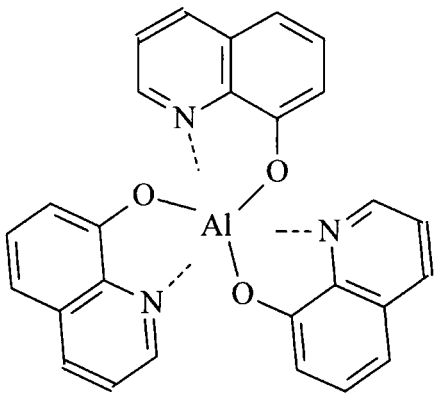

Alq3

Figure 2.1 Chemical structure of Alq_3

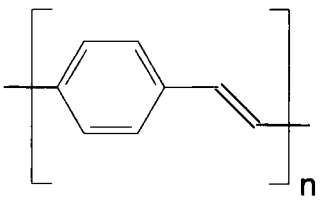

PPV

Figure 2.2 Chemical structure of PPV

The second category of organic materials to have been the subject of significant research in the field of electroluminescence is polymers. One of the most frequently cited publications is that of Friend and co-workers [5] in 1990 in which this group demonstrated a polymer light emitting device with the active layer formed from a thin film of the organic polymer poly(p-phenylene vinylene) (PPV) (Figure 2.2). The emissive layer was fabricated by spin-coating a precursor polymer which was subsequently thermally converted to PPV.

The next innovation came in 1991 when Braun and Heeger synthesised a fully solution-processable derivate of PPV called poly(2-methoxy-5-(5'-ethylhexyloxy)-p-phenylenevinylene), abbreviated as MEH-PPV [6]. With the development of a solution-processable polymer came a proliferation in international research interest because, if such a technology could be incorporated into a commercial device, major savings could be made in terms of reduced manufacturing cost and complexity compared with other display technologies.

Both the above types of organic material have since been used to develop organic light emitting devices (OLEDs) and the two technologies have become known as small molecule OLED (SMOLED) and polymer LED (PLED)..

In most cases, the fabrication techniques for SMOLED and PLED technologies differ significantly. Most emissive polymers have been developed so as to dissolve in a range of solvents and be processed easily from solution. As a result, spin coating, inkjet printing and screen printing have become popular for depositing thin polymer films. The size of polymer chains makes it difficult to deposit them by thermal evaporation as the materials invariably dissociate. By contrast, small molecules generally have a low sublimation temperature, making them appropriate for thermal evaporation. Small molecules are not suitable for depositing from solution since they tend to crystallize into discrete regions. Thermal evaporation allows easy control of the rate of deposition and film thickness but it is expensive and time consuming as it must be performed under vacuum. Spin coating is more complicated to control due to the high number of variables involved but the fact that it is not performed under vacuum means that the costs are lower. Inkjet printing and screen printing techniques are the least expensive methods as, not only do they require no vacuum, but also they are compatible with continuous, roll-to-roll processing.

Since the first demonstrations of electroluminescence, a range of materials with a variety of band gaps has been developed which has lead to the possibility of full colour displays. A number of techniques have been proposed [7] to integrate red, green and blue (RGB) emitters in order to create lighting cells capable of producing colours across the visible spectrum. The techniques that have been investigated are described in section 2.5.

2.2.2 Benefits of OLEDs

The potential advantages of OLEDs are two-fold. OLEDs are likely to offer benefits over established technologies not only through reduced cost of manufacture but also through enhanced capabilities.

The processes involved in OLED manufacture are simpler and therefore require less investment in capital-intensive, state-of-the-art micro-fabrication facilities. As stated previously, solution processable thin films used in PLEDs can be deposited by a range of low cost methods including spin coating and inkjet printing. The costs of these fabrication methods are in marked contrast to the high precision micro-fabrication techniques, such as those used in the production of LCDs, which attract high costs.

Enhanced capabilities are likely to include lower power consumption, wider viewing angle, thinner profiles, and larger areas. There is also the potential for ultra-thin large-area ambient lighting modules, low cost disposable devices and physically flexible displays.

2.2.3 Current situation

Despite intense research over the past twenty years there are few examples of commercially available OLED displays compared with the more established technologies of cathode ray tube (CRT), liquid crystal display (LCD) and plasma induced phosphors. The first OLED to come to market, in 1996, was a monochrome car radio display by Pioneer, fabricated using small molecule technology [8]. At the time of writing, small molecule OLEDs can be seen in a select range of car radio displays (some Pioneer and TDK models), a number of MP3 players (including some by Sony) and as the small secondary screen on some mobile telephones (including some of those manufactured by Motorola, Samsung and LG). Until recent years these devices displayed a select range of discrete colours. In 2003 Kodak launched their first digital camera to incorporate a SMOLED screen, which was one of the first full colour displays. Philips launched an electric razor in 2002 which used a monochrome polymer LED (PLED) as the battery indicator display.

All these commercially available OLEDs have in common the fact that they are restricted to devices with low lifetime demands by comparison with, for example, computer monitors and televisions. Displays mounted in digital cameras, shavers, car radios and MP3 players need only be operational for a fraction of the life of the device, while mobile telephones have an average life of only 18 months. Additionally, the great majority of these displays are not capable of achieving the density necessary for a high information-content display such as in a laptop computer.

Almost all of the commercial products to date have been limited to the small molecule OLED technology. However, because SMOLEDs require more complex processing and are more difficult to scale up, they are less likely than PLEDs to compete in the large area display market.

Prototypes of larger displays and OLEDs for ambient lighting applications have been showcased by a range of companies over several years but none has yet come to market.

Competition in the display market is fierce. Current technologies such as the liquid crystal display (LCD) are being produced affordably at high specifications in great numbers. Any potential OLED manufacturer must therefore be confident that the benefits of their product will provide effective competition with established technology. In short, OLEDs must provide more advanced capability or lower price, but preferably both. Until OLED technology has developed beyond its current interim state there is reluctance among

manufacturers to invest heavily in it. The major potential advantage in the fabrication of the PLED is roll-to-roll manufacture. Investment in a large scale fabrication facility is unlikely at a time when this method is not capable of delivering the necessary high accuracy on the industrial scale. The long term goal is a full-colour, high-content, flexible display with lifetime comparable to or surpassing that of existing technology; only once this is commercially feasible is the technology likely to succeed in the display market.

2.3 The structure and the principles of operation of OLEDs

2.3.1 Basic structure

The basic structure of an organic electroluminescent device is illustrated in Figure 2.3. OLEDs comprise at least three layers deposited in succession on a substrate, which is transparent to the wavelength of light produced. The organic active layer, which must include the electroluminescent component (emitter), is sandwiched between two electrodes. Electrons and holes are injected into the active layer via the cathode and anode, respectively. One electrode, usually the anode, must in common with the substrate be transparent so as to transmit the light produced by the emitter. Energy transfer will be discussed in Section 2.3.2.

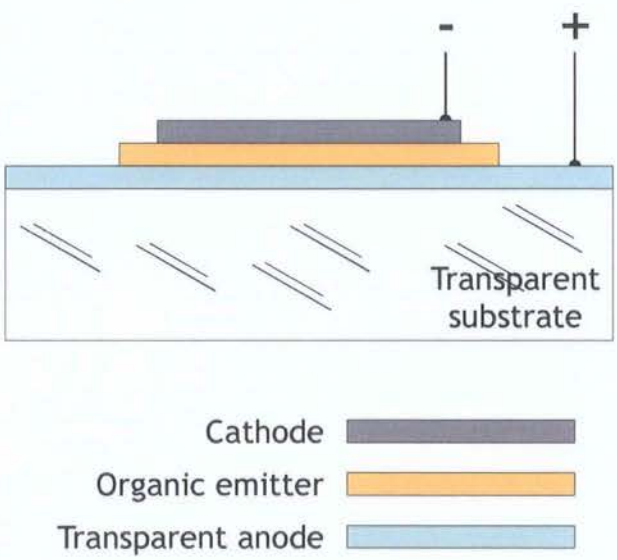

Figure 2.3 Basic structure of an OLED

The necessary characteristics of each layer, and the arguments for and against incorporating one or more additional layers, are better understood following a discussion on the principles of operation.

2.3.2 Principles of operation

In most cases, electronic energy band theory provides a convincing model of the operating principles of OLEDs [9].

The energy band structure of the basic OLED, illustrated in Figure 2.3, is shown in Figure 2.4. Under an applied field, electrons and holes are injected from the cathode and anode, respectively, into the active emitting layer. These carriers travel in the active layer but with mobilities much lower than those in inorganic semiconductors. Electron-hole recombination occurs in the active layer and an exciton is produced. Some exciton formation results in the release of a photon, as described in more detail below.

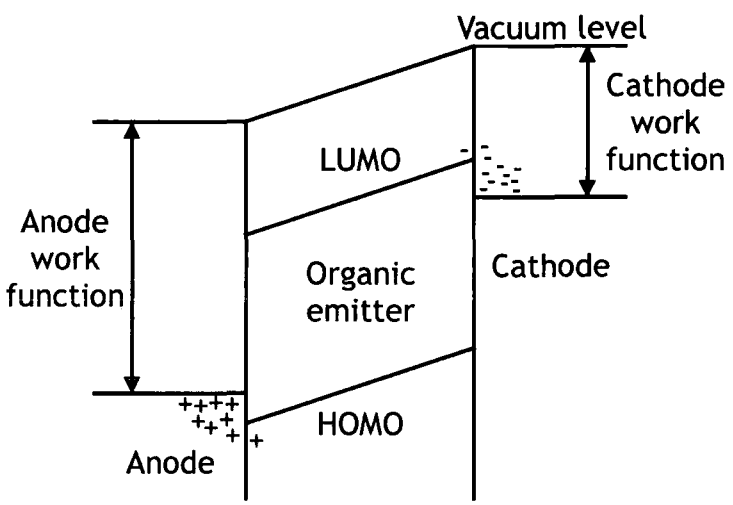

Figure 2.4 Schematic energy level diagram for a basic OLED under applied bias

The following sections describe in more detail the functions which occur in each of the device layers.

2.3.3 The electroluminescent layer

The emission occurs in the electroluminescent layer, which is formed either from a small molecule thin film or polymeric thin film, generally less that 100 nm in thickness. The semiconductor properties of organic materials result from the presence of π-bonds which produce a delocalised electron distribution above and below the bond axis. The HOMO (highest occupied molecular orbital) and LUMO (lowest unoccupied molecular orbital) of the individual molecules determine the electronic structure of the organic material.

Unlike the highly ordered structure of crystalline semiconductors, which is conducive to carrier transport, organic materials have a more amorphous structure. This means that carrier transport is more difficult. Specifically, the amorphous nature of small molecule films provides a more restrictive environment for carriers, while in polymer films carriers are largely confined to a single chain.

For this reason, electron-hole recombination is more localised. Electrons and holes recombine in the organic emitter layer and form an exciton, which is a charge-neutral bound excited state. Excitons can either be in the singlet or triplet form, according to the alignment of the spins of the electrons involved relative to one another. If the spins are antiparallel the state is a singlet with a total spin of zero; if they are parallel, a triplet is formed with a spin of unity. Only singlets produce a photon of visible light. In the majority of organic materials the ratio of singlet to triplet is one to three, so increasingly researchers have adopted methods for harnessing the triplet state energy by exciting a phosphor [10].

Singlet excitons produce a photon whose frequency, υ, is calculated using the following equation

$$E = h\upsilon \qquad (2.1)$$

where E is the energy represented by the band gap in Joules and h is the Planck constant.

In most electroluminescent organic materials, the electron mobility is orders of magnitude smaller than hole mobility. Antoniadis *et al.* calculated the drift distance (alternatively known as the mobility lifetime product) of charge carriers in the presence of an electric field in the polymer PPV [11]. For electrons and holes they calculated 10^{-12} cm^2 V^{-1} and 10^{-9} cm^2 V^{-1}, respectively. Due to this imbalance, it has become common to introduce a means of improving the electron injection and transport (*vide infra*).

The spin coating process commonly used to deposit polymers from solution influences electron mobility in the resulting film. Reducing the solution concentration and increasing the spin speed results in greater polymer stretching and alignment. Typically, stretching the polymer chains results in better conjugation of the π-electrons [12].

Also, spin coating a polymer solution results in the polymer chains lying in the plane of the film [13]. During operation of a polymer-based device, the charge carriers travel perpendicular to the plane of the film, so charge transport is dependent on inter-chain hopping. It is therefore favourable for charge transport if the π-bonds are located at the edge of each polymer chain, closest to the adjacent chains, to promote inter-chain hopping. The location of the π-bonds in a spin-coated polymer film is influenced by solvent choice. In the case of the polymer MEH-PPV, it is desirable for the backbone (which includes the π-bonds) of each polymer chain to be exposed at the edge of the chain and to envelop the insulating side chains [14]. By selecting a solvent which dissolves the backbone of the polymer in preference to the side chains, the side chains are likely to entangle and be surrounded by the backbone. This leaves the backbone exposed and increases the likelihood of charge carriers hopping from one chain to the next.

The internal quantum efficiency is defined as the number of photons emitted per charge carrier flowing in the external circuit. In contrast, the external quantum efficiency takes account of the fact that not all photons are emitted through the substrate. External quantum efficiency, η_{ext}, can be described by

$$\eta_{ext} = \xi \gamma r_{ST} \eta_{PL} \qquad (2.2)$$

where ξ is the fraction of photons emitted through the front surface of the device, γ is the ratio of recombination events to electrons flowing in the external circuit, r_{ST} is the proportion of excitons which are of the singlet variety and η_{PL} is the radiative yield of the singlet excitons [15].

Increasing the quantum efficiency has been the subject of much interest in the literature. As discussed previously, r_{ST} is generally limited to 0.25. Various mechanical techniques have been adopted to increase the proportion of photons emitted through the substrate (ξ). Increasing the number of electron-hole pair recombinations per charge carrier injected (γ) is achieved by balancing the number of electrons and holes injected through the electrodes.

2.3.4 Electrodes

Electrodes perform the role of injecting carriers into the emissive organic layer. Two significant factors influence the choice of electrodes. First, it is necessary for one of the electrodes to be transparent to the wavelength of light produced by the emitting material.

Secondly, to maximise device efficiency and minimise turn-on voltage, the work functions of the anode and cathode must closely match the energy levels for the HOMO and LUMO, respectively, of the organic semiconductor.

Indium tin oxide (ITO) is one of very few transparent conductors and its work function of -4.8 eV is close to the HOMO level of a wide variety of organic materials. For this reason it is used almost ubiquitously as the anode in OLEDs, despite the fact that it has many disadvantages. Cathodes are commonly made from low work function materials such as aluminium or calcium, which have work functions of approximately -4.2 eV and -2.9 eV, respectively [6].

Assuming the band model of electronic structure is applicable, as advocated by Parker [9], the efficiency is reduced when the energy offset between the HOMO and the anode is different to that between the LUMO and the cathode. In order to minimise this loss, Parker suggests matching these energy offsets.

A further method of improving the efficiency is by matching the number of electrons and holes being injected into the EL material. The balance of charge carrier injection is usually limited by the electron injecting characteristics of the negative electrode. So the current is largely composed of holes which have little opportunity for recombination. Cases have been demonstrated where only one carrier-type is successfully injected [9]. Where this is the case, the current will result from just one carrier type, but carrier recombination will never be achieved so there will be no light output.

For this reason methods have been employed to increase injection of the minority carrier [16].

2.3.5 Interfacial regions

Researchers have commented on the importance of the cathode-polymer interface [17]. If there are no oxygen species in the polymer then it is possible for the metal cathode to diffuse into the near surface region and to donate electrons to the polymer. If there are oxygen species at the surface of the organic material then during the thermal evaporation of the cathode the first few metal atoms can produce a thin (2 to 3 nm in thickness) insulating oxide film at the interface. The device efficiency has been seen to improve in the latter case as the thin oxide layer acts as a barrier to holes which can result in balancing the number of carriers injected into the polymer.

It has also been shown that the interfaces between layers are common sites for degradation [18]. Delamination is a particularly common problem as is the reaction or electromigration of a material in one layer with material in an adjacent layer, or with material trapped between two layers. Degradation mechanisms are discussed further in Chapters 5 to 7.

2.4 Carrier injection and carrier transport

The incorporation of additional organic materials in OLEDs has been the subject of much research. Additional materials are used to increase device efficiency through balancing the numbers of electrons and holes and maximising the likelihood of an electron-hole pair recombining in the emissive layer. These additional materials are exploited either as supplementary layers in multi-layer devices, or by combining more than one material in a single blended layer. Methods for improving transport are different for PLEDs and SMOLEDs.

2.4.1 Multi-layer devices

Multi-layer devices feature one or more additional layers between the emissive material and one or both of the electrodes. This approach is commonly employed in SMOLEDs deposited by evaporation, where each material is evaporated to form a discrete layer. It is more complicated to deposit multi-layer PLEDs which are commonly processed from solution because each solvent must not cause the previous layer to re-dissolve.

Improving electron transport

For devices where the electroluminescent layer transports holes preferentially, a multi-layer device includes an electron-transport layer (ETL) between the emitter and the cathode. The energy levels for such a device are illustrated in Figure 2.5.

The purposes of the electron transport layer are twofold. One objective is to reduce the energy offset between the cathode and the adjacent LUMO, so improving electron injection. The other is to establish a barrier for holes by introducing a large disparity between the HOMO level of the emitter and the HOMO of the ETL. The barrier prevents holes from passing through the device without recombining with an electron.

The distribution of the field across the device is uneven because holes accumulate in the region of the organic emitter close to the interface with the ETL. Therefore, a small proportion of the field is dropped across the emitter while a larger proportion is dropped across the ETL.

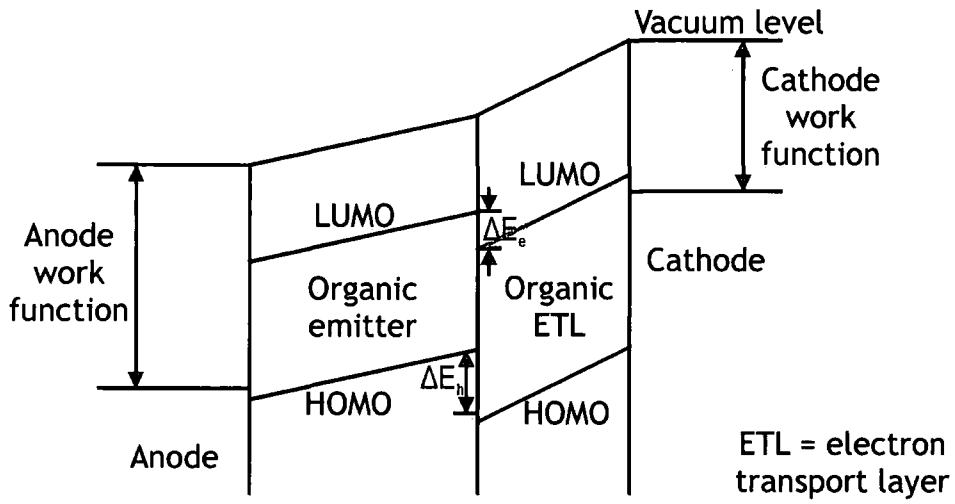

Figure 2.5 Schematic energy level diagram for an OLED including an electron transport layer, under applied bias

In the example of Figure 2.5, the energy required (ΔE_h) for holes to be injected from the emitter into the ETL is greater than the energy required for the electrons to be injected from the ETL into the emitter (ΔE_e). Therefore, recombination is most likely to occur in the emitting material where the size of the band gap (the energy gap between the HOMO and LUMO) is such that the recombination will result in light emission. As well as avoiding the possibility of current flow by only one carrier type, this approach reduces the likelihood of recombination occurring close to the cathode which quenches the emission and is common where electron-transport is poor. Any electron-hole pairs which recombine in the ETL may produce a photon the wavelength of which is governed by the band gap of the electron-transport (ET) material. In this case, the electroluminescent spectrum of the device would include a component from the ET material as well as that from the emissive material. Heeger and co-workers were among the first to advocate the use of an ETL. They demonstrated a five fold increase in the quantum efficiency of devices which included this additional layer [19].

Improving hole transport

Some small molecule emissive materials are more effective in the transport of electrons than holes. In such devices, the multi-layer approach requires a hole-transport layer (HTL) between the cathode and the emitting layer. The HTL prevents recombination from occurring close to the cathode which can result in quenching of the emission. An example of the energy level profiles of such a device is illustrated in Figure 2.6.

A larger proportion of the field falls across the HTL than across the emitter since electrons tend to accumulate in the region of the emitter close to the interface with the HTL.

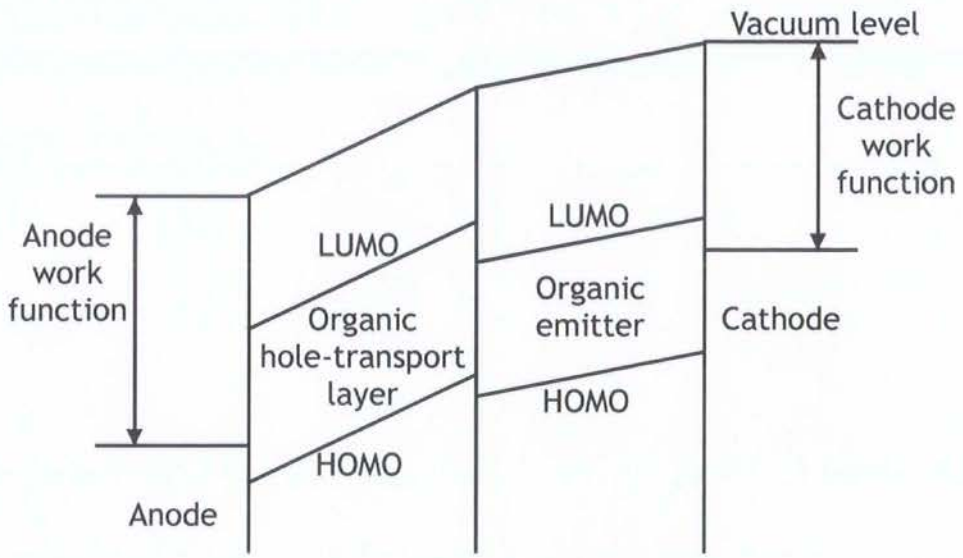

Figure 2.6 Schematic energy level diagram for a device which includes a hole-transport layer, under applied bias

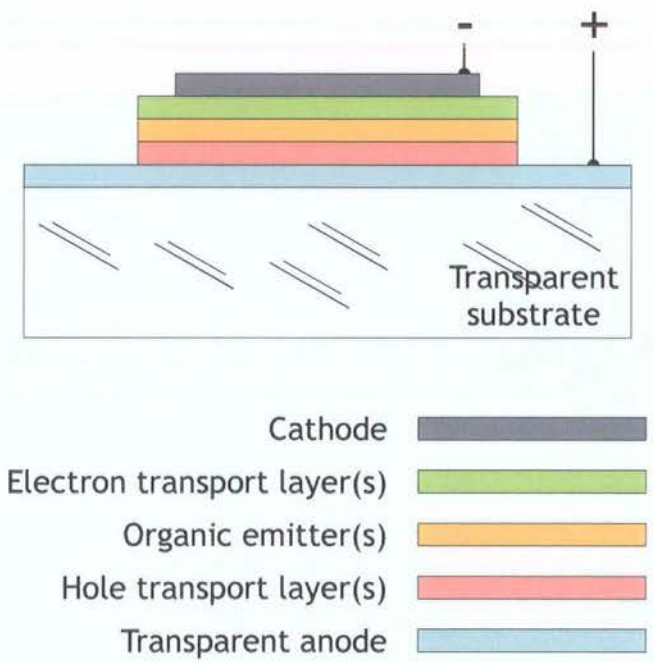

Figure 2.7 Schematic diagram of a multi-layer device with emitting layer, together with electron and hole transporting layers

Increases in efficiency of more than an order of magnitude have been observed by employing an additional ETL and HTL [20]. It has become usual, particularly in the fabrication of SMOLEDs, to introduce a number of injection, transport and blocking

layers. Theoretically, it is possible to fabricate increasingly intricate multiple-layer devices to exploit the electroluminescent, charge injection and charge carrier properties of each material. Figure 2.7 shows a schematic diagram of an OLED with both an ETL and a HTL in addition to an emissive layer.

As indicated previously, the multi-layer approach has been less widespread among the advocates of PLED technology. This is because there are difficulties involved in solution processing of successive multiple layers. Specifically, the solvent used for each successive layer must not dissolve the previously deposited layer [10]. This complication removes many of the advantages of single-step solution processing. However, there are some successful examples of multi-layer PLEDs. Brown *et al.* observed an order of magnitude increase in efficiency by adding a polymer ETL to a PLED [21].

There are also more general disadvantages inherent in multi-layer devices. Research has suggested that degradation commonly nucleates at the interface between two layers [18]. This provides a compelling argument for minimising their number. Also, cost of manufacture is related to the number of layers. Increasing the number of layers inevitably increases the cost. As simplicity of manufacture is one of the main advantages of OLEDs, it seems that such an approach is unlikely to be commercially attractive [22].

2.4.2 Blended layer devices

The alternative to the multi-layer approach is to produce a device with a single organic layer consisting of an electroluminescent material blended with additional material(s) which influence the carrier injection and transport [23-25]. For example, those materials used to form ETLs and HTLs might instead be blended into the emissive material. This approach is popular for the fabrication of PLEDs [26] due to the simplicity of depositing a mixture of materials from a single solution. Blended layer SMOLEDs have also been fabricated by simultaneous evaporation of multiple materials [27].

The effect on charge injection and transport of the dopant material in a blend is similar to that of the extra discrete layer(s) in multi-layer devices. The major difference is that, rather than discrete layers contributing different characteristics to the device, the attributes of the constituent materials are spread more evenly across a single layer.

As stated previously (Section 2.2.3), the currently available display technologies are well established and highly profitable. There are two commonly held strategies for launching a

new technology into the display market. One strategy is to produce an OLED with a specification manifestly superior to that currently available from existing technologies. The other strategy, which is likely to succeed sooner, is to produce an OLED with a similar specification to existing technologies, but at a lower price. The cost of manufacture, and hence the price of the product, is influenced by the cost of each process and the number of processes. By combining the emission and charge transport requirements into a single layer, the number of manufacturing processes is reduced to the minimum. This is a significant argument in favour of blended layer devices.

It is also clear that the cost of manufacturing for (blended or pure) polymer devices is less than for (blended or pure) small molecule devices. Films of small molecules cannot generally be produced from solution and must be thermally deposited in a vacuum. This requires a batch approach to manufacturing which is more expensive than a continuous fabrication facility. Polymers can be processed from solution which makes them highly suitable for a roll to roll manufacturing method.

The following section is a review of what has already been demonstrated with blended PLEDs.

A brief review of blended layer devices

The two most popular groups of polymeric emitting materials are those based on PPV and those based on polyfluorines [22]. One of the first publications to describe the blended layer approach was by Heeger and co-workers [28]. They blended a derivative of the emissive polymer PPV with a small molecule ET material containing the electron-deficient oxadiazole group. This resulted in an 18-fold improvement in the quantum efficiency compared to a similar device without the ET material.

Blended layers are most commonly used to increase device efficiency. More recently, a 500 fold increase in quantum efficiency has been shown through blending MEH-PPV with an electron transporting material, compared with pure MEH-PPV devices [29]. It was also argued that this approach removed the necessity for a low work function cathode material such as calcium, which is particularly unstable in atmospheric conditions. The other reason for using blended emissive layers is to influence the device emission spectrum [30, 31]. This has become more widespread in the pursuit of white OLEDs for ambient lighting applications (*vide infra*).

There are many more publications which describe multi-layer devices than blended layer devices. To this author's knowledge, no publications have referred to the effects of blending on device stability.

Strukelj *et al.* have reported that that the stability of a PLED was improved by adding an additional electron transport layer using a multi-layer approach with PPV [32]. Given that, in general, the multi-layer approach is thought to have a negative influence on device stability, it seems logical to pursue the effect on stability of electron transporting materials exploited in blended layer PLEDs.

Polymer blends, and particularly their influence on device stability, are discussed at length in Chapters 6 and 7.

2.5 Colour displays and white light OLEDs

With the improvement in performance of organic electroluminescent devices, researchers have begun to investigate the possibility of full colour displays and white light OLEDs.

2.5.1 Colour displays

There are three widely described techniques for producing full colour displays [7, 8].

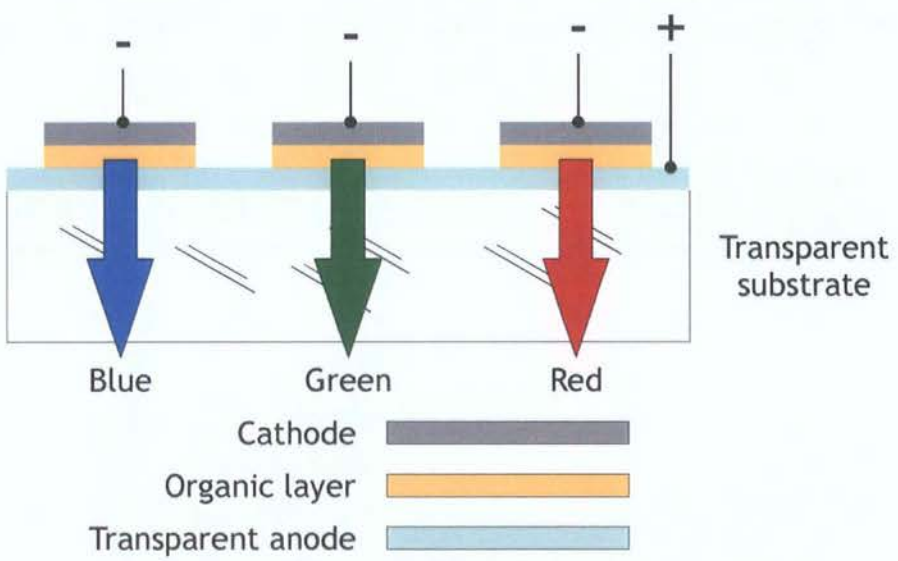

Figure 2.8 Schematic cross section showing the technique which uses discrete RGB elements to produce a full colour display

The schematic in Figure 2.8 illustrates a layout in which independent red, green and blue (RGB) emitters are deposited on the substrate. This technique requires a large number of processing steps. When viewed from above the three pixels would usually be arranged in a

triangular formation. The disadvantages of this approach include the poor aperture ratio and the different degradation rates of the three colour emitters.

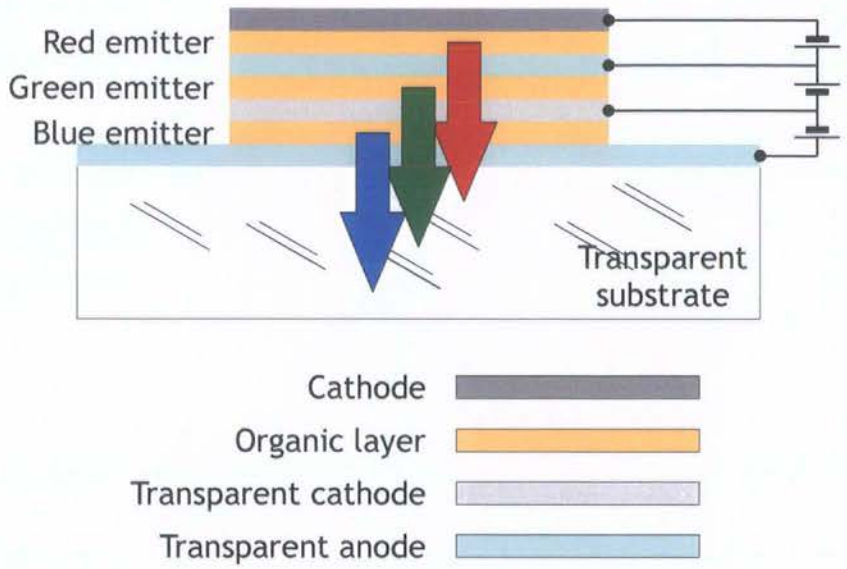

Figure 2.9 Schematic cross section showing the technique which uses stacked RGB elements to produce a full colour display

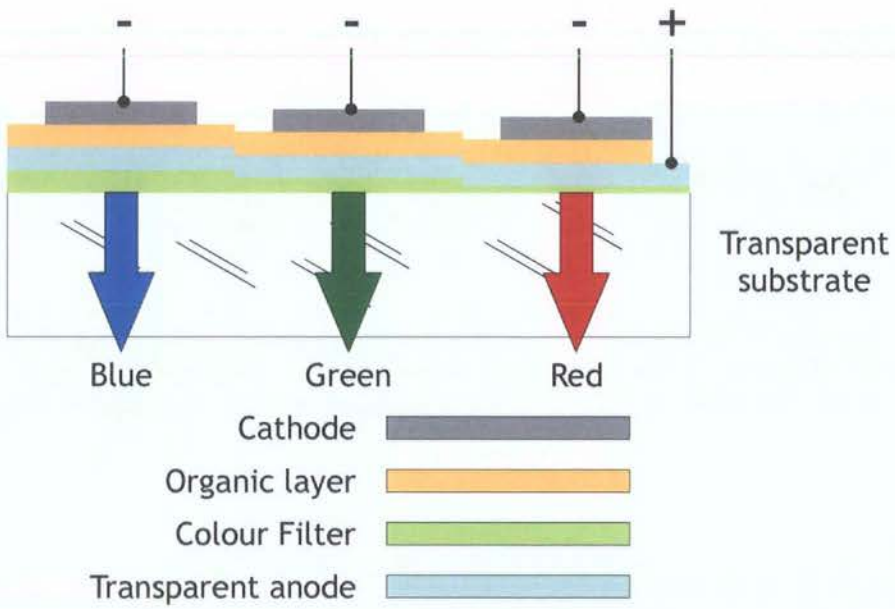

Figure 2.10 Schematic cross section showing the technique which uses filtering of white light or down-converting of blue light to produce a full colour display

Figure 2.9 shows the three RGB emitters stacked vertically, one on top of each other, between transparent electrodes [33]. This method saves space on the substrate and reduces pixel pitch but processing complexity is high.

The third technique, shown in Figure 2.10, uses a single type of emitter to produce light of one colour or range of colours which is subsequently altered where necessary [34]. The light initially produced is usually either white, in which case different filtering elements are used to permit passage of one of the three colours, or blue, in which case down-converters (phosphors) are used to convert the frequency of the light down to green or red. The advantage of this method is simplicity of fabrication by a reduction in the number of materials and layers required, although pixel pitch is as low as for the first technique.

2.5.2 White light OLEDs

Recently, research has diversified to incorporate the field of white light emitters for ambient lighting applications [35-37] as well as displays. In 2001, lighting consumed approximately 30 % of all the electricity generated for buildings in the U.S.A., and cost the consumer $58 billion [38]. Compared with traditional incandescent lamps, which dominate the lighting market and produce 12 to 17 lm W^{-1}, prototype white OLEDs (WOLEDs) have already been shown to produce as much as 60 lm W^{-1} [35]. It seems clear that by exploiting OLEDs for ambient lighting applications, significant savings could be made in terms of energy consumption and cost. For WOLEDs to compete with incandescent light sources, brightness and cost must compare favourably.

Techniques are being developed for fabricating WOLEDs from small molecules and polymers [35]. One approach has been to fabricate multi-layer devices, where each layer is required either to influence some aspect of the emission spectrum or to maximise the efficiency. For example, Forrest *et al.* have demonstrated a multi-layer device which includes six small molecule organic layers between the anode and the cathode, some doped with phosphorescent materials [39]. Using the blended polymer approach, Tasch and co-workers have achieved white emission by blending a broad blue emitting polymer with one which emits red-orange light [40]. The major problem with these two approaches is the differential ageing of the colour emitters, which results in the light spectrum changing with time. To avoid this, devices have been developed that emit a single colour, which is subsequently converted to white light. For instance, Duggal *et al.* used a single polymer layer to emit blue light which was converted into white light using down-conversion layers consisting of organic molecules and inorganic phosphor particles [41].

2.6 Major issues for the future of OLEDs

In order to break into an already highly competitive market, OLEDs will need to compete favourably on both price and specification. As it stands, the few commercially available OLEDs have lower specifications than other display technologies, particularly in terms of lifetime and full colour capability, and they are only able to compete financially with other technologies in small area, low content applications.

Though much has been invested in efforts to increase the relatively low efficiencies of OLEDs, it is arguable that the greatest barrier to commercialisation is that of insufficient lifetime for mainstream applications.

2.6.1 Limited lifetimes

Short lifetimes by comparison with other technologies have long been considered one of the most significant barriers to commercialisation for most applications [42]. Component instability and delamination are regarded as the major causes of low lifetimes and these issues are discussed in more detail in Chapter 5 *et seq.* The problem of short lifetimes, as well as restricting the applications in which monochrome OLEDs can be used, is compounded by the fact that colours degrade differentially. This has implications for the production of full colour RGB displays, as discussed below.

2.6.2 Differential rates of degradation between colour elements

Figure 2.11 shows the relative lifetimes (half-lives) for PLEDs across a range of colours extrapolated from data obtained during accelerated degradation testing by Cambridge Display Technology (CDT) [43]. These are estimated data and are dependent on the brightness required from the device. To give an absolute figure, the lifetime of the most stable device (which emits orange light) was estimated at 320,000 h when emitting at a constant brightness of 100 cd m^{-2}.

As stated previously, two of the three techniques used to produce a full colour display require red, green and blue emitters. The lifetime of blue devices has consistently been lower than for red and green, which introduces considerable difficulty when designing a full colour display product. If an RGB device were to be made where the blue contributor had a shorter lifetime than the other colours, either the intensity of blue elements would degrade more rapidly than the other colours which would result in continually changing colour balance, or complex feedback electronics would be required to drive the blue

emitter at higher voltages to maintain constant intensity with time. For this reason much research has been focused on increasing the lifetime of blue emitters to be similar to that of red and green.

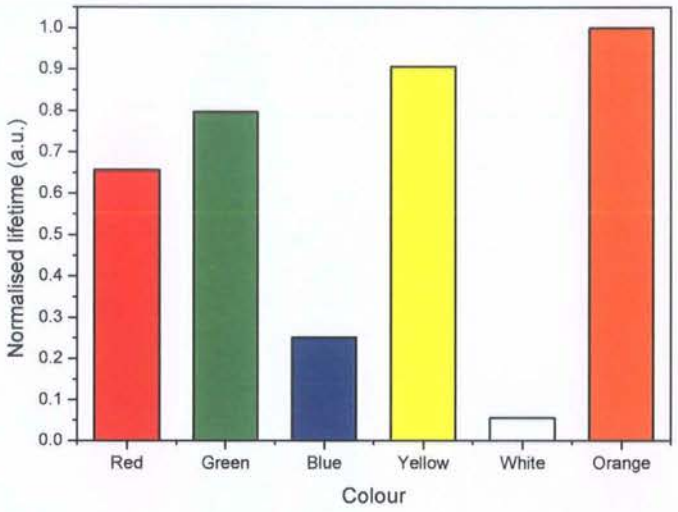

Figure 2.11 Relative lifetimes for PLEDs across a range of colours, as supplied by Cambridge Display Technology in February 2005 [43]

Products have been released to the market with very low lifetimes. For example, in February 2006 Art Lebedev Studio released a three key keyboard with an OLED mounted in each key to allow the image to change with the functionality of the key. The lifetime quoted by the manufacturer was 8000 hours [44] which equates to less than one year of continuous use. It is questionable whether devices with such low lifetimes will have any serious commercial impact. It may be the case that a device such as this, which has no LCD equivalent, could become a commercial success despite the low lifetime. However, for applications where there is an alternative technology which provides a longer lifetime OLEDs are unlikely to compete until lifetimes are comparable.

2.7 Summary and conclusion

An introduction to the field of OLEDs has been given. This included a brief history of research into electroluminescence in organic materials and a discussion of the present and probable future advantages of OLED technology. The structure and principles of operation of OLEDs have been discussed with reference to the role of each component and how they interact. Multi-layer and blended layer device structures have been introduced, and the merits of each have been reviewed.

This chapter has also introduced many of the issues which need to be addressed before OLED technology can have a significant impact on the highly lucrative display and ambient lighting markets. In particular, the technological challenges of the limited device lifetime and complexity of manufacture have been discussed. Also, the need to compete with existing technologies in terms of cost and functionality has been highlighted. These are the issues which profoundly influence the direction of this thesis.

The research recorded here concentrates on stability issues in PLEDs. PLEDs were selected in favour of SMOLEDs because polymer-based devices can be produced by role-to-role fabrication processes, whereas small molecule devices require an inherently more expensive vacuum deposition approach. The investigation of degradation mechanisms and methods for increasing device stability is justified by the fact that device lifetime is one of the principal barriers to commercialisation for most potential OLED applications [42].

Many of the devices which feature in this thesis are derived from blends of MEH-PPV with electron transporting materials. Adopting the blended layer approach has favourable implications for both cost and lifetime. By combining multiple characteristics in a single layer the cost and complexity of manufacture are minimised. Furthermore, minimising the number of interfaces between films reduces the number of nucleation sites for degradation mechanisms.

2.8 References

1 A. Bernanose, M. Compte and P. Vouaux, Journal de Chimie Physique, 50, 65 (1953).

2 M. Pope, H.P. Kallmann and P. Magnate, *Electroluminescence in organic crystals.* Journal of Chemical Physics, 38, 2042 (1963).

3 W.A. Hartman and H.L. Armstrong, *Electroluminescence in organic polymers.* Journal of Applied Physics, 38, 2393 (1967).

4 C.W. Tang and S.A. Van Slyke, *Organic electroluminescent diodes.* Applied Physics Letters, 51, 913 (1987).

5 J.H. Burroughes, D.D.C. Bradley, A.R. Brown, R.N. Marks, K. Mackay, R.H. Friend, P.L. Burns and A.B. Holmes, *Light-emitting diodes based on conjugated polymers.* Nature 347, 539 (1990).

6 D. Braun and A.J. Heeger, *Visible light emission from semiconducting polymer diodes.* Applied Physics Letters, 58, 1982 (1991).

7 P.E. Burrows, G. Gu, V. Bulovic, Z. Shen, S.R. Forrest and M.E. Thompson, *Achieving full-color organic light-emitting devices for lightweight, flat-panel displays.* IEEE Transactions on Electron Devices, 44, 1188 (1997).

8 A. Ghosh and S.A. Van Slyke, *OLEDs: The challenges ahead.* Information Display, 22, 26 (2006).

9 I.D. Parker, *Carrier tunneling and device characteristics in polymer light-emitting diodes.* Journal of Applied Physics, 75, 1656 (1994).

10 K. Meerholz, *Device physics: Enlightening solutions.* Nature 437, 327 (2005).

11 H. Antoniadis, M.A. Abkowitz and B.R. Hsieh, *Carrier deep-trapping mobility-lifetime products in poly(p-phenylene vinylene).* Applied Physics Letters, 65, 2030 (1994).

12 Y. Shi, J. Liu and Y. Yang, *Device performance and polymer morphology in polymer light emitting diodes: The control of thin film morphology and device quantum efficiency.* Journal of Applied Physics, 87, 4254 (2000).

13 D. McBranch, I.H. Campbell, D.L. Smith and J.P. Ferraris, *Optical determination of chain orientation in electroluminescent polymer films.* Applied Physics Letters, 66, 1175 (1995).

14 Y. Shi, J. Liu and Y. Yang, Organic-light emitting devices, A survey, Springer-Verlag New York, 155 (2004).

15 J. Shinar and V. Savvateev, Organic-light emitting devices, A survey, Springer-Verlag New York, 30 (2004).

16 A.P. Kulkarni, C.J. Tonzola, A. Babel and S.A. Jenekhe, *Electron transport materials for organic light-emitting diodes.* Chemistry of Materials, 16, 4556 (2004).

17 J. Birgerson, M. Fahlman, P. Bröms and W.R. Salaneck, *Conjugated polymer surfaces and interfaces: a mini-review and some new results.* Synthetic Metals, 80, 125 (1996).

18 V.N. Savvate'ev, A.V. Yakimov, D. Davidov, R.M. Pogreb, R. Neumann and Y. Avny, *Degradation of nonencapsulated polymer-based light-emitting diodes: Noise and morphology.* Applied Physics Letters, 71, 3344 (1997).

19 S. Aratani, C. Zhang, K. Pakbaz, S. Höger, F. Wudl and A.J. Heeger, *Improved efficiency in polymer light–emitting diodes using air-stable electrodes.* Journal of Electronic Materials, 22, 745, (1993).

20 X. Gong, S. Wang, D. Moses, G.C. Bazan and A.J. Heeger, *Multilayer polymer light-emitting diodes: white-light emission with high efficiency.* Advanced Materials, 17, 2053 (2005).

21 A.R. Brown, D.D.C. Bradley, J.H. Burroughes, R.H. Friend, N.C. Greenham, P.L. Burn, A.B. Holmes and A. Kraft, *Poly(p-phenylenevinylene) light-emitting diodes: Enhanced electroluminescent efficiency through charge carrier confinement.* Applied Physics Letters 61, 2793 (1992).

22 M.T. Bernius, M. Inbasekaran, J. O'Brien and W.S. Wu, *Progress with light-emitting polymers.* Advanced Materials, 12, 1737 (2000).

23 J. Kido, M. Kohda, K. Okuyama and K. Nagai, *Organic electroluminescent devices based on molecularly doped polymers.* Applied Physics Letters, 61, 761 (1992).

24 M. Uchida, C. Adachi, T. Koyama and Y. Taniguchi, *Charge carrier trapping effect by luminescent dopant molecules in single-layer organic light emitting diodes.* Journal of Applied Physics, 86, 1680 (1999).

25 S.Y. Quana, F. Teng, D. Wang, D. Liu, Z. Xu, Y. Wang, and X. Xu, *Charge carrier injection and transport in polymer blend films.* Solid State Communications, 134, 291 (2005).

26 D.R. Baigent, N.C. Greenham, J. Grüner, R.N. Marks, R.H. Friend, S.C. Moratti and A.B. Homes, *Light-emitting diodes fabricated with conjugated polymers – recent progress.* Synthetic Metals, 67, 3 (1994).

27 M. Pfeiffer, K. Leo, X. Zhou, J.S. Huang, M. Hofmann, A. Werner and J. Blochwitz-Nimoth, *Doped organic semiconductors: Physics and application in light emitting diodes.* Organic Electronics, 4, 89 (2003).

28 C. Zhang, S. Höger, K. Pakbaz, F. Wudl and A.J. Heeger, *Improved efficiency in green polymer light-emitting diodes with air stable electrodes.* Journal of Electronic Materials, 23, 453 (1994).

29 I.-N. Kang, D.-H. Hwang, H.-K. Shim, T. Zyung and J.-J. Kim, *Highly improved quantum efficiency in blend polymer LEDs.* Macromolecules, 29, 165 (1996).

30 B. Hu, Z. Yang and F.E. Karasz, *Electroluminescence of pure poly(N-vinylcarbazole) and its blends with a multiblock copolymer.* Journal of Applied Physics, 76, 2419 (1994).

31 C. Zhang, H. von Seggern, K. Pakbaz, B. Kraabel, H.-W. Schmidt and A.J. Heeger, *Blue electroluminescent diodes utilizing blends of poly(p-phenylphenylene vinylene) in poly(9-vinylcarbazole).* Synthetic Metals, 62, 53 (1994).

32 M. Strukelj, F. Papadimitrakopoulos, T.M. Miller and L.J. Rothberg, *Design and application of electron-transporting organic materials.* Science, 267, 1969 (1995).

33 S.R. Forrest, P.E. Burrows, Z. Shen, G. Gu, V. Bulovic and M.E. Thompson, *The stacked OLED (SOLED): a new type of organic device for achieving high-resolution full-color displays.* Synthetic Metals, 91, 9 (1997).

34 A. Dodabalapur, L.J. Rothberg, T.M. Miller and E.W. Kwock, *Microcavity effects in organic semiconductors.* Applied Physics Letters, 64, 2486 (1994).

35 B.W. D'Andrade and S.R. Forrest, *White organic light-emitting devices for solid-state lighting.* Advanced Materials, 16, 1585 (2004).

36 C.W. Ko and Y.T. Tao, *Bright white organic light-emitting diode.* Applied Physics Letters, 79, 4234 (2001).

37 Y. Sun, N.C. Giebink, H. Kanno, B. Ma, M.E. Thompson and S.R. Forrest, *Management of singlet and triplet excitons for efficient white organic light-emitting devices.* Nature, 440, 908 (2006).

38 U.S. Department of Energy, *National Lighting Inventory and Energy Consumption Estimate, Volume 1,* U.S. Government Printing Office, Washington DC, 2001, page x.

39 B.W. D'Andrade, M.E. Thompson, S.R. Forrest, *Controlling exciton diffusion in multilayer white phosphorescent organic light emitting devices.* Advanced Materials, 14, 147 (2002).

40 S. Tasch, E.J.W. List, O. Ekström, W. Graupner, G. Leising, P. Schlichting, U. Rohr, Y. Geerts, U. Scherf, and K. Müllen, *Efficient white light-emitting diodes realized with new processable blends of conjugated polymers.* Applied Physics Letters, 71, 2883 (1997).

41 A.R. Duggal, J.J. Shiang, C.M. Heller and D.F. Foust, *Organic light-emitting devices for illumination quality white light.* Applied Physics Letters, 80, 3470 (2002).

42 L.J. Rothberg and A.J. Lovinger, *Status of and prospects for organic electroluminescence.* Journal of Materials Research, 11, 3174 (1996).

43 Data compiled from Cambridge Display Technology (CDT) press releases, accessed 30th June 2006, available at: www.cdtltd.co.uk.

44 Data available on Art Lebdev Studio company website, accessed 30th June 2006, at: www.artlebedev.com/portfolio/optimus-mini/answers/

45 L.S. Hung and C.H. Chen, *Recent progress of molecular organic electroluminescent materials and devices.* Materials Science and Engineering R, 39, 143 (2002).

Chapter Three

Experimental techniques

3.1 Introduction

The first part of this Chapter records all of the experimental techniques used to fabricate devices, including descriptions of the apparatus. Section 3.4 introduces the methods for analysing the physical characteristics of devices and their components, while the techniques used to establish the operational characteristics of devices are explained in section 3.5.

3.2 Device fabrication

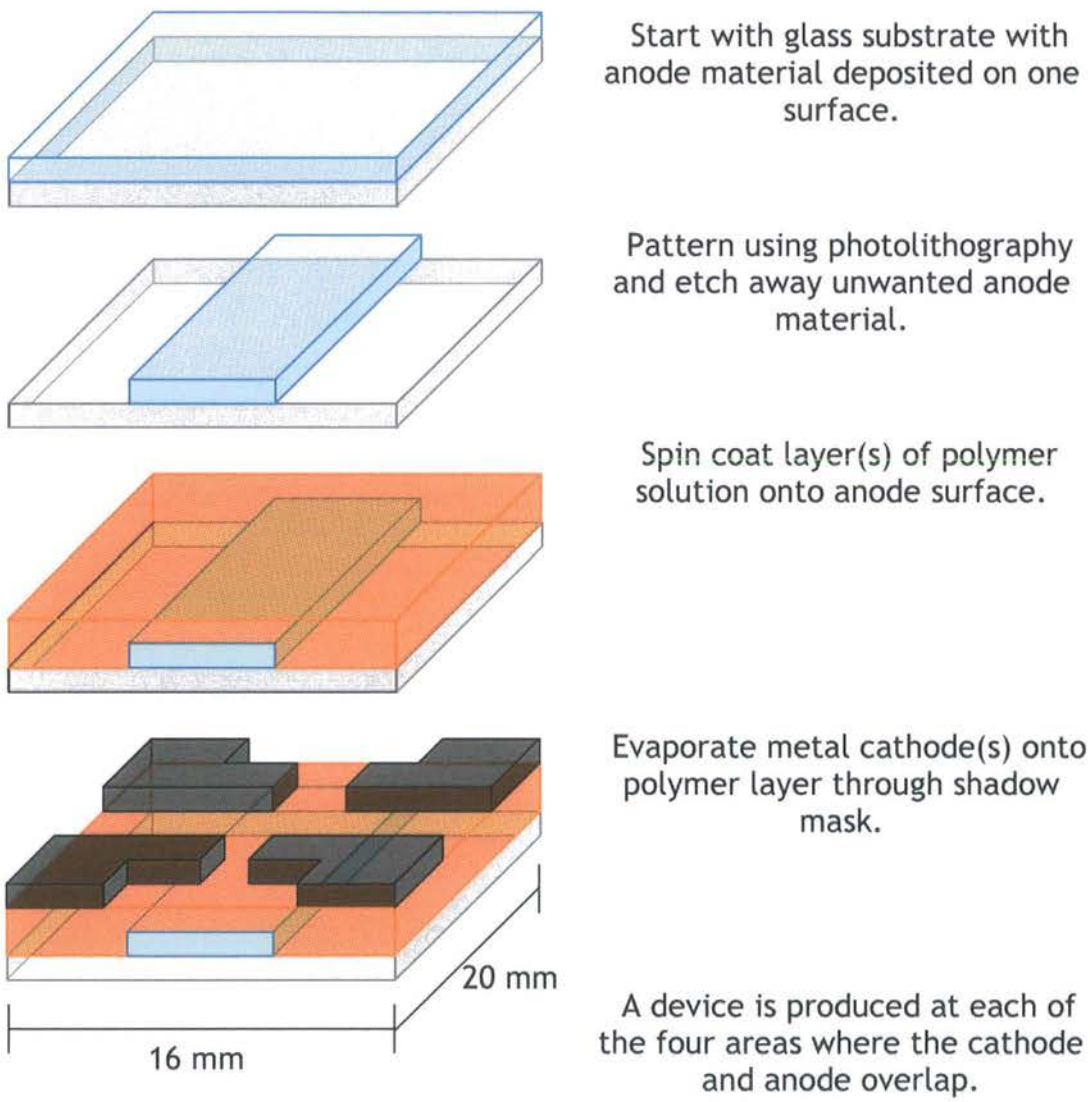

Figure 3.1 Layer by layer illustration of device construction process

Devices were fabricated by stacking at least three thin films on a transparent substrate material. Films were deposited using spin coating and thermal evaporation techniques. The

steps in the process of fabricating the principal components of an OLED on a glass substrate are illustrated in Figure 3.1.

3.2.1 Glovebox

All processing (subsequent to anode patterning) was undertaken in a bespoke glovebox (Figure 3.2) manufactured by Glovebox Technology Ltd.

Figure 3.2 Photograph of glovebox

The atmosphere inside the glovebox was continuously purged with dry nitrogen. This was to eliminate atmospheric oxygen and water vapour, to which OLEDs are particularly sensitive. When in standby mode the rate of flow of dry nitrogen was maintained at 4 l min^{-1} which increased to 10 l min^{-1} when in use. An Edwards 306 thermal evaporator and purpose designed spin coater were incorporated into the glovebox. The design also included a purgable ante chamber to allow samples to be passed in and out. This is visible on the right hand side.

3.2.2 Anode patterning

Anodes were fabricated from either indium tin oxide (ITO) or aluminium-doped zinc oxide (AZO). The films were supplied already deposited on polished soda lime glass. Merck (Germany) supplied glass with a 100 nm thick sputtered layer of ITO with sheet resistance 7.8 Ω □$^{-1}$. Cranfield University provided glass with a 500 nm thick sputtered layer of AZO of sheet resistance 118 Ω □$^{-1}$.

The sheets of coated glass were cut into 60 mm by 64 mm pieces, then cleaned by ultrasonication in acetone and iso-2-propanol (IPA) for 30 min each. They were dried using a nitrogen gun and baked on a hotplate at 120 °C for 5 min to evaporate any residual liquid. A 1.3 μm layer of Shipley S1813 photoresist was spun onto the anode film at a speed which increased over 20 s to 3700 rpm for 45 s. Each sample was placed on a hotplate at 95 °C for 5 min to allow the photoresist to bake, after which it was flood exposed to broadband UV light through a printed acetate mask (Figure 3.3) for 3 s using an EVG620 mask aligner.

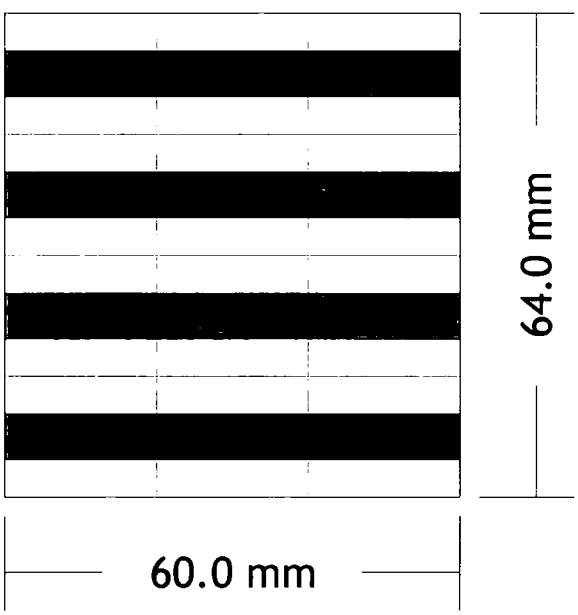

Figure 3.3 Pattern used for anode etching

The sample was baked on a hotplate at 50 °C for 5 min before developing the pattern in a NaOH-based developer (AZ2351B) diluted 1:1 with pure water to remove the exposed photoresist. Continuously flowing pure water was used to rinse the sample and it was dried using a nitrogen gun. The exposed anode material was etched off the glass by submerging the sample in an acidic bath of HCl:HNO_3:H_2O (20:1:20) at 50 °C for 3 min. The sample

was again rinsed in pure water and then cleaned by ultrasonication in acetone and IPA for 30 min each and dried using the nitrogen gun. The patterned anode glass sheets were cut into twelve individual substrates (20 mm by 16 mm), each with a single 6 mm wide strip of anode material across the centre of one face. Prior to the next processing stage the substrates were cleaned by further ultrasonication in acetone and IPA.

3.2.3 Spin coating of organic layers

Solution preparation

Electroluminescent polymers and electron-transporting molecules were obtained in powder form. The details of each material, including its chemical nature, source and purity, are given in subsequent chapters. Solutions were produced with chloroform of the 'Aristar' grade sourced from BDH with a purity of 99.0 to 99.4 %. Ethanol (0.6 to 1.0 %) was present in the purchased solvent as a preservative and other contaminants were quoted in the range 1 to 100 parts per billion. The solution concentrations were adjusted (between 5 and 16 mg ml^{-1}) to produce films of consistent quality and thickness. In the case of blended layer devices, the ratio of materials was measured by weight when solid.

A layer of PEDOT:PSS was included in many devices. PEDOT:PSS was sourced as a dispersion (sold as BAYTRON P) from H.C. Starck. This was diluted with pure water (1:1) immediately prior to spin coating.

Spin coating

Spin coating is a fabrication method employed for producing thin film coatings over large areas. The spin coater was designed and made at Durham University. Its main component was a horizontal chuck which could be spun by an electric motor at up to 3000 rpm. The substrate was placed onto the chuck with the anode surface facing up. A vacuum line was used to fasten the substrate to the chuck. Between 200 and 300 µl of solution was dispensed onto the substrate surface, then the chuck rotated at between 750 and 1500 rpm (depending on the solution concentration and the desired thickness) for a period of 1 min. The centrifugal force caused much of the solution to fly off the substrate, but the attractive force between the substrate and the solution caused a thin layer of the solution to remain. The solvent in this thin layer evaporated rapidly due to the large ratio of surface area to volume, leaving a thin solid film of the electroluminescent material(s) [1]. The spin coater is shown in Figure 3.4 and Figure 3.5.

In the case of devices with PEDOT:PSS, after this layer was deposited by spin coating the substrate was placed under vacuum for one hour in order to evaporate residual water content before spin coating the electroluminescent layer.

Figure 3.4 Photograph of the spin coater

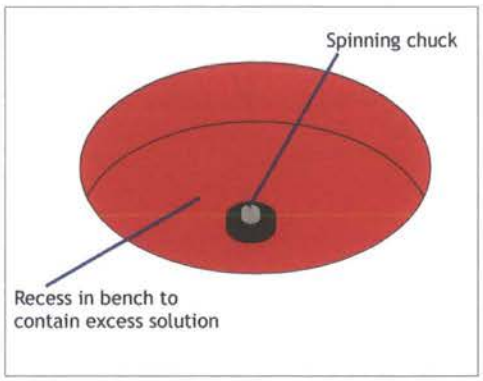

Figure 3.5 Diagram of the spin coater

3.2.4 Thermal evaporation of cathode

Metal cathodes were deposited by thermal evaporation through a metal shadow mask at a pressure of 10^{-6} mbar at a rate of 1 nm s^{-1}. The design of the shadow mask for fabricating cathodes on six substrates is shown in Figure 3.6.

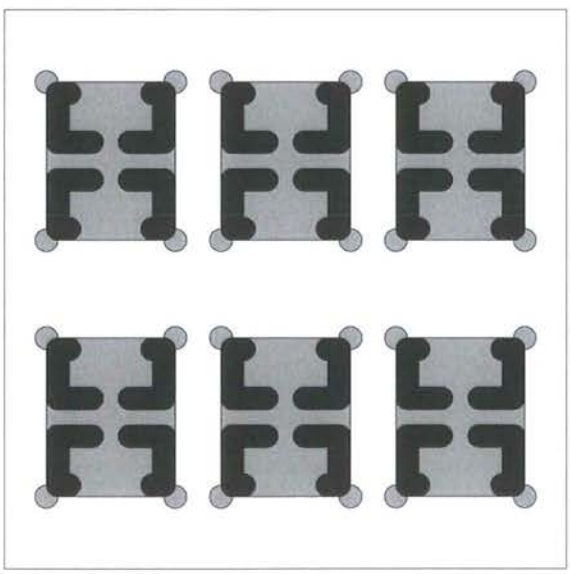

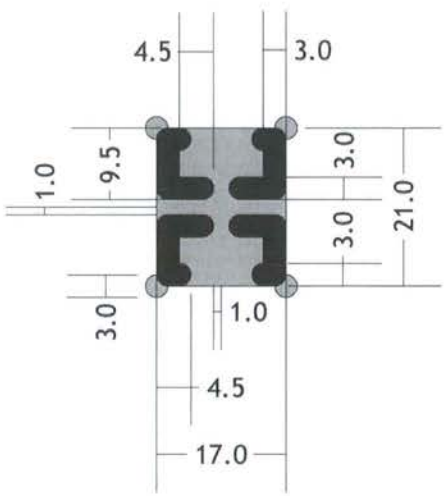

Dimensions in mm

White regions: brass (3 mm thick)
Grey regions: 1.5 mm recess in brass
Black regions: aperture

Figure 3.6 Shadow mask for cathode evaporation

Rate of deposition and film thickness were monitored by a quartz crystal sensor during the evaporation. The thickness of aluminium cathodes was 100 nm. Some devices included a 10 to 15 nm layer of calcium beneath the aluminium.

3.3 Standard device layout

Figure 3.7 illustrates how the patterning of the layers defined the device configuration. An electroluminescent region (or device) of approximately 5 mm^2 was formed at each of the four regions where the anode and cathode overlapped. Figure 3.8 is a photograph of a sample containing four devices. The (orange) organic film and (metallic) cathode can be identified clearly. The transparent anode layer is not visible in the photograph.

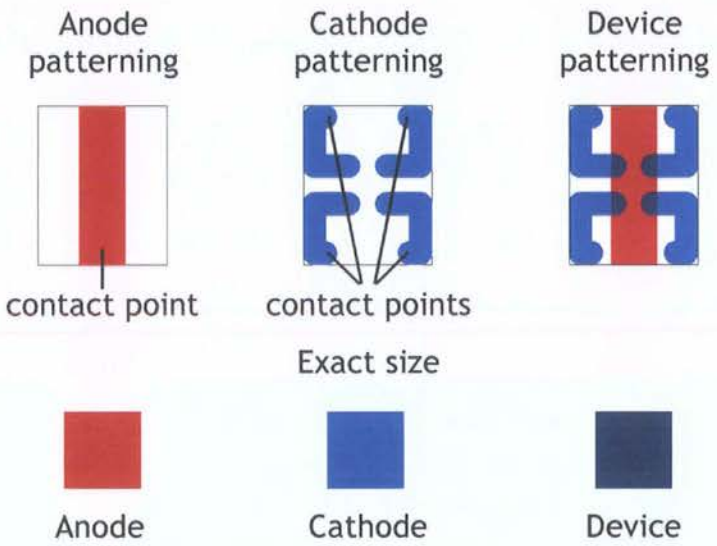

Figure 3.7 Device patterning

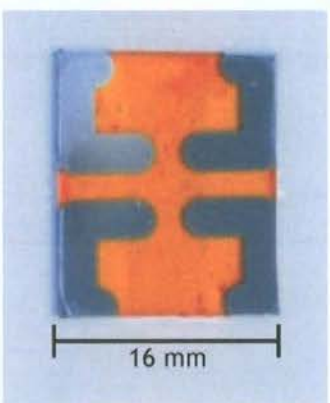

Figure 3.8 Photograph of standard device

To access the anode beneath the polymer material, a small region (~ 5 mm^2) of polymer was removed either with a blade or by dissolving in chloroform.

3.4 Analysing physical characteristics of devices

Device films were characterised using the following methods.

3.4.1 Optical microscopy

The film morphology was assessed initially using a Vickers optical microscope. Lenses with magnification factors of 10, 20, 40 and 100 times were available. Micrographs were produced using a Canon EOS D30 digital camera.

The same camera was used without magnification to photograph devices under operation.

3.4.2 Absorption spectroscopy

Absorption spectra were measured using a Perkin Elmer Lambda 19 spectrophotometer. The operation of the spectrophotometer is shown schematically in Figure 3.9.

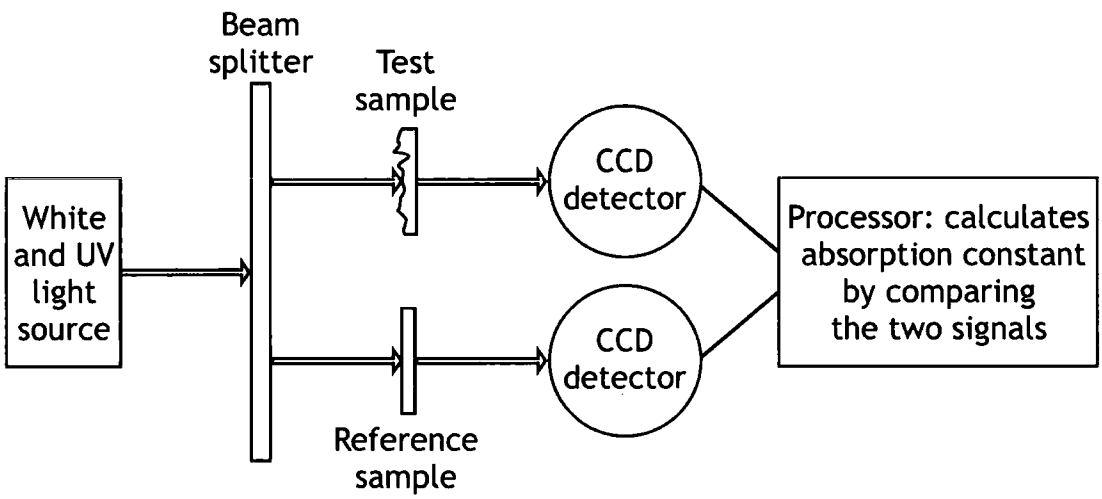

Figure 3.9 Schematic of spectrophotometer

The spectrophotometer's light source emitted a beam in the wavelength range 350 nm to 1100 nm. The absorption was measured at each wavelength sequentially in steps of 1 nm. The light beam was split in two and each of the two beams passed through a sample container. The two sample containers initially housed two reference samples during the calibration cycle. After calibration, one of the reference samples remained in place and the other was replaced by the sample under test. Two charge coupled devices (CCD) detected the light transmitted through each of the two samples and a processor calculated the absorption constant of the test sample by comparing it with the reference sample according to the equation

$$A = -\log_{10}\left(\frac{I}{I_0}\right) \tag{3.1}$$

where A is absorption, I_0 is the initial intensity and I is the measured intensity.

3.4.3 Atomic force microscopy

A Topometrix Explorer™ atomic force microscope (AFM) was used to produce a three dimensional profile of the surface being analysed. Figure 3.10 illustrates the principles of operation of the AFM.

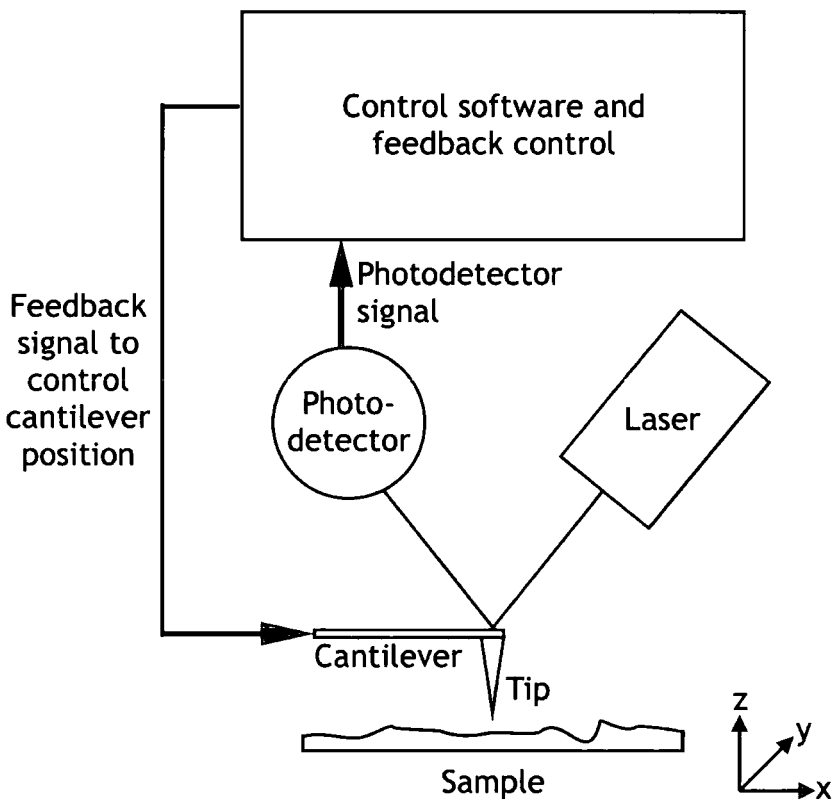

Figure 3.10 AFM schematic diagram

The AFM consisted of a cantilever at the end of which was mounted a tip with a radius of curvature of approximately 1 nm. The sample under test was placed on the scanning table and the cantilever tip was lowered into close proximity with the top surface of the sample. The scanning table moved in the x-y plane which allowed the tip to scan the surface of the sample one row at a time. The attractive force between the tip and the sample caused the tip to deflect in sympathy with the profile of the sample. A laser was focused on the cantilever and reflected onto a photodetector. As the cantilever deflected, the reflected laser beam moved relative to the photodetector. In order to avoid the likelihood of the tip

crashing into the surface of the sample, a feedback loop caused the table to move in the z-dimension such that a constant force between the cantilever and the sample was maintained.

3.4.4 White light interferometry

A Zygo NewView™ 5010 white light interferometer was also used to produce a three-dimensional profile of a sample surface. The maximum field of view for a single scan was 17.5 mm, but this could be expanded using the field stitching option. Peak lateral resolution was 0.45 μm, and peak vertical resolution was 0.1 nm. The general principles of operation of the white light interferometer are illustrated in Figure 3.11.

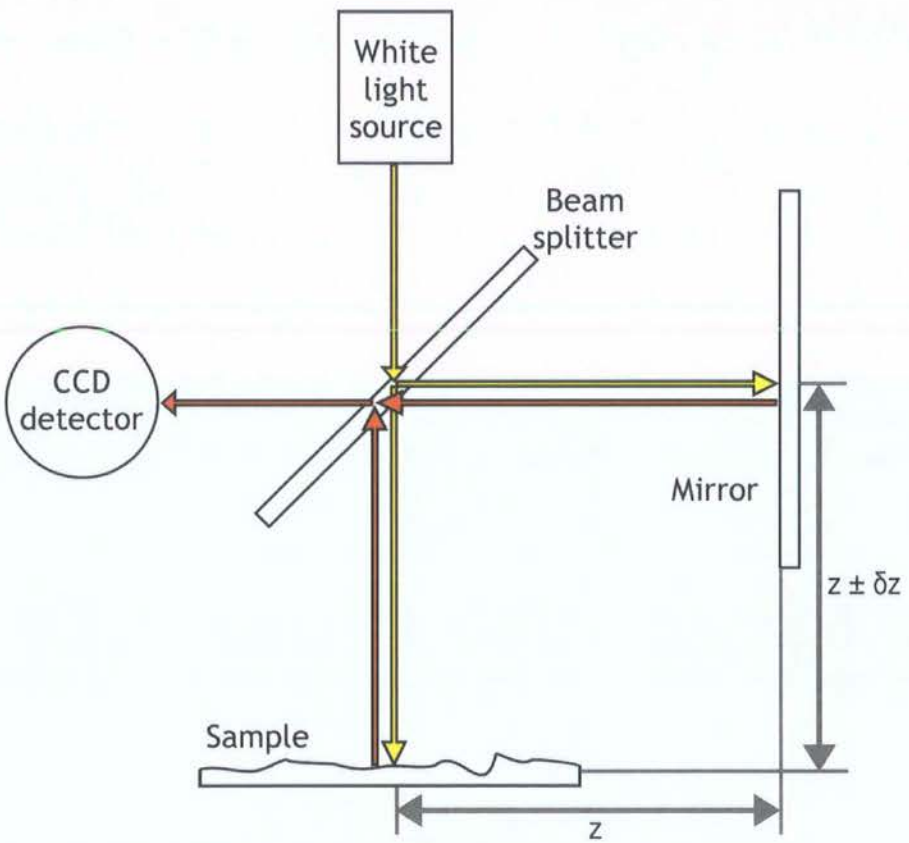

Figure 3.11 Schematic diagram of white light interferometer

The white light interferometer transmitted a beam of white light through a beam splitter so that 50 % of the light fell onto the surface of the substrate and 50 % fell onto a mirror. Both light beams were reflected and recombined at the beam splitter before falling onto a charge couple device (CCD) detector. Where the distance to the surface ($z \pm \delta z$) differed from the distance to the mirror (z) the light beams returned to the beam splitter out of phase. This appeared on the CCD detector as a pattern of interference fringes. The Zygo

software calculated the surface height, to within 0.1 nm, by analysing the frequency and wavelength of the interference fringes. The equipment was calibrated to move the sample table through the beam in 0.22 μm steps to enable height data to be recorded across a range of x-y coordinates. The data were plotted to produce a three dimensional model of the sample.

3.4.5 Surface profilometry

A Tencor Instruments Alpha-Step 200 stylus profilometer was used to measure film thickness. It measured the surface profile of a sample by recording the vertical and horizontal positions of a stylus as it scanned across whilst in contact with the sample. Scanning the perimeter of a film on a substrate provided the step profile and height of the film.

3.4.6 Impedance spectroscopy

Alternating current (a.c.) impedance spectroscopy was used as a technique to establish the equivalent circuit of a device. Measurements were performed using a Hewlett Packard 4192 Impedance Analyser with a four terminal configuration to connect to the device electrodes. The capacitance and conductance of the devices were measured at logarithmically spaced a.c. voltages in the frequency range from 1 Hz to 13 MHz. Parasitic capacitance and conductance in the test leads were automatically removed from the data by first performing a calibration scan. The real and imaginary parts of the impedance were plotted in the complex plane. This allowed the device to be modelled as a number of discrete resistances and capacitances.

3.5 Analysing the operational characteristics of devices

The operational characteristics of sets of devices were compared according to their values for peak light emission, turn-on voltage required for current flow, turn-on voltage required for light emission, quantum efficiency and luminance efficiency. Details of how these data were obtained are given below.

3.5.1 Current-voltage and light-voltage characteristics

Current-voltage (I-V) and light-voltage characteristics were analysed using purpose designed characterisation apparatus, details of which are given in Chapter 4. The measurement technique involved applying a voltage across each device, which was

incremented at appropriate time intervals. At each voltage, the current was measured and simultaneously the light emission was estimated by measuring the current generated in a photodiode which was in contact with the device.

3.5.2 Quantum efficiency

Quantum efficiency is defined as the ratio of the number of photons emitted from the device to the number of charge carriers injected into the device. Values of quantum efficiency were estimated at each voltage increment from the current-voltage and light-voltage data.

3.5.3 Electroluminescence spectroscopy

The electroluminescent spectra were obtained using an Ocean Optics USB 2000 miniature fibre optic spectrometer. Devices were held at constant voltage and positioned inside an integrating sphere which acted to diffuse the light evenly throughout the sphere (diameter 50 mm). A fibre optic cable (diameter 0.1 mm) was positioned through a hole in the sphere such that the end of the fibre was flush with the internal surface of the sphere. The opposite end of the fibre was connected to the spectrometer, which was composed of an array of 2048 charge-coupled devices (CCDs). In the spectrometer, a movable diffraction grating split the light into narrow (between 0.3 nm and 0.4 nm) bandwidths. Each narrow band was directed towards a separate element of the CCD array which was calibrated to the incoming wavelength.

The surface area of a sphere is $4\pi r_s^2$ (where r_s is the radius of the sphere) and the area of a circle is πr_c^2 (where r_c is the radius of the circle). Therefore, the ratio of the amount of light incident on the (circular) fibre optic to that incident on the internal surface of the integrating sphere is $r_c^2/4r_s^2$. In this case, r_c = 0.1 mm and r_s = 25 mm, so 1/250,000 of the light emitted by the device fell onto the fibre optic cable.

3.5.4 Luminous efficiency

It has been argued that OLED efficiency is most universally meaningful when quoted in terms of luminous efficiency (cd A^{-1}) or luminous power efficiency (lm W^{-1}) at a stated value of luminance (cd m^{-2}) [2, 3]. Since the publication by Forrest *et al.* [2], quoting efficiency in such units has become increasingly popular.

The lumen (lm) is the unit of luminous flux which equates to the visible power or light energy per unit of time. Luminous intensity, the SI base unit measured in candela (cd), is

the luminous flux per solid angle emitted or reflected from a point. The lumen is related to the candela in terms of solid angle, whereby cd = lm sr^{-1}. Luminance is the measurable quantity which most closely corresponds to the subjective quantity perceived as brightness. Therefore, any efficiency quoted in terms of lumens per Watt (lm W^{-1}) or candela per Ampere (cd A^{-1}) is objectively linked to the intensity of light perceived by a human observer. By quoting the efficiency at a fixed luminance this ensures that the efficiency corresponds to a visible brightness and avoids the likelihood of stating high efficiencies at luminance values which are too small to be of practical relevance. The photometric units are summarised in Table 3.1.

Term	Unit	Notes
Luminous intensity	candela (cd)	SI base unit
Luminous flux	lumen (lm) = cd sr	Luminous intensity multiplied by solid angle (in steradians)
Luminance	cd m^{-2}	Luminous intensity per unit area
Luminous efficiency	cd A^{-1}	Luminous intensity per Ampere
Luminous power efficiency	lm W^{-1}	Luminous flux per Watt

Table 3.1 Photometric units

To estimate the luminous efficiency, the electroluminescent spectrum of the device was obtained using the integrating sphere (*vide supra*). The spectrometer provided a value for the total energy emitted by the device and this was used to estimate the luminous intensity in candela. Luminance was not measured directly, as to force the device to operate at an exact luminance would have required complex feedback circuitry. As no such circuitry was available, a number of measurements were made providing a range of luminance values. Further luminance values were extrapolated together with the corresponding luminous efficiency values.

3.5.5 Electrical and emission stability

The equipment used for the I-V characterisation was also employed to assess the electrical and light emission stability of devices. In the early stages of this research, the device stability was measured by applying a constant voltage across the device and measuring

(a) the current through the device and (b) the photocurrent generated by the emitted light. Following preliminary trials, it was established that applying a constant current through the device resulted in greater stability. Subsequently, the device stability was measured by applying a constant current through the device and measuring (a) the voltage across the device and (b) the photocurrent generated by the emitted light.

3.6 Summary

The anode patterning, spin coating and thermal evaporation processing methods have been described. Explanations have been given for the techniques of microscopy, absorption spectroscopy, electroluminescence spectroscopy, atomic force microscopy, white light interferometry surface profilometry and impedance spectroscopy, which were used to analyse the physical characteristics of devices. Procedures used to analyse the operational characteristics of devices including current-voltage and light-voltage characterisation, quantum efficiency estimation, luminous efficiency characterisation and stability analysis have been discussed.

3.7 References

1 K. Norrman, A. Ghanbari-Siahkali and N.B. Larsen, *Studies of spin-coated polymer films.* Annual reports on the progress of Chemistry, Section C, 101, 174 (2005).

2 S.R. Forrest, D.D.C. Bradley and M.E. Thompson, *Measuring the Efficiency of Organic Light-Emitting Devices.* Advanced Materials, 15, 1043 (2003).

3 Discussions of photometric variables and the relationships between them were found in: (a) K. Gieck and R. Gieck, Technical Formulae, 8th Edition, Gieck Verlag, (1996) (page V1); and (b) C.P. Halsted, "Brightness, luminance, and confusion," originally published in Information Display (March 1993), since made available online at http://www.crompton.com/wa3dsp/light/lumin.html (accessed 12th May 2006).

Chapter Four

Characterisation equipment

4.1 Introduction

Automated device characterisation equipment was necessary for two reasons:

- to characterise large numbers of devices in batches so as to identify data trends and easily distinguish anomalous data; and
- to characterise devices automatically, rapidly and (in the case of stability routines) simultaneously.

Identifying data trends was important because of the variation observed between the characteristics of identically fabricated devices. Devices were fabricated in batches of 24 (6 substrates each with 4 devices).

Manual characterisation was time and labour intensive. It took approximately 3 hours to characterise all 24 devices, and the user had to be present throughout to load each substrate, align the probes, close the chamber, wait for vacuum and initiate each routine in the software interface. During this period the devices were subjected to an intermittent vacuum and the user had to be present throughout.

Another limitation with manual characterisation was that stability data could be obtained for only one device at a time. In particular, if each of 6 devices were to be tested for a period of a week, the sixth device had to remain untested for the first five weeks following fabrication. During this time the device may have undergone degradation.

An automated measurement system was designed such that no user intervention was required once the routine was initiated. All the samples were loaded into the chamber at the start of the characterisation. This system required only 2 min of user input, whereas the manual system required 3 hours. Once initiated, it took approximately 45 min for the system to perform two standard I-V characterisations on each of 24 devices, consecutively. All the substrates were present in the chamber throughout the 45 min routine, the vacuum was maintained and, once started, the process was fully automated. Stability characteristics were performed on up to 6 devices simultaneously (hence the delay between fabrication and testing was the same for all 6 devices) and once the routine was initiated, no user input was required.

All data presented in this thesis were obtained using the automated characterisation equipment.

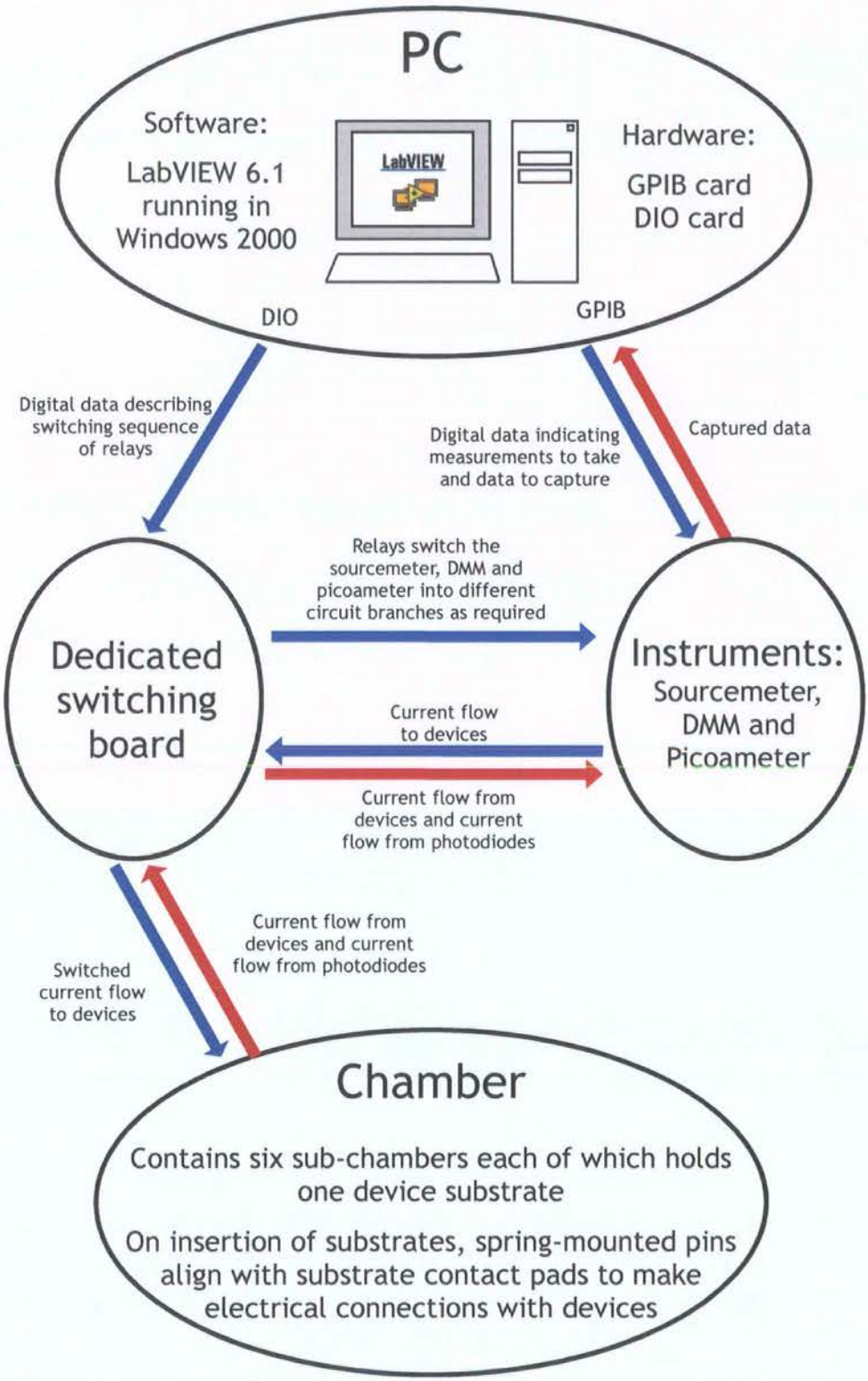

Figure 4.1 Schematic of characterisation equipment

The automated characterisation equipment consisted of a measurement chamber, switching hardware, instruments, a rotary pump and a PC with software to provide control and a user

interface. The equipment was located in a cleanroom with the temperature maintained at 20 °C ± 2 °C, which minimised temperature-induced behaviour variation. The relationship between the constituent parts is illustrated schematically in Figure 4.1. A photograph of the equipment (excluding the rotary pump) is shown in Figure 4.2.

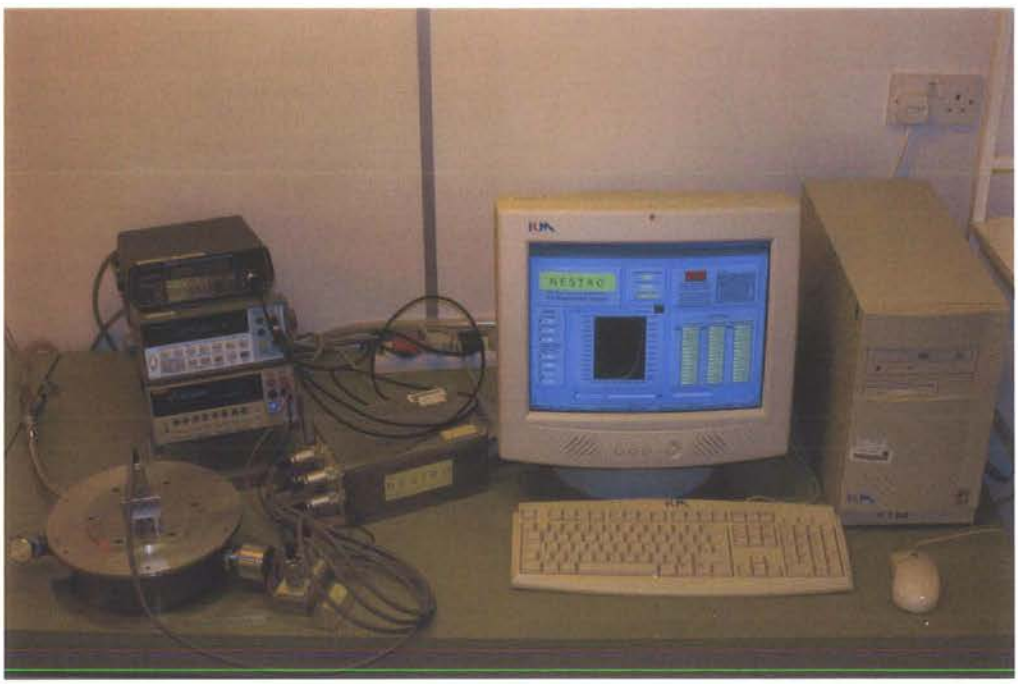

Figure 4.2 Photograph of characterisation equipment

4.2 Chamber

The chamber provided a controlled environment for substrates during testing. A photograph and an annotated diagram of the chamber are given in Figure 4.3 and Figure 4.4, respectively. The chamber capacity was six substrates, with each substrate being placed in one of the six identical device-holders or sub-chambers. A photograph of a sub-chamber is shown in Figure 4.5, while Figure 4.6 shows an annotated diagram. Each sub-chamber included a recess to cradle the substrate in the appropriate position so that spring mounted pins in the sub-chamber made contact with the relevant pads on the substrate. Two tubes with valves were fastened into one side of the main chamber to allow control of the atmosphere within. One was connected to a rotary pump, which was used to provide a vacuum of 0.1 mbar in the chamber, and the other was to allow gases into the chamber. On the opposite side of the chamber was a 30-pin feed-through to provide electrical connections to the devices without compromising the atmosphere inside the chamber.

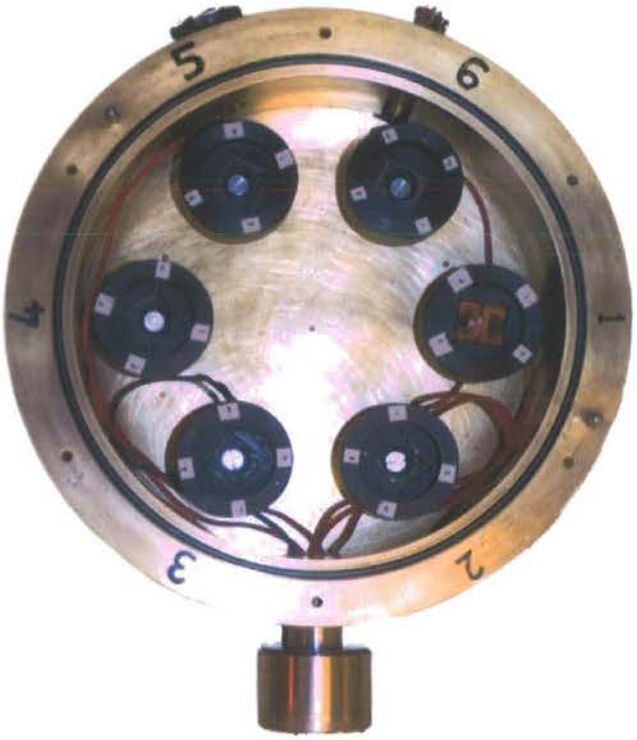

Figure 4.3 Photograph of chamber (without the lid)

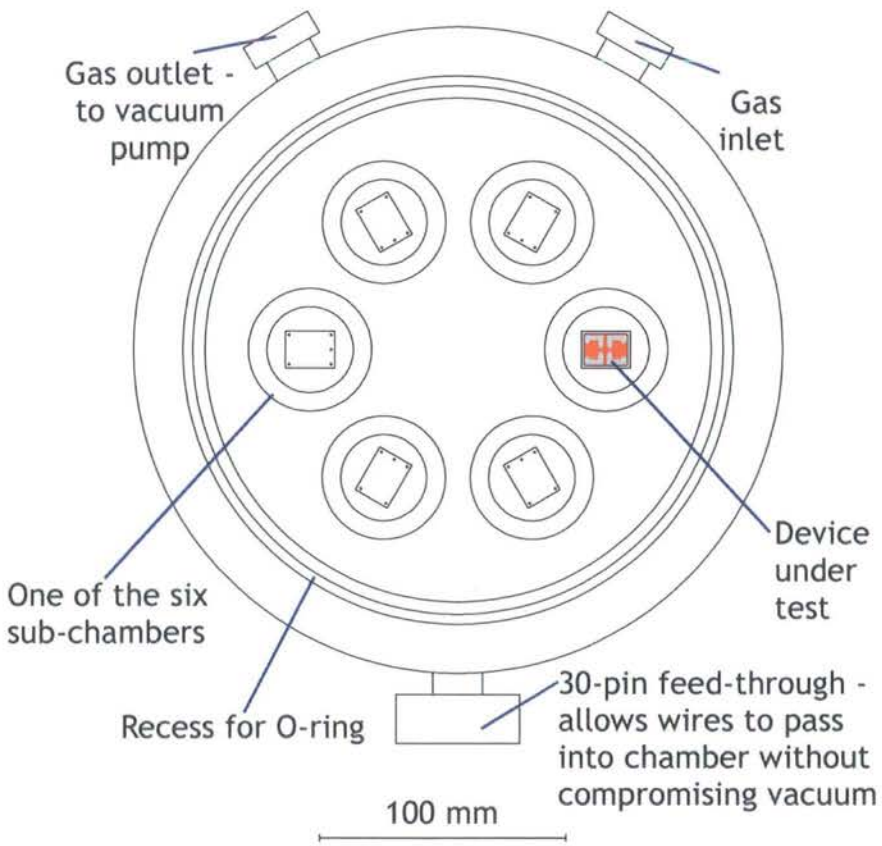

Figure 4.4 Chamber (without the lid)

Figure 4.5 Photograph of sub-chamber

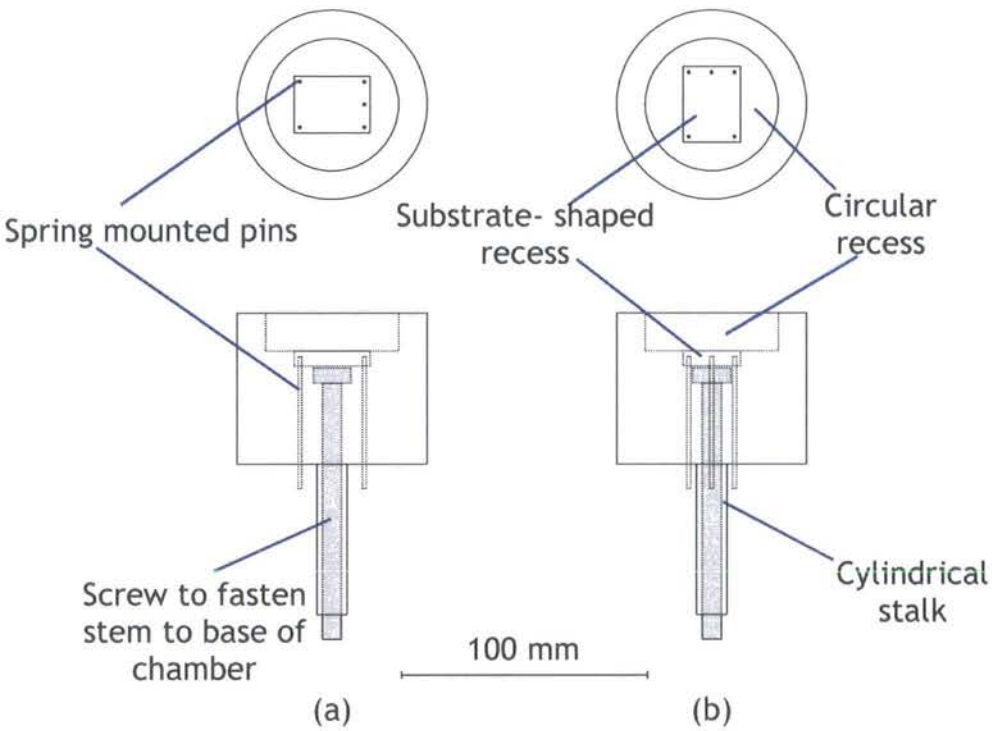

Figure 4.6 Sub-chamber: (b) is rotated through 90° with respect to (a)

Six identical wide-area photodiodes (15 mm in diameter) were mounted on stems on the underside of the chamber lid. A photograph and diagram of the lid are shown in Figure 4.7 and Figure 4.8. Each photodiode corresponded with one of the six sub-chambers. By positioning the lid in the correct alignment, the photodiodes applied pressure to the device substrates to ensure contact between the device contact pads and the spring-mounted pins inside the sub-chamber. The six photodiodes each generated photocurrents proportional to the light emission from up to six devices simultaneously. An O-ring provided the vacuum seal between the chamber and lid. When closed, it was not possible for ambient light to pass into the chamber. Seals on each sub-chamber ensured that the light produced within would not escape. A total of 12 wires, two wires for each photodiode, passed out through a 12-pin vacuum feed-through mounted in the lid.

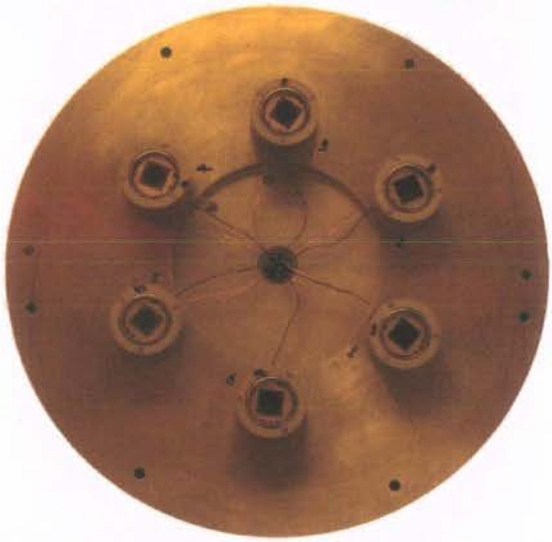

Figure 4.7 Photograph of the internal face of the chamber lid

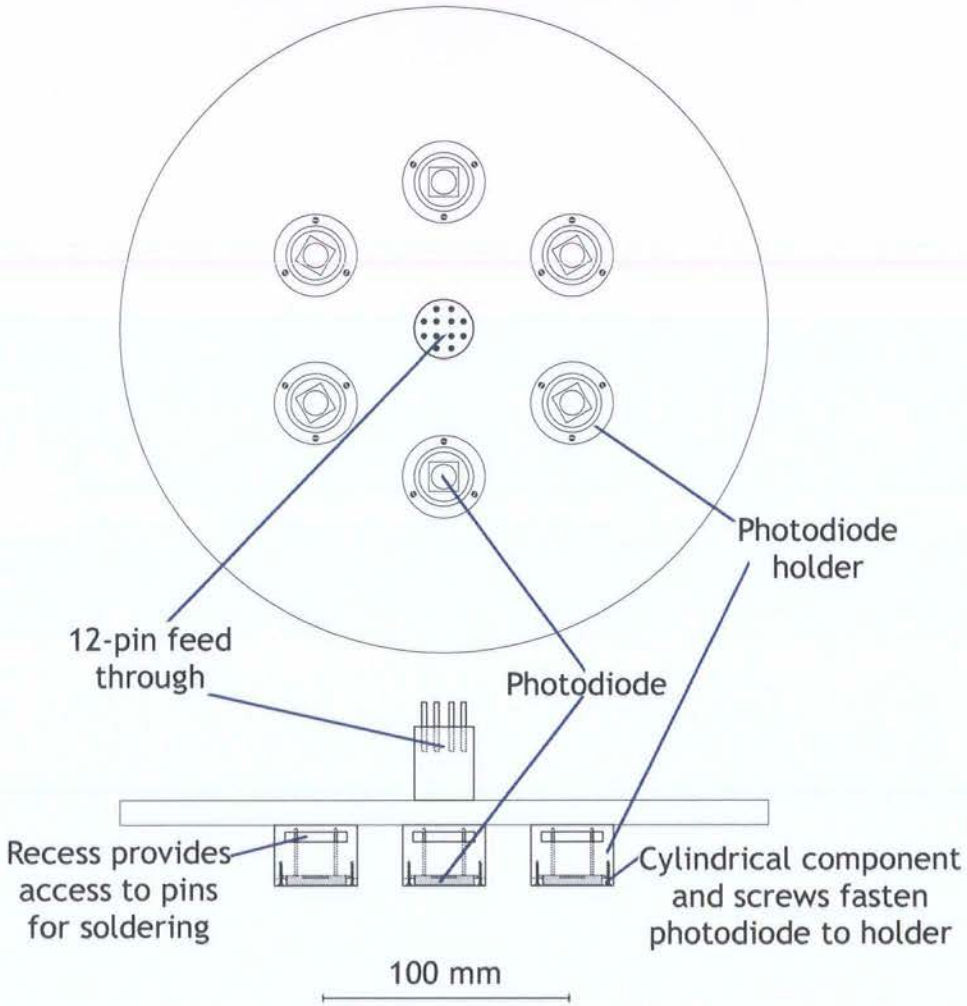

Figure 4.8 Chamber lid (above: internal face; below: side profile with the internal face downwards)

4.3 Switching circuitry

Characterisation routines were either sequential or simultaneous. In the case of the former, each device was switched into the characterisation circuit sequentially. For simultaneous routines, several devices operated concurrently but the instruments were continuously switched into and out of each circuit branch in sequence. Two switching circuits were designed to achieve this.

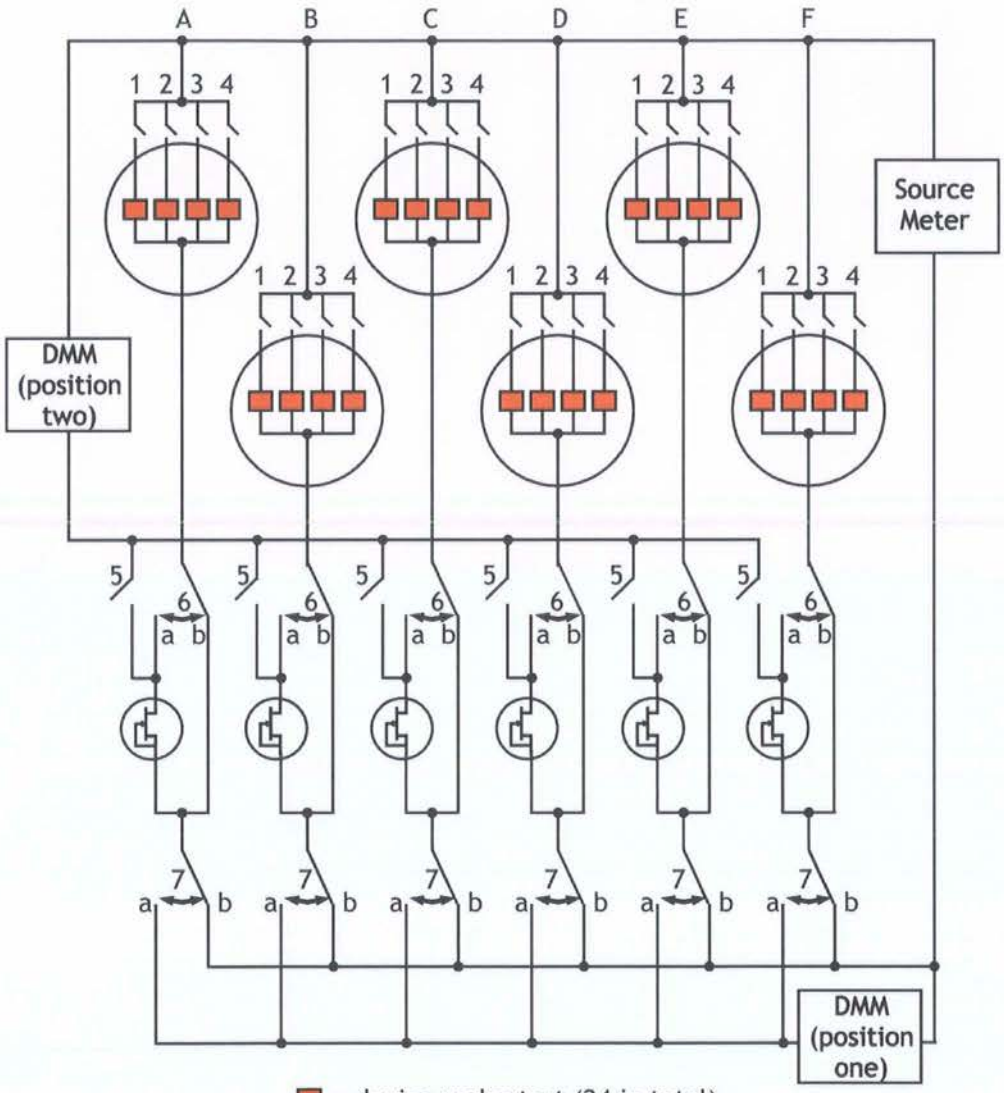

Figure 4.9 Chamber switching circuit

Relays:	Rows 1 - 4	Row 5	Row 6	Row 7
Consecutive routines	Each of the 24 relays in rows 1 to 4, columns A to F, are closed and opened consecutively one at a time.	All row 5 relays open.	All row 6 relays at position b.	All row 7 relays at position b.
Simultaneous routines (constant voltage)	At any time, one of relays 1 to 4 in each of the six columns is closed. (Six relays are closed in total.)	All row 5 relays open.	All row 6 relays at position b.	At any time, one relay in row 7 is at position a. All others are at position b.
Simultaneous routines (constant current)	At any time, one of relays 1 to 4 in each of the six columns is closed. (Six relays are closed in total.)	At any time, one relay in row 5 is closed. All others are open.	All row 6 relays at position a.	All row 7 relays at position b.

Table 4.1 Relay sequence

Figure 4.9 shows the main circuit used for switching devices and two of the instruments. The rules which govern the relay behaviour for the three different types of routine are given in Table 4.1. A second circuit associated only with the chamber lid hardware is shown in Figure 4.10.

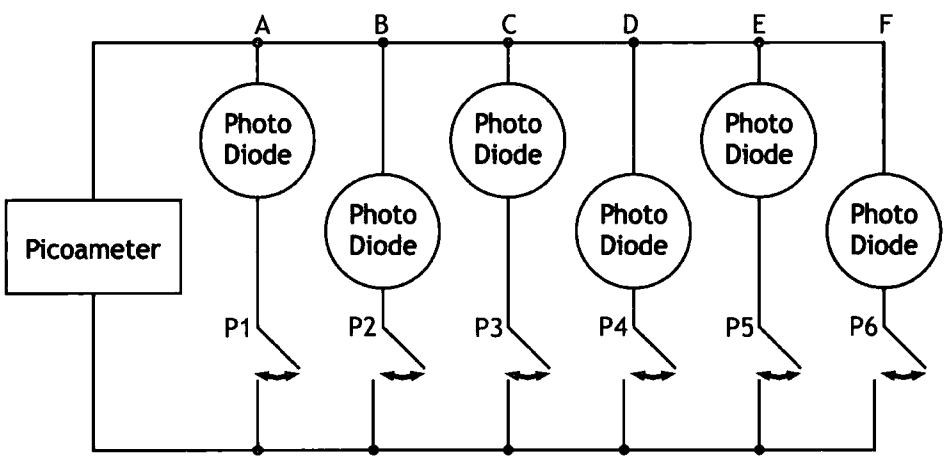

The six photodiodes are mounted on the inside of the chamber lid
Each photodiode is positioned in line with the corresponding sub-chamber
Only one relay from row P (P1-P6) is closed at any time

Figure 4.10 Lid switching circuitry

4.4 Instruments

The characterisation equipment required three instruments. A Keithley 2400 Sourcemeter was used either as a voltage source and to measure the current flow in the whole circuit, or

to provide a current source and to measure the voltage across the whole circuit. For simultaneous routines (where several devices were powered simultaneously) a meter had to be switched into each circuit branch in turn to measure the currents or voltages relating to individual devices. An Agilent 34401A DMM was selected for this purpose. A Keithley 385 Picoameter was used to measure the currents generated by each individual photodiode. This current is subsequently referred to as photo current.

4.5 Data interface

Interfaces were required to transfer data between the software (section 4.6) which ran on a PC, the switching circuitry (section 4.3) and the instruments (section 4.4).

4.5.1 PC to instruments interface

The interface between the PC and the instruments was provided by a general purpose interface bus (GPIB). The instruments and the PC all had GPIB cards installed. These were linked to the single bus by daisy-chaining cables from one card to the next.

4.5.2 PC to switching circuitry interface

A digital input /output (DIO) card was installed in the PC for the purpose of triggering the switching circuitry relays. The 48 lines were connected to the coil of each of 48 relays. A relay was closed by applying a 'voltage low' and opened by applying a 'voltage high' to the relevant line.

4.6 Software

4.6.1 Requirements

Software was designed and written to perform characterisation functions on the devices under test. To achieve this objective the software:

- provided a graphical user-interface (GUI) from which to control the equipment;
- generated and sent control information to the switching circuitry (via DIO lines);
- requested the sourcemeter to provide the necessary source conditions (via GPIB);
- requested data from the instruments (via GPIB); and

- saved the data in a format ready for analysis and plotted the collected data on the screen in real time.

4.6.2 Characterisation functions

Three measurement characterisation functions were written in LabVIEW:

- a current-voltage (I-V) function to ramp the voltage between user-defined limits and measure the corresponding sample currents and photo currents;

- a stability function which held the sample at a constant voltage over an extended period and measured the sample current and photo current at user-defined intervals; and

- a stability function which held the sample at a constant current over an extended period and measured the voltage across the sample and the photo current at user-defined intervals.

As it took less than five minutes to measure the I-V characteristics of each device, the I-V function performed the same routine, consecutively, on each of the 24 devices. Figure 4.11 shows the basic flow for a consecutive routine. By contrast, the stability functions were simultaneous routines because the characterisation of each device was carried out over extended periods, up to a few weeks. Figure 4.12 shows the basic flow for a simultaneous routine.

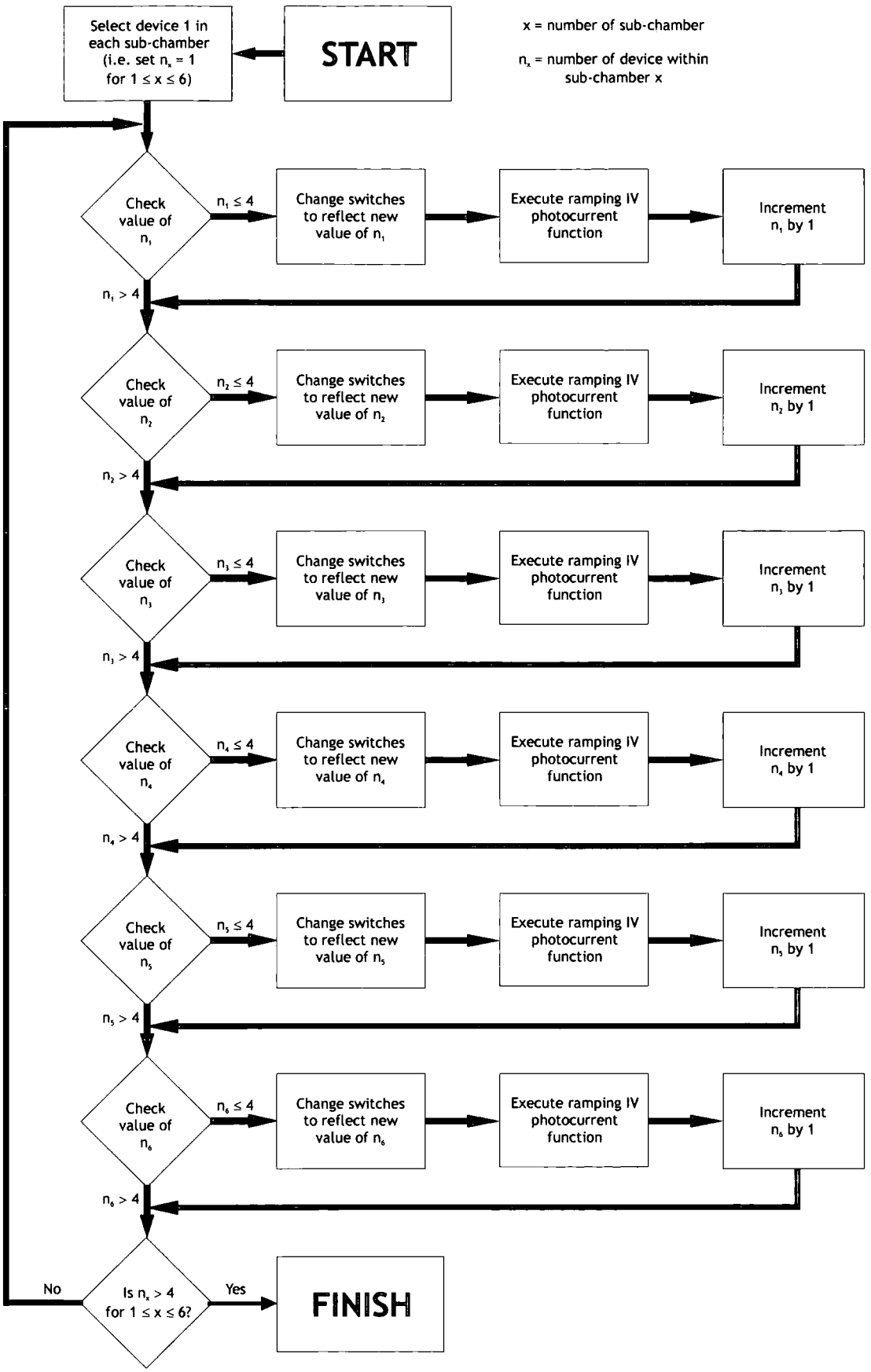

Figure 4.11 Flow chart for consecutive routine

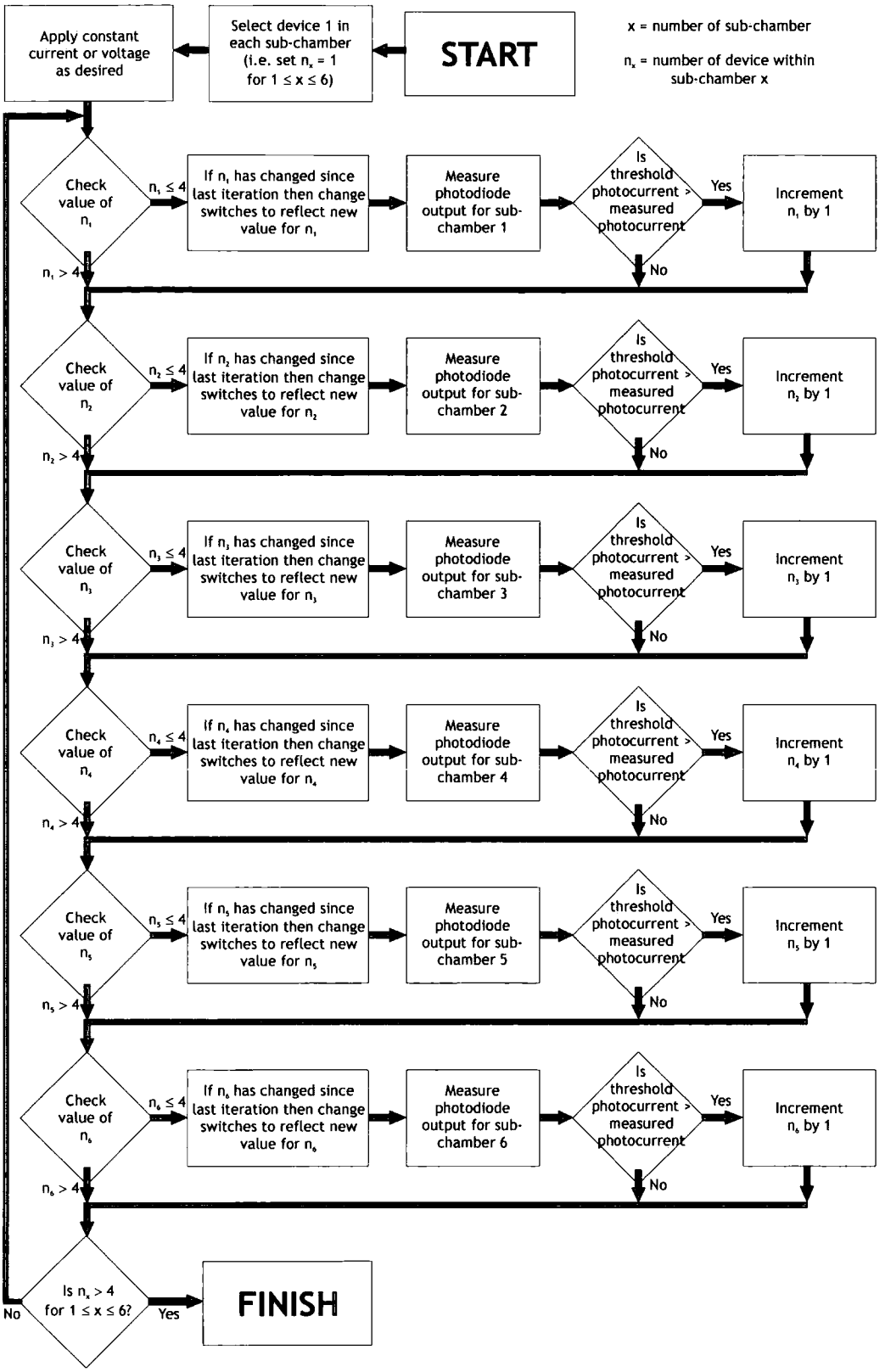

Figure 4.12 Flow chart for simultaneous routine

4.6.3 Data manipulation

The data collected by the I-V characterisation function were used to estimate the quantum efficiency of each device under test. The quantum efficiency is the ratio of the number of photons produced to the number of electrons injected. Values for these were estimated using the data (sample current and photocurrent) from the I-V characterisation.

The method of calculation was as follows:

$$QE = \frac{\text{number of photons emitted per second}}{\text{number of electrons injected per second}} = \frac{n_p}{n_e} \tag{4.1}$$

The number of electrons injected per second, n_e, was estimated by dividing the value for the current through the device (I_s) by the charge on each electron, $e = 1.602 \times 10^{-19}$ C.

$$n_e = \frac{\text{sample current}}{\text{charge on an electron}} = \frac{I_s}{e} \tag{4.2}$$

An estimate for the number of photons emitted per second, n_p, was given by:

$$n_p = \frac{\text{radiant power}}{\text{energy of a photon}} \tag{4.3}$$

where

$$\text{radiant power} = \frac{\text{photodiode current}}{\text{photodiode responsivity}} = \frac{I_P}{R} \tag{4.4}$$

(photodiode responsivity is measured in Ampere per Watt); and

$$\text{energy of a photon} = \frac{hc}{\lambda} \tag{4.5}$$

Substituting 4.4 and 4.5 into 4.3 gives:

$$n_p = \frac{I_P \lambda}{Rhc} \tag{4.6}$$

and so, substituting 4.6 and 4.2 into 4.1 gives the estimate for quantum efficiency:

$$QE = \frac{I_P \lambda e}{I_S R h c} \tag{4.7}$$

4.6.4 Graphical user interface

The graphical user-interface (GUI) for each of the three measurement functions was constructed from a common framework. Screen grabs from the GUI for an I-V characterisation and a stability characterisation are shown in Figure 4.13 and Figure 4.14, respectively.

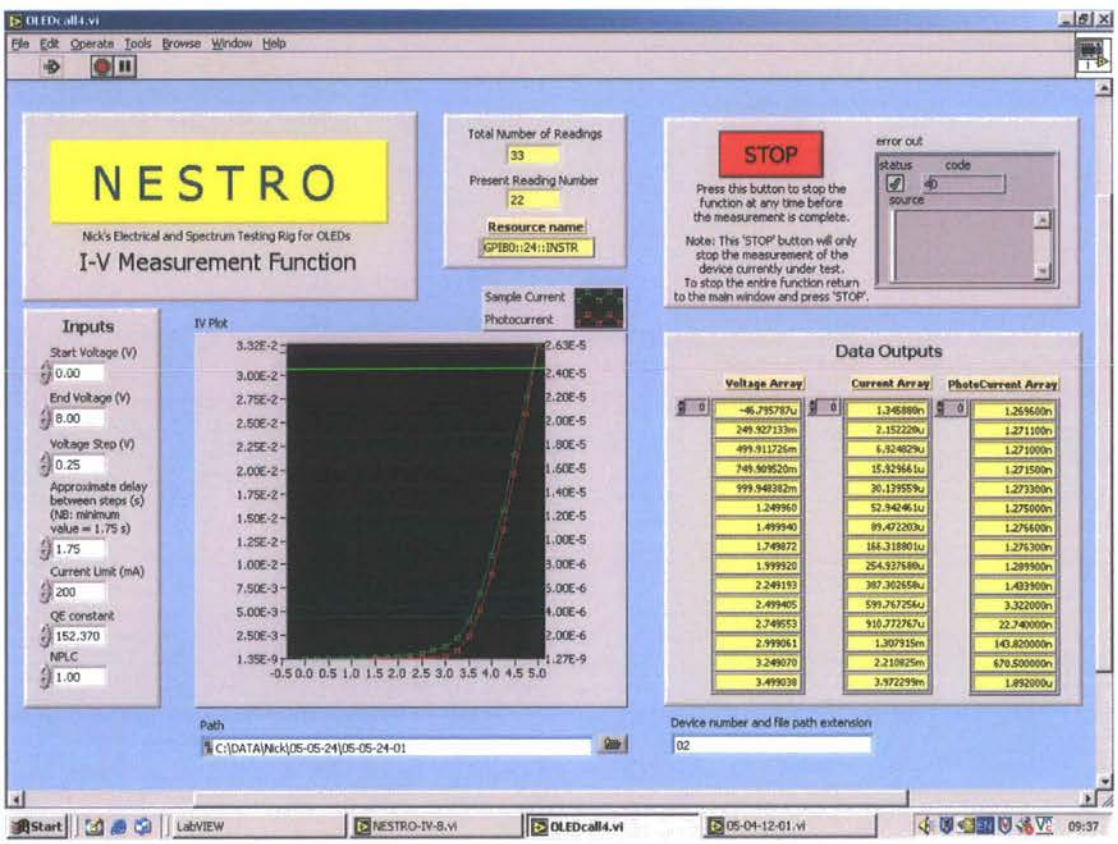

Figure 4.13 Screen grab of GUI for I-V function

For each function, all available information was displayed on a single screen without the need for additional menus or scrolling. User inputs were collected in a column at the left and the remainder of the screen displayed the collected data in real time, graphically and numerically.

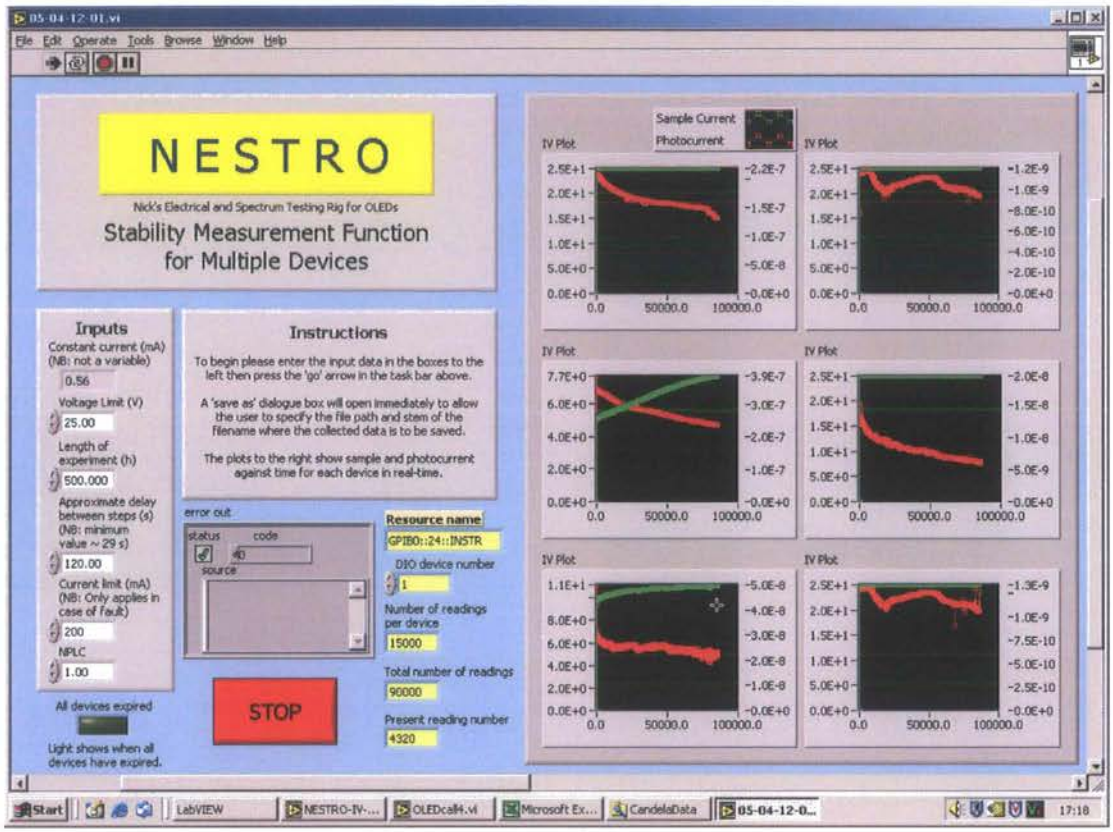

Figure 4.14 Screen grab of GUI for (simultaneous) stability function

4.7 Equipment calibration

After fabrication of the equipment, it was necessary to confirm the calibration for measurement integrity. This was performed using commercially available zinc oxide doped gallium phosphide red LEDs (Figure 4.15) manufactured by Multicomp with known and consistent outputs. Repeated testing of these devices using the equipment yielded consistent, accurate results with minimal noise (Figure 4.16). The measured behaviour was within the specification described in the Multicomp data sheet.

Figure 4.15 Photograph of Multicomp LED

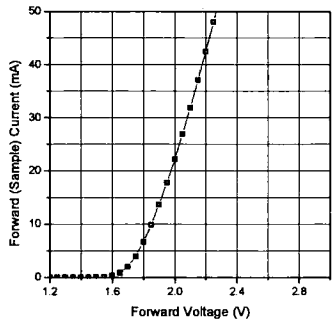

Figure 4.16 I-V characteristics as measured using equipment

It was also necessary to eliminate inconsistencies between the six sub-chambers. Measurements were taken to investigate whether the six photodiodes were consistent with one another and with results obtained from another photodiode independent of the switching circuitry. The currents generated by a photodiode independent of switching circuitry were highly consistent (± 0.005 nA over one hour), and the average generated current in darkness was 0.04 nA. Where the switching circuitry was in use, the currents were less consistent (± 0.01 nA over one hour) and the average generated current in darkness was 0.12 nA. This indicated that small currents (~ 0.08 nA) were generated within the switching circuitry, and that the switching circuitry was slightly more susceptible to external noise. The threshold at which light emission became visible by eye was in the region of 5 nA. By comparison, the magnitude of the noise was insignificant.

4.8 Typical data

Typical I-V data from the automated measurement equipment are shown in Figure 4.17. As discussed previously, the capacity of the equipment was six substrates each containing four devices. In this case, the figure shows data for devices where each of the six substrates was produced to a different specification. For this reason, each substrate is represented by a different colour, which means that the four devices of the same specification are plotted in the same colour.

As there was often considerable variation in the photocurrents produced between the most and least emissive devices, the photocurrents were often plotted against a log scale.

In obtaining multiple data from the characterisation equipment and plotting them all on one curve it was possible to identify anomalous devices, such as those with short circuits

which exhibited Ohmic characteristics. Data from anomalous devices were not analysed further.

Figure 4.18 shows a plot of the typical stability data obtained by the automated measurement equipment, in constant current mode. When characterising stability, the maximum number of devices was six: one from each substrate.

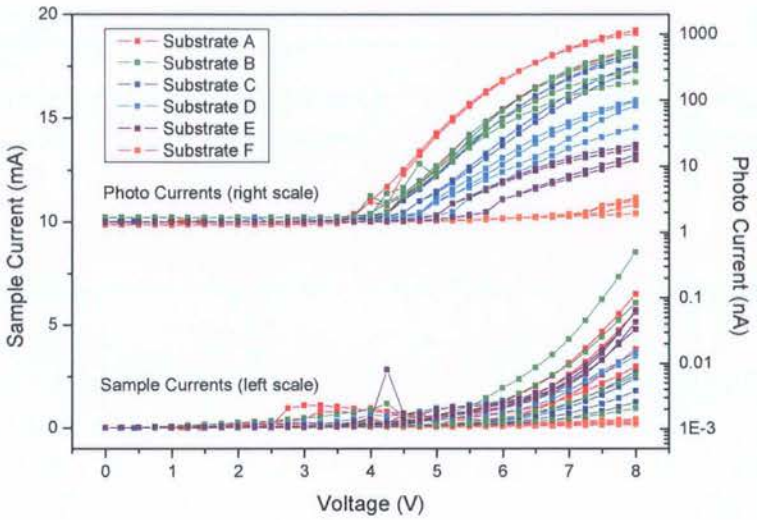

Figure 4.17 Typical I-V data produced when characterising six arbitrary substrates (A-F) using the automated measurement equipment

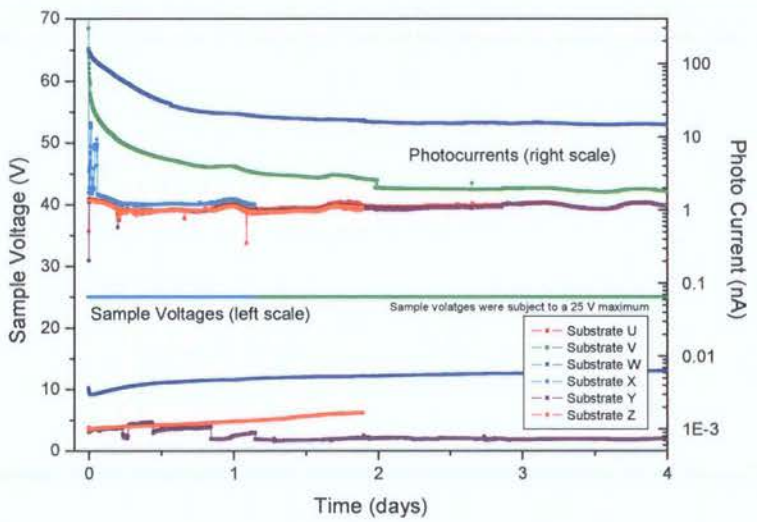

Figure 4.18 Typical stability data produced when characterising six arbitrary substrates (U-Z) using the automated measurement equipment

4.9 Conclusions

The justification for automated characterisation equipment has been presented in light of the time taken to characterise devices manually. An outline of the design and operation of the equipment has been provided and the components have been described and illustrated.

The means of communication between each constituent part has been specified. A broad outline of the software including a skeleton of the two modes of characterisation routine and a description of the GUI has been provided. Evidence has been presented to confirm the validity of data generated by the equipment. Finally, some sample data obtained using the characterisation equipment have been shown and explained.

Chapter Five

Anode materials and the PEDOT layer

5.1 Introduction

Indium tin oxide (ITO) is the most widely used OLED anode material. The sputtering process by which it is commonly deposited produces a rough film with many spikes. The number and size of these have been seen to influence the stability of the resulting devices [1-3]. ITO is also known to be a source of oxygen [4], the presence of which causes oxidation of polymer materials. As a consequence, the polymers lose conjugation, reducing charge carrier mobility [5-7].

The ITO used in the following investigation was purchased from Merck, ready sputtered on glass sheets. It was shown to have an approximate sheet resistance of 7.8 $\Omega\,\square^{-1}$ and an RMS roughness value equivalent to 11 % of the total film thickness. Figure 5.1 shows an AFM image of a region of glass substrate across an ITO-glass step. Patterned photoresist protected the ITO region on the back left portion of the substrate while the front right portion of the ITO was etched off the substrate. The surface of the ITO was highly non-planar with spikes covering the entire surface area. The glass surface was also non-planar but to a lesser extent. The spikes were smaller and fewer in number.

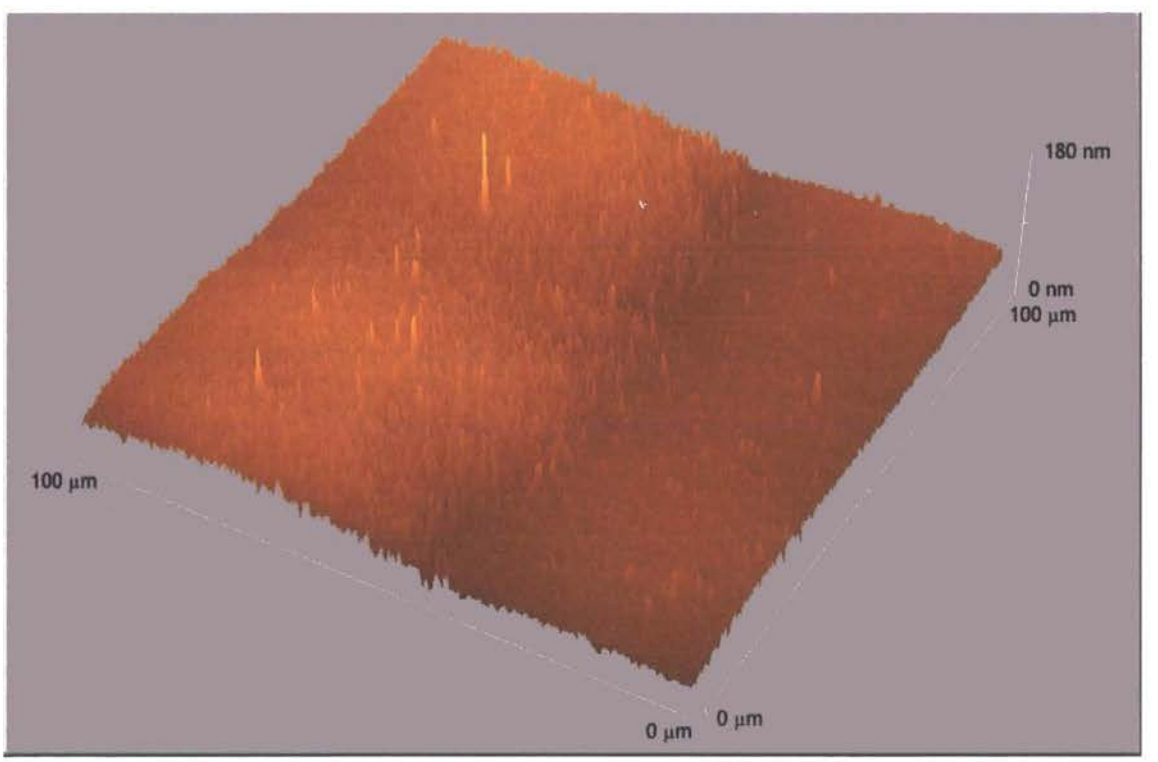

Figure 5.1 AFM image of ITO step on glass substrate

This chapter records an investigation into the influence of the material and surface profile of the anode on the behaviour of OLEDs. Spiked regions were present in the freshly

prepared ITO and they were seen to have grown and developed following device operation. Experiments were carried out to investigate the influence on device stability of spiked regions on the anode. The application of a layer of PEDOT:PSS to compensate for the roughness between the anode and the polymer is examined in Section 5.2. Section 5.3 describes an investigation of aluminium-doped zinc oxide (AZO) as an alternative anode material to ITO.

5.2 The PEDOT:PSS layer

Poly(3,4-ethylenedioxythiophene) poly(styrenesulfonate) (PEDOT:PSS) has commonly been used in OLEDs to form a 'smoothing' and hole-injection layer between the anode and the electroluminescent polymer film [4, 8]. The chemical structures of the polymers PEDOT and PSS are shown in Figure 5.2 and Figure 5.3, respectively [9].

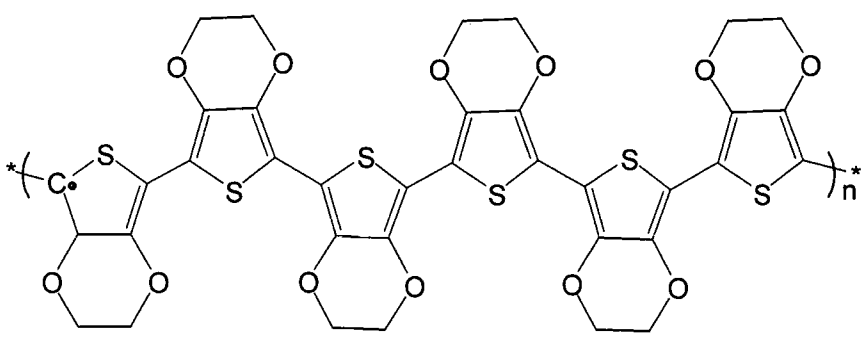

Figure 5.2 Chemical structure of PEDOT

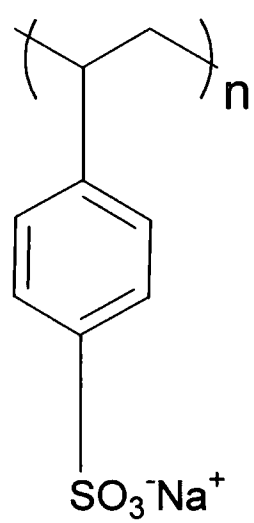

Figure 5.3 Chemical structure of PSS

An aqueous dispersion at a ratio by weight of 2 parts PEDOT to 5 parts PSS was supplied by H.C. Starck under the trade name Baytron P. The highest occupied molecular orbital

(HOMO) and lowest unoccupied molecular orbital (LUMO) values of PEDOT:PSS are -5.0 eV and -3.2 eV, respectively.

An investigation was first undertaken of the influence of a spin coated layer of PEDOT:PSS (hereafter referred to as PEDOT) on the electrical, morphological and stability characteristics of devices before and after operation.

5.2.1 Device fabrication

Devices were fabricated using the techniques described in Chapter 3. For half of the devices, a layer of PEDOT was deposited between the ITO and the polymer blend layer. 200 µl of PEDOT solution diluted with 50 % pure water was applied to the substrate and spun at 1500 rpm for 60 s. The devices were placed in a vacuum at 10^{-1} mbar for 1 h to remove residual water vapour before spin-coating the blended polymer layer. The polymer blend used was 80 % MEH-PPV and 20 % PDPyDP. (These materials and their blending are discussed in detail in Chapter 6.) The proportion of each (solid) material was measured by weight; solutions were then produced by dissolving the blended solids in chloroform. The solutions were spin-coated to form the electroluminescent film on top of the PEDOT layer where applicable. Device cathodes were deposited by evaporating a 100 nm layer of aluminium.

5.2.2 Polymer film deposition and quality

The behaviour of the blended polymer solution when dispensed onto the substrate was affected by the surface treatment. It was not possible to measure the contact angle of the chloroform-based solution on any substrate because the chloroform evaporated too rapidly. Water was observed to have a similar contact angle to chloroform on the two different surfaces. Optical micrographs of the same volume of water on ITO and PEDOT, in Figure 5.4 and Figure 5.5, respectively, showed contact angles of 60 ° for the hydrophobic ITO surface and 3 ° for the hydrophilic PEDOT film. This had implications on the quality and adhesion of the spun films [10].

In general, a film formed of polar molecules will result in a hydrophilic surface while a hydrophobic surface will be created from non-polar molecules. The materials used in this project had differing polarities. For example, the ionic salt PEDOT is highly polar; water and chloroform are less polar and MEH-PPV and ITO are only slightly polar.

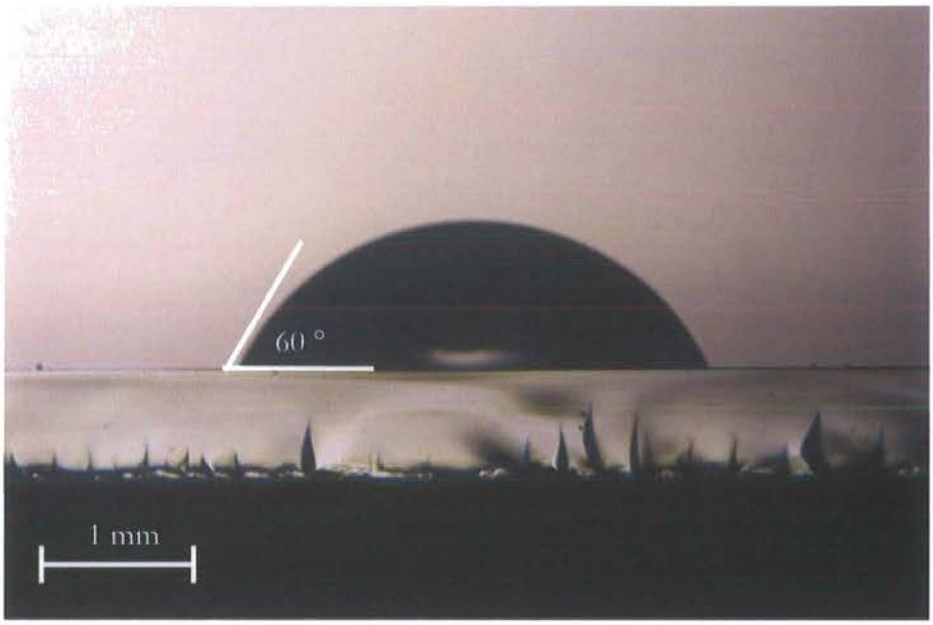

Figure 5.4 Micrograph of a drop of water on an ITO-coated glass substrate

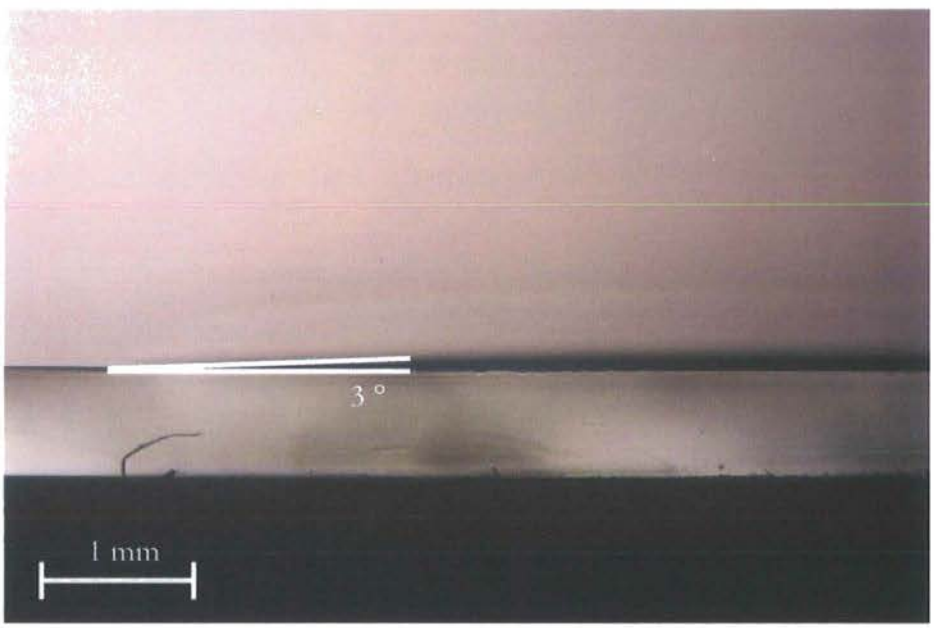

Figure 5.5 Micrograph of a drop of water on a glass substrate coated with ITO and PEDOT

When fabricating a device without a PEDOT layer, the blended MEH-PPV chloroform-based solution was spun directly onto the ITO. The large wetting angle indicated poor contact between the solution and the substrate. Also, as the chloroform began to evaporate immediately, even before spinning, there was little opportunity for the polar nature of the chloroform to influence the surface adhesion. When the substrate was spun, the film formed without making good contact with the surface contours of the ITO. The

result was a film which exhibited poor adhesion to the substrate and possessed a high concentration of pin holes.

To fabricate a device with the PEDOT layer, the PEDOT water dispersion was applied to the ITO substrate. The highly polar nature of the PEDOT combined with the fact that the water did not evaporate before spinning, meant that the dispersion spread more effectively over the substrate. This resulted in fewer pin holes forming during spin coating. Once the PEDOT film was dry, it provided the surface onto which the chloroform-based MEH-PPV solution was applied. As PEDOT and chloroform were both polar, the chloroform solution was attracted to the surface and spread quickly. Even though the chloroform began to evaporate rapidly, the solution was already in more intimate contact with the PEDOT film below. The result was a film with few pin holes and which adhered well to the PEDOT over the full area. These attributes increased the area for current flow between the films and reduced the likelihood of subsequent delamination.

The difference in adhesion was also observed during attempts to remove the films. When placed in a solvent in an ultrasonic bath, the films coated directly on ITO became detached before redissolving, but the films on PEDOT-coated substrates were firmly attached and were only removed by redissolving gradually in the solvent.

5.2.3 Device characteristics

Electrical characteristics

The use of a PEDOT layer made a considerable improvement to the current and light emission characteristics. The current-voltage (I-V) and light-voltage data are shown in Figure 5.6.

The current generated in a photodiode (photo-current) gave an indication of the light output from each device and is plotted in units of nA. In order to produce similar currents and light outputs to those seen in the PEDOT devices at 8 V, the non-PEDOT devices were tested to 14 V.

These data also provide a good example of the extent of the variation that was often observed within batches of identically produced devices. There are a large number of possible reasons for the variation, which include: differences in device area due to poor electrode patterning; inconsistent polymer film thicknesses due to differences in the solution compositions or the spinning properties; small variations in the thickness of metal

cathodes; and non-conductive and non-emissive regions within the device due to delamination and short circuit defects. As discussed in Chapter 4, this level of variation was one of the justifications for producing a measurement rig capable of measuring batches of devices.

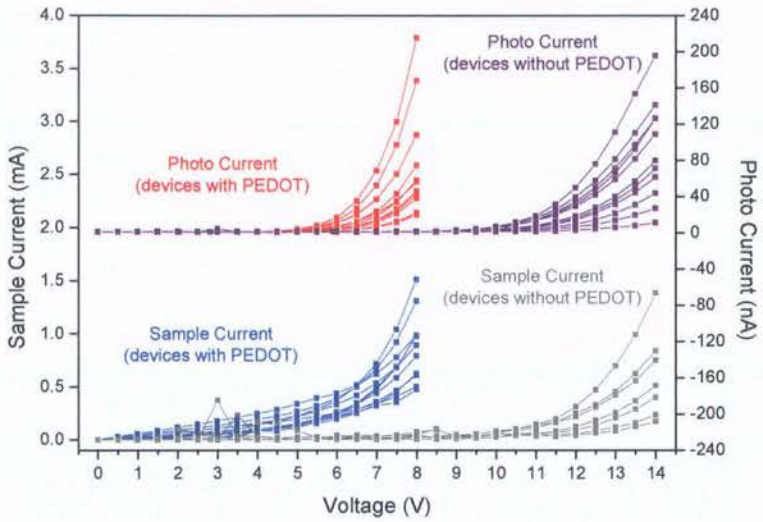

Figure 5.6 I-V and light-voltage characteristics for MEH-PPV : PDPyDP (80 : 20) aluminium-cathode devices with and without PEDOT

Several theories have been suggested to account for the current-voltage behaviour of OLEDs. The dependence of the injection-limited current is said to be similar to, but not the same as, Fowler-Nordheim tunnelling, where charge tunnels through a triangular energy barrier [11]. There is also a similarity with the Schottky-Richardson mechanism of thermally-stimulated emission, and many data reveal space-charge-limited injection characteristics [12]. There is, however, no single theory which models all the current behaviour in OLEDs, and this thesis does not attempt to give detailed explanation of the charge flow mechanisms.

The most obvious benefit of the devices with PEDOT was the much reduced turn-on voltage. The turn-on voltage (for light output) of the devices with PEDOT (~ 5 V) was approximately half that of those without (~ 10 V). This was attributed to the increased area for current flow made possible by the improved adhesion. Van Dijken *et al.* suggest that the PEDOT layer behaves also as a hole injection layer, so increasing the number of available holes in the electroluminescent layer [13]. Consideration of the energy levels (diagram shown in Figure 5.7) would seem to suggest, however, that any influence of the PEDOT on hole injection was minimal because the HOMO levels for PEDOT and

MEH-PPV were the same. Though, obviously, this depends on the accuracy of the quoted HOMO levels. Further discussion of this issue is given at section 6.2.

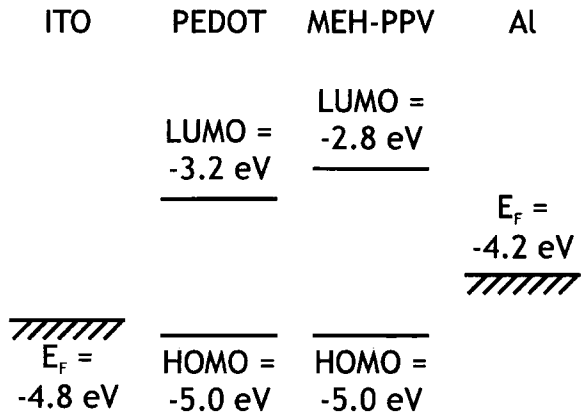

Figure 5.7 Energy diagram showing the HOMO and LUMO levels of the organic materials and the Fermi levels of ITO and aluminium

Recent research has indicated that energy level alignment may be different at the interface between an organic emissive material and a polymer (i.e. the MEH-PPV / PEDOT interface) and the interface between the same emissive material and a metal (i.e. MEH-PPV / ITO). Koch *et al.* observed that, on contact of metal to organic emissive material, molecular adsorption at the surface resulted in the HOMO level of the organic material being lowered [14]. This would provide an increase in the 0.2 eV nominal hole injection barrier between ITO and MEH-PPV, but no increase in the injection barrier for devices which included PEDOT as an intermediate layer.

This is an attractive explanation of the increased hole injection for PEDOT devices, given that the nominal (*ex situ*) HOMO level appeared to be the same as that for MEH-PPV.

Figure 5.6 also indicates differences in terms of the turn-on voltages for light output compared with the turn-on voltages for current flow. For non-PEDOT devices, the average turn-on voltage for current flow was the same as that for light output (10 V). By contrast, for the PEDOT devices there was an offset of approximately 3 V between the turn-on voltage for current flow (~ 2 V) and the turn-on voltage for light output (~ 5 V). Therefore, between 2 V and 5 V, power was consumed but no light was emitted. This is probably because the PEDOT provides additional paths for leakage current outside the device area, perhaps, though not necessarily, via pin holes in the emissive layer. The two possible current paths are illustrated in Figure 5.8. Such leakage paths are not present in

devices without PEDOT as the emissive material outside the device region lies directly on the insulating glass substrate.

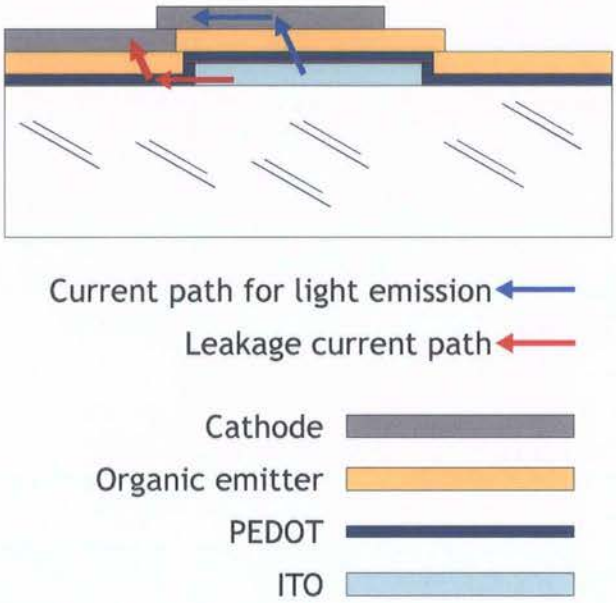

Figure 5.8 Schematic diagram showing current path for light emission and leakage current path in a device with a PEDOT layer

The reason for the offset between the two turn-on voltages may be explained by further findings of van Dijken *et al.* [13]. This group suggests that the vinylene bond in MEH-PPV can react with protons in the PEDOT to produce bonds capable of trapping charge carriers. Until all the potential trap sites are occupied, hole transport is reduced and so light emission is lower.

Quantum efficiency characteristics

Quantum efficiency (QE) data are shown in Figure 5.9. At low currents the QE values for non-PEDOT devices were greater than for PEDOT devices. This may be explained by the leakage currents which appeared only in PEDOT devices (*vide supra*), where voltages between 2 V and 5 V resulted in current but no light emission (Figure 5.6). Therefore, when the devices were operated within this voltage range, the efficiency was low compared to the non-PEDOT devices. At higher currents, equivalent to voltages above 5 V and where light emission was observed, the QE values matched those of the devices without PEDOT.

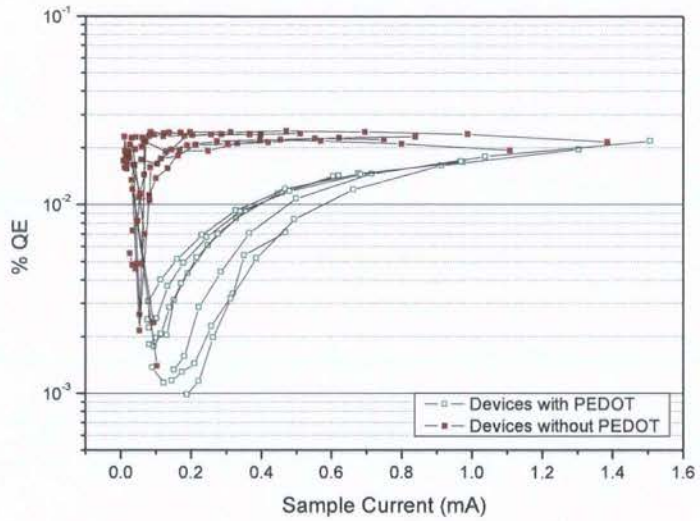

Figure 5.9 QE characteristics for MEH-PPV : PDPyDP (80 : 20) aluminium-cathode devices with and without PEDOT

5.2.4 Stability characteristics

Figure 5.10 shows the results of a stability study.

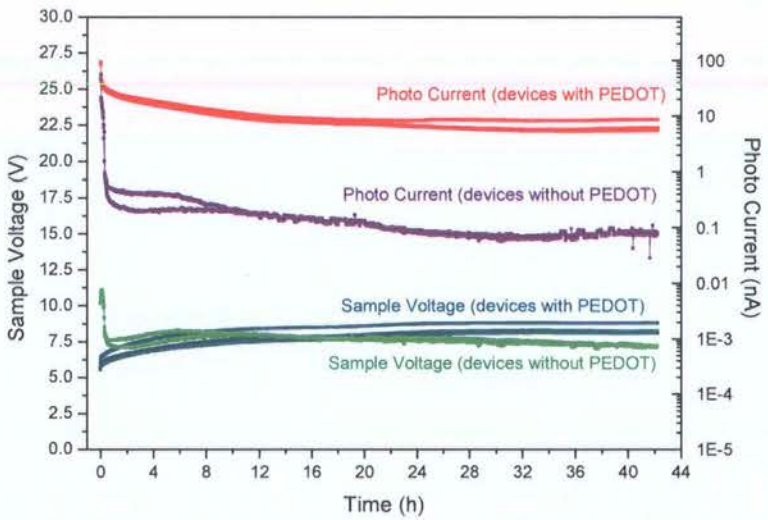

Figure 5.10 Stability characteristics for MEH-PPV : PDPyDP (80 : 20) aluminium-cathode devices with and without PEDOT

A constant current of 0.56 mA passed through each device for an extended period and the device characteristics were continuously monitored. The upper four curves are plots of photo-current and the lower four curves represent the voltages across each sample resulting from the constant current. While the voltages for devices both with and without PEDOT remained fairly similar throughout the period, the photo-currents for those devices without PEDOT dropped dramatically over the first few minutes of the test.

Given that the threshold for visibility was approximately 5 nA, the devices without PEDOT ceased to emit visible light almost immediately. The photo-current measured from the light output of the devices with PEDOT decayed more gradually and even after the 42 hour period the light output remained visible.

5.2.5 Effect of operation on anode

After investigating the operational stability of devices, the quality of the ITO and PEDOT layers was examined by atomic force microscopy (AFM) and scanning electron microscopy (SEM) including energy dispersive spectroscopy (EDAX).

To access the ITO or PEDOT layers, the upper layers were removed. After operation, the devices were placed in a beaker of chloroform in an ultrasonic bath to dissolve the electroluminescent layer. This also caused the metal cathode to separate from the device. Following this process, only the ITO layer and PEDOT layer (where applicable) remained on the glass substrate.

In a typical PEDOT device, the step where the ITO region ended was not obvious, as indicated by the AFM scan in Figure 5.11. This was because the PEDOT layer had the effect of smoothing the ITO step to produce a gentle gradient rather than a sharp profile. The figure shows one large defect in the substrate in the form of a single tall spike of material. This was surrounded by a crater, with a depth of 150 nm, which was equivalent to the full thickness of the PEDOT and ITO combined.

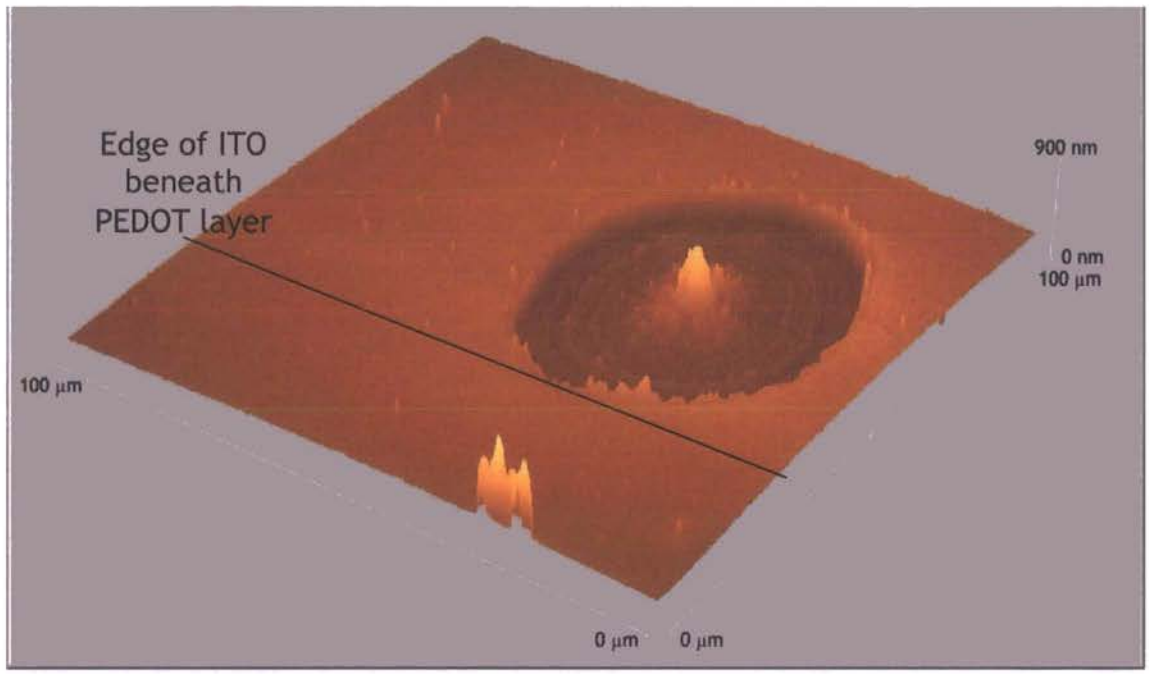

Figure 5.11 AFM image of an operated device with PEDOT (with upper layers removed) showing the sloped region between ITO and glass

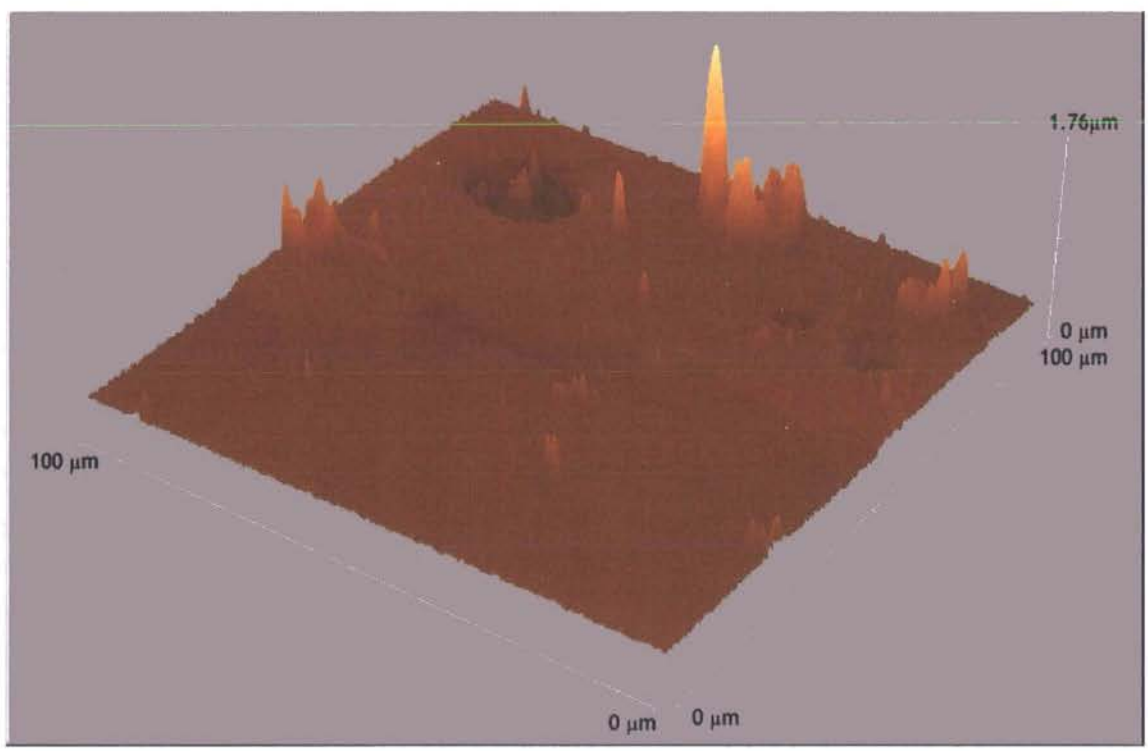

Figure 5.12 AFM image of an operated device without PEDOT (with upper layers removed) showing the step region between ITO and glass

The AFM image of the device without PEDOT (Figure 5.12) revealed a clearer step at the boundary of the ITO. The surface roughness of the ITO was considerable with several spikes extending up to 1.76 µm from the lowest point on the scan. There were also many smaller spikes on the surface of the glass.

To this author's knowledge, spikes and craters of such magnitudes have not previously been reported in OLED anodes, but damage of similar appearance has been observed in ceramic materials. For example, sol-gel produced on lead zirconate titanate (PZT) films have exhibited spikes and craters [15].

Liu *et al.* suggested that migration of indium is a common degradation mechanism in OLEDs caused by high electric field during operation [16]. The maximum electric field experienced by the devices in this chapter was estimated to be 1.4×10^8 V m^{-1}. It has also been reported that migration of the anode into the organic layers increased drive voltage and reduced luminescence efficiency, which agrees with these findings [17].

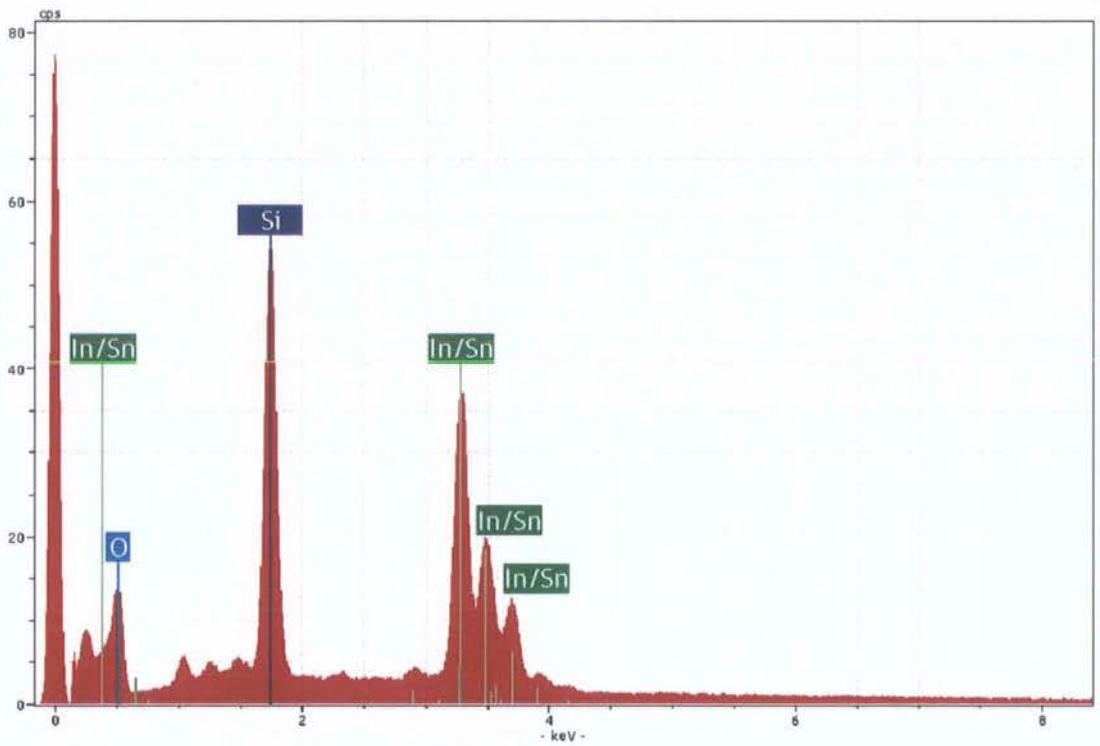

Figure 5.13 EDAX spectrum for an anode spike

Energy dispersive X-ray spectroscopy (EDAX) was used to establish the material composition of the spikes on both substrate types (PEDOT and non-PEDOT). Each sample was placed inside a scanning electron microscope (SEM) and an electron beam excited the atoms in the sample. This resulted in X-rays, characteristic of the emitting atoms, forming a series of peaks in the spectrum. The EDAX spectrum for one of the samples is shown in Figure 5.13. The spectra for devices with and without PEDOT were almost identical, indicating that the material composition of the spikes was the same in both types of device.

The peak at 1.75 keV is indicative of silicon which was one of the major constituents of the glass substrate, and the peak at 0.5 keV is typical of oxygen. Most of the other spectral peaks are characteristic of indium and tin. As indium and tin are close in atomic number (49 and 50, respectively) they produce peaks at similar energies. The EDAX data therefore verify that the anode spikes consisted of ITO and not some foreign material. In addition to the observations of Liu *et al.*, each spike was also surrounded by a crater (Figure 5.11 and Figure 5.12). This confirms that, rather than the indium migrating independently of the tin, the entire local region of ITO substrate reformed as a spike.

Devices with PEDOT possessed better film adhesion and fewer pin holes. These factors decreased the likelihood of ITO migration despite the high electric field. The fact that there was only one defect in an area of 10,000 μm^2 (Figure 5.11) and that this region was typical of the wider area, suggests that there were few sites for nucleation. This spike was probably located at the site of the only pin hole in the PEDOT within the scanning region. When the blended polymer was spin coated on the PEDOT, a pin hole formed in the polymer at the same position. Only at this one location (a) was there no physical protection from the PEDOT; and (b) was the emissive polymer film adhesion poor. During operation the electric field caused ITO to migrate, in the form of spikes, into the poorly adhered MEH-PPV blend film. Each spike nucleated at a pin hole location and material was drawn from the surrounding region leaving a crater. With continued operation, the spikes grew taller and more ITO was drawn from the surrounding region. The low number of pin holes resulted in a small number of spikes, which were generally taller than the spikes in the devices without PEDOT. In extreme cases, the ITO spikes grew tall enough to reach the cathode, causing a short circuit, and the crater extended to the full thickness of ITO. The spike shown in this AFM scan was tall enough to pierce the blended polymer film (approximate thickness 100 nm). The process is described schematically in Figure 5.14.

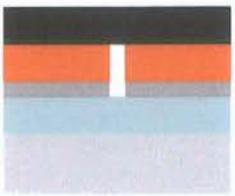

1. Spin coating PEDOT from solution produced pin holes in the film. Pin holes were formed at the same locations in the spin-coated MEH-PPV film.

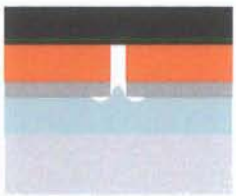

2. During operation the electric field caused ITO to diffuse in the form of columnar spikes.

3. With continued operation, the spikes grew taller and more ITO was drawn from the surrounding region.

4. In extreme cases the ITO spike grew tall enough to reach the cathode.

Figure 5.14 Schematic diagram showing the process of ITO spike and crater formation in devices which include a PEDOT layer

1. Spin coating the blended polymer from solution produced pin holes in the film. Without PEDOT, film adhesion was poor and pin holes were more likely.

2. During operation the electric field caused ITO to diffuse in the form of columnar spikes.

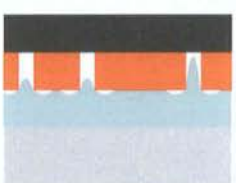

3. With continued operation, the ITO spikes and craters grew and more appeared.

Figure 5.15 Schematic diagram showing the process of ITO spike and crater formation in devices which do not include a PEDOT layer

The major disadvantage for devices without PEDOT was that the emissive film was spin coated directly onto the hydrophobic substrate rather than onto the hydrophilic PEDOT. This resulted in a large number of pin holes, which acted as nucleation sites for ITO migration. The location of the pin holes was probably governed by the surface profile of the ITO which was influenced by the sputter deposition process and by defects in the glass surface. During operation the electric field caused ITO to migrate at the nucleation sites in the form of columnar spikes, in the same way as seen in the PEDOT devices. Material was drawn from the surrounding region leaving craters. With continued operation the ITO spikes and craters grew and more appeared. The process of ITO migration in devices without PEDOT is illustrated schematically in Figure 5.15.

By comparison with the PEDOT device (a) the number of spikes was greater because there were more nucleation sites for ITO migration, (b) the spikes were shorter because only the same amount of energy was available to instigate a larger number of necessarily smaller spikes; and (c) the average crater size was smaller because smaller spikes required less material.

5.3 Aluminium-doped zinc oxide anodes

As shown above, many properties of ITO (including surface morphology and high propensity for migration into the polymer film during operation) made it undesirable for use as the anode in OLEDs. Although the use of a PEDOT layer was seen to compensate for many of its undesirable properties, a second approach was to investigate the substitution of ITO with a more suitable material. Suggested alternatives have included Ga-In-Sn-O, Zn-In-Sn-O, Ga-In-O, and Zn-In-O [18]. In addition, a few examples have been proposed which include no oxygen, such as titanium nitride [19]. When comparing anode materials there is always a trade-off between conductivity, work function and optical transparency.

In this study, the feasibility of employing an aluminium-doped zinc oxide (AZO) film as the anode in a PLED was investigated. The inexpensive and non-toxic nature of AZO has attracted interest for use as the anode in SMOLEDs with limited success [20, 21] but the surface morphology of AZO and its influence on lifetime in PLEDs has not previously been investigated.

5.3.1 Material properties

AZO films, up to 500 nm in thickness, were provided on glass substrates by Cranfield University. These were formed by sputter deposition from an AZO ceramic target in a Balzers RF (radio frequency) sputter coater at a power ranging between 200 and 250 W.

Film quality and surface roughness

Figure 5.16 shows an AFM image of a square region (100 μm by 100 μm) of glass substrate where the step in the centre represents the boundary of the AZO layer.

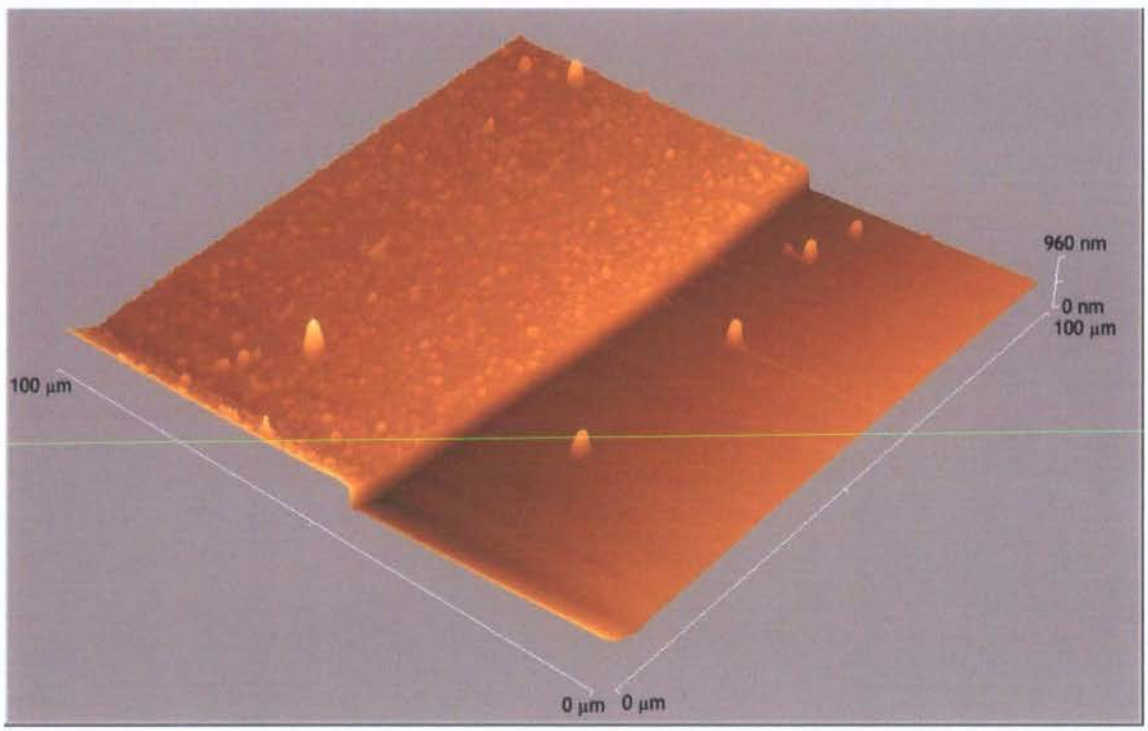

Figure 5.16 AFM image of AZO step on glass substrate

The AZO was deposited across the full area of the substrate to a thickness of approximately 500 nm and a standard photolithographic process (the same in all respects as that used for ITO) was employed to pattern it. The glass surface at the front of the image included a small number of AZO spikes which were not successfully removed by the etching process. These were unlikely to be defects similar to those seen in Figure 5.1 (on a 180 nm z-scale) because they projected from the surface by 500 nm, approximately the same thickness as the adjacent AZO film. Apart from these few irregularities, the glass was smooth by comparison with the AZO surface, which contained a large number of defects of varying heights and areas. The RMS roughness value for the AZO region was 289.9 nm, equivalent to almost 60 % of the average film thickness.

By comparison, Figure 5.1 shows a square region of a glass substrate across an ITO-glass step. (Note the different vertical scales used in Figure 5.1 and Figure 5.16.) The thickness of the ITO was approximately 100 nm (5 times thinner than the AZO). There were a small number of areas where either the ITO had not etched successfully from the glass or the glass was particularly non-planar. In addition, there were a number of small area spikes in the ITO region. The RMS roughness value for the ITO surface was 10.9 nm, equating to 11 % of the film's average thickness. By this measure the AZO film was more than five times rougher than the ITO film.

The unevenness of the AZO film was more regular and consistent across its surface than was the case for the ITO film. The less frequent, irregular spikes were taller and narrower in the ITO than in the AZO, making them potentially more damaging.

Optical properties

One method of maximising the efficiency of an OLED is to maximise the light transmitted through the anode layer. It is particularly important that the anode absorbs minimally in the region of the wavelength of the emitted light.

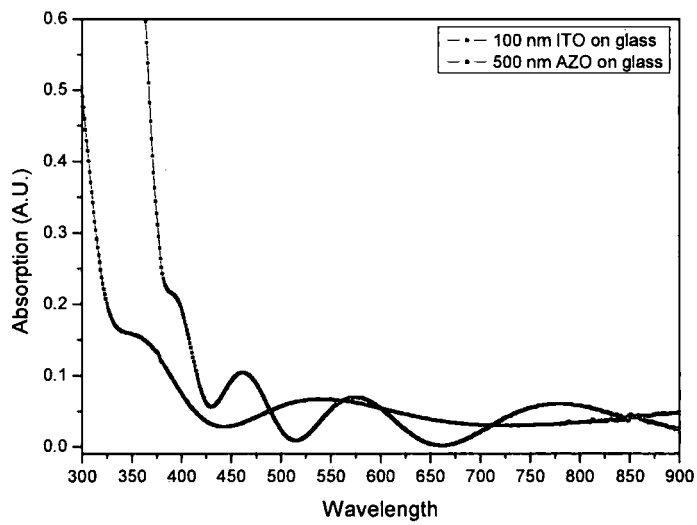

Figure 5.17 Absorption spectra for AZO and ITO films on glass substrates

Absorption spectra for AZO and ITO were obtained using a Perkin Elmer Lambda 19 spectrometer and are shown in Figure 5.17. The absorption spectra for the two substrate materials were for the most part similar with absorption coefficients fluctuating around 0.05 A.U. throughout the visible spectrum. The absorption coefficient varied by a maximum of 10 % in the region 10 nm either side of the peak emission wavelength for

MEH-PPV devices of 590 nm. The peaks and troughs in the absorption profile were the result of constructive and destructive interference (an example of Bragg's law).

Electrical properties

The sheet resistance of anode materials was measured using a four point probe, averaged over five samples of each material. The sheet resistance was 118 $\Omega\,\square^{-1} \pm 2\,\Omega\,\square^{-1}$ for the AZO substrates and 7.8 $\Omega\,\square^{-1} \pm 0.1\,\Omega\,\square^{-1}$ for the ITO substrates. The difference in sheet resistance of more than one order of magnitude contributed to the lower efficiency of devices with AZO anodes.

Different values for the Fermi level of AZO are quoted in the literature. Estimates range from -4.0 eV [21] to -5.2 eV [20], depending on the composition of the material and method of deposition. Although facilities were not available to measure the value of the Fermi level, it was possible to reduce the range of values by considering the device behaviour.

5.3.2 Device fabrication

Devices were fabricated using the techniques described in Chapter 3. The anode material employed was either AZO or ITO.

A layer of PEDOT was applied between the ITO or AZO and the polymer blend layer in some devices. For those devices with the PEDOT layer, 200 µl of PEDOT solution diluted with 50 % pure water was deposited onto each substrate, which was then spun at 1500 rpm for 60 s. The subsequent processing steps were as described previously in section 5.2.1.

5.3.3 Device characteristics

Electrical characteristics

The current-voltage (I-V) and (log) light-voltage characteristics are shown in Figure 5.18 for a batch of devices of which one half had ITO and the other half had AZO anodes. All the devices included a layer of PEDOT. As with all batches presented in this thesis, all 24 devices in the batch were fabricated in one session and characterised immediately after fabrication. The devices were the same in all respects, apart from the fact that 12 were produced with ITO and 12 with AZO.

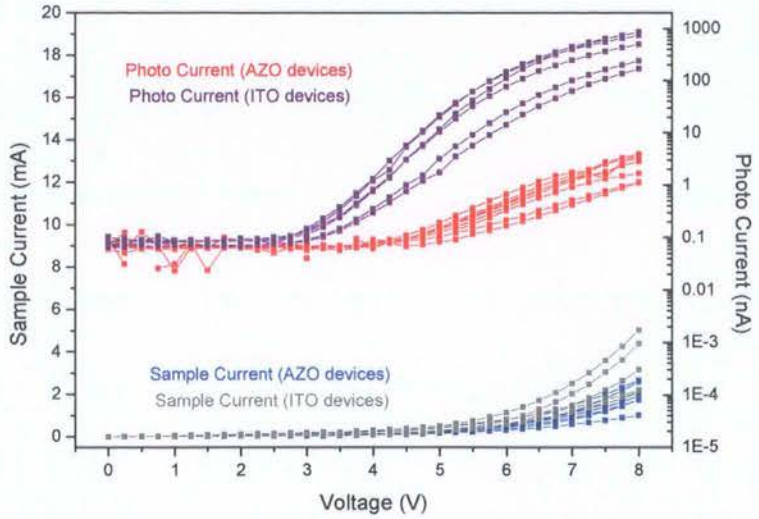

Figure 5.18 I-V and (log) light-voltage characteristics for MEH-PPV : PDPyDP (80 : 20) aluminium-cathode devices with AZO or ITO anodes and a layer of PEDOT

Before comparing the characteristics of the two anode materials it is important to note that the ITO / PEDOT devices were produced no differently from the ITO / PEDOT devices with characteristics shown in Figure 5.6, but the range of light emission values was different. In Figure 5.6 the variation was between 20 nA and 220 nA, whereas in Figure 5.18 the values ranged from 200 nA and 900 nA. This was an extreme example of the differences between devices that, although fabricated at different times, were intended to be the same in all respects. Some possible reasons for the inconsistencies between batches are presented in section 5.2.3.

Figure 5.18 indicates that the photo-currents in AZO devices were lower than those for ITO devices by approximately two orders of magnitude. Given that the threshold for visibility was approximately 5 nA, the light output from the AZO devices was only just seen by eye.

A small quantity of AZO with a lower sheet resistance of 35 $\Omega\,\square^{-1}$ was obtained from Cranfield University. Devices were made using this low resistance AZO and a layer of PEDOT to prove that visible light emission could be achieved using AZO anodes. The I-V characteristics for these devices are shown in Figure 5.19. Even with all factors maximised, the light emission remained almost an order of magnitude lower than the equivalent ITO devices. (Note that the average light emission from the ITO devices in this batch was approximately 200 nA, which was similar to that seen in Figure 5.6.)

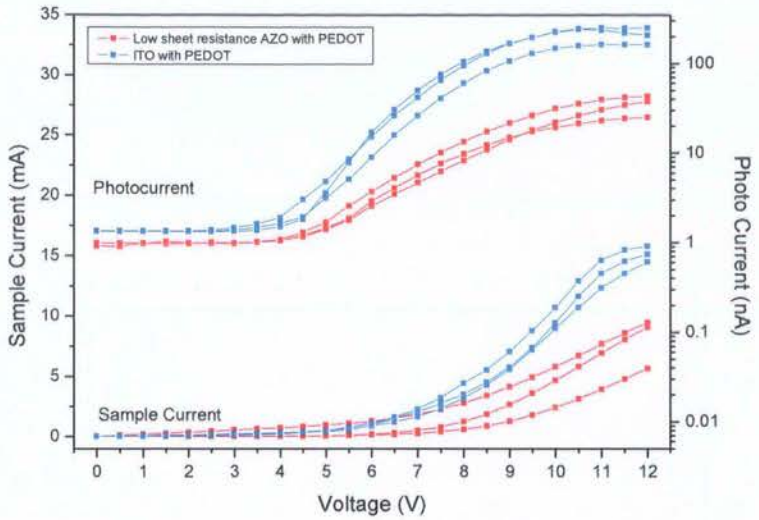

Figure 5.19 I-V and (log) light-voltage characteristics for MEH-PPV : PDPyDP (80 : 20) aluminium-cathode devices with (low resistance) AZO or (standard) ITO anodes and all with a layer of PEDOT

There was probably a combination of factors which resulted in the light emission from both batches of AZO devices being significantly less than from ITO devices.

It is widely known that the I-V characteristics of PLEDs, including the turn-on voltages, are highly sensitive to the band offset between the polymer and the electrodes [22-24]. The energy diagrams for ITO and AZO devices (both including PEDOT) are shown in Figure 5.7 and Figure 5.20, respectively.

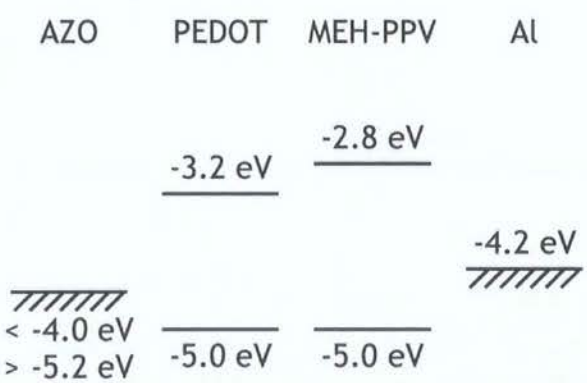

Figure 5.20 Energy diagram showing the HOMO and LUMO levels of the organic materials and the Fermi levels of AZO and aluminium

The I-V and light-voltage data suggest it is likely that the AZO devices included a larger barrier to hole injection than those with ITO anodes. As stated previously (Section 5.3.1), a range of values for the Fermi level of AZO are quoted in the literature. It is certain that there must have been at least some barrier to hole injection. If this were not the case, current would have been predominantly through the flow of holes, and no light emission

would have occurred. Therefore, the Fermi level of AZO cannot be below the HOMO level for PEDOT, which occurs at -5.0 eV. Secondly, given that the I-V characteristics (including turn-on voltages for current and light emission) were worse for AZO devices compared to ITO devices, it is likely that the barrier to hole injection was larger for AZO than for ITO devices. This suggests that the Fermi level for AZO was above -4.8 eV.

It may also be that the surface properties of the AZO resulted in a large voltage drop across the AZO / polymer interface, which reduced the effective voltage drop across the polymer. This provides a second explanation for the differences between the I-V characteristics of the two sets of AZO devices (Figure 5.18 and Figure 5.19). The thicker film, as well as having lower sheet resistance, was likely to have a smoother surface morphology. A smoother surface probably resulted in better contact, and therefore a smaller voltage drop, at the interface between the two materials. In reducing the voltage lost across the interface region, a greater proportion of the voltage fell across the polymer which increased current flow and light emission.

Quantum efficiency characteristics

Values for quantum efficiency were estimated from the I-V data and plotted in Figure 5.21.

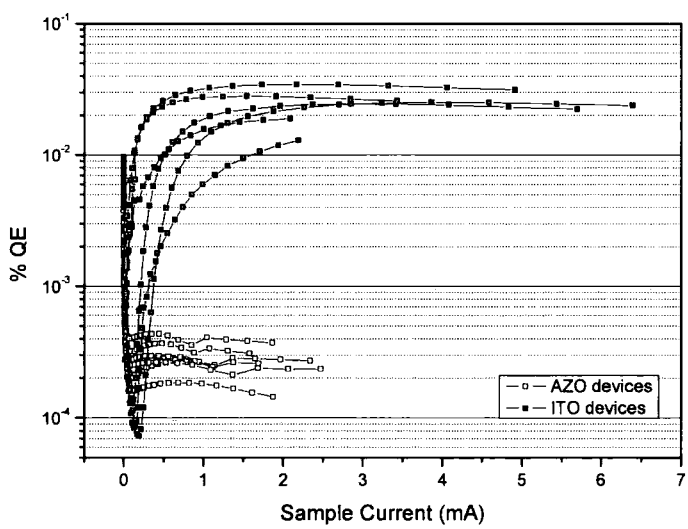

Figure 5.21 QE characteristics for MEH-PPV : PDPyDP (80 : 20) aluminium-cathode devices with (high resistance) AZO or ITO anodes and a layer of PEDOT

The average QE for the devices with (high resistance) AZO was two orders of magnitude less than the average for ITO devices. The 12 times greater sheet resistance of the AZO film contributed significantly to lower sample currents and lower light outputs, which led to the relatively poor quantum efficiency. The other negative influence on the quantum

efficiency was the increased regular roughness of the AZO surface which affected the quality and adhesion of the polymer film.

Electroluminescent spectra

The luminous flux at peak wavelength was 3100 A.U. in the case of the ITO devices and 350 A.U. for the AZO devices, which was consistent with the difference seen in the generated photo-currents.

The electroluminescent spectra of AZO and ITO devices are illustrated in Figure 5.22. Given the difference in light output for the two kinds of device, for comparison purposes the light intensities were normalised. It is debatable to what extent the apparent spectral shift between the two scans is real and what is attributable to the data normalisation. As the light output from the AZO device was two orders of magnitude less than from the ITO device, the normalisation process caused a greater degree of noise to be visible on the AZO plot. This is particularly obvious in the 400 to 500 nm wavelength range.

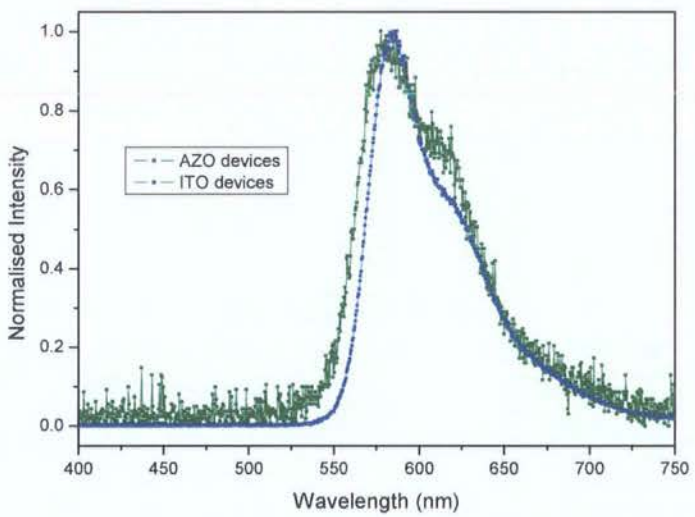

Figure 5.22 Normalised electroluminescent spectra for MEH-PPV : PDPyDP (80 : 20) aluminium-cathode devices with AZO or ITO anodes and a layer of PEDOT

Nevertheless, some variations between the spectra were likely to be caused by real differences in the anode materials. For example, the shoulder region which occurs in both spectra at approximately 625 nm is higher for the AZO device. The absorption spectra of AZO and ITO, shown in Figure 5.17, indicate that at this wavelength the absorption of AZO is approximately half that of ITO.

Another possible reason for the variation in shoulder height was dissimilar polymer aggregation caused by different surface morphology of AZO and ITO. The shoulder

which is often observed in the emission spectra for MEH-PPV films is strongly influenced by polymer aggregation [25]. A more detailed discussion on the influence of polymer aggregation on emission spectrum is given in Section 6.9.

Impedance spectroscopy

Impedance spectroscopy was used to establish the equivalent circuits of the devices. Figure 5.23 shows a simple equivalent circuit of the devices consisting of parallel resistance capacitance combination and a series resistance.

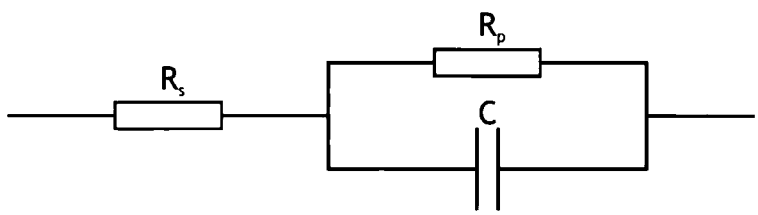

Figure 5.23 Equivalent circuit of an OLED

R_s represents the resistance of the electrodes and contacts while R_p and C represent the resistance and capacitance of the electroluminescent layer, respectively.

At low frequencies the capacitor behaves as an open circuit, so the total resistance is:

$$R = R_s + R_p \qquad (5.2)$$

At high frequencies the capacitor effectively short-circuits R_p, making the total resistance:

$$R = R_s \qquad (5.3)$$

In Figure 5.24 the measured resistance, R, is plotted against frequency.

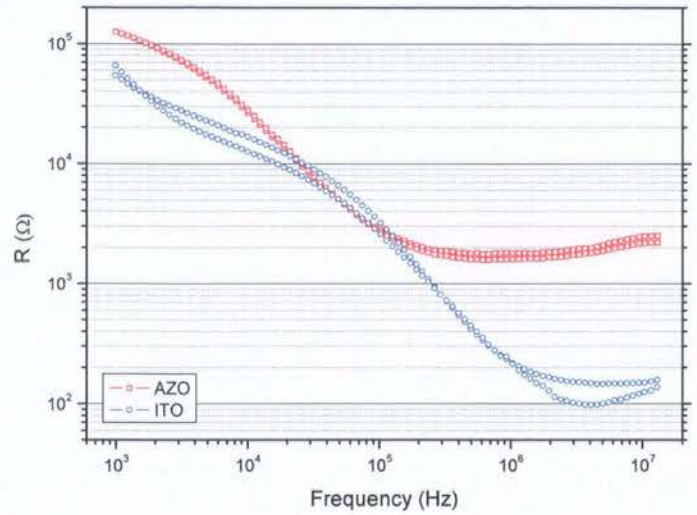

Figure 5.24 Impedance spectroscopy for MEH-PPV : PDPyDP (80 : 20) aluminium-cathode devices with AZO and ITO anodes: Resistance versus frequency

At frequencies above 0.3 MHz for AZO and above 3 MHz for ITO, R was constant suggesting this was the region where $R = R_s$ (Equation 5.3). Therefore, the combined resistance of the electrodes and contacts for devices with AZO and ITO anodes was approximately 2,000 Ω and 200 Ω, respectively. This order of magnitude variation was attributed to the difference in sheet resistance, which was 118 Ω □ $^{-1}$ for AZO and 7.8 Ω □ $^{-1}$ for ITO.

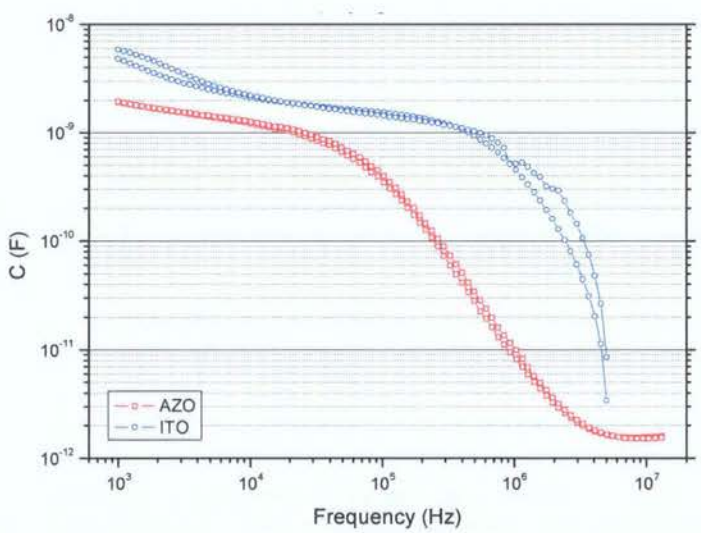

Figure 5.25 Impedance spectroscopy for MEH-PPV : PDPyDP (80 : 20) aluminium-cathode devices with AZO and ITO anodes: Capacitance versus frequency

Figure 5.25 shows capacitance against frequency. This plot confirms the assumption made above that the capacitance values become less significant at frequencies greater than 0.3 MHz for AZO and 3 MHz for ITO.

Stability characteristics

The stability behaviour for typical devices with AZO and ITO anodes measured at a constant current of 0.56 mA are shown in Figure 5.26. Over the course of a week, the light emitted by the ITO-anode devices decayed by approximately one third. Nevertheless, throughout the testing period the light emission was visible and the voltage required to maintain the constant sample current remained stable at approximately 6 V. By contrast, it is unlikely that the AZO-anode devices produced any light, as the photocurrent level was similar to that obtained when the photodiode was in complete darkness. The voltage required to hold the constant current increased by 130 % over the course of the 7 days suggesting continually increasing instability, even though no light was emitted.

Following the stability test, the polymer and cathode device layers were stripped in the way described in 5.2.5. The ITO device showed considerable damage after operation (Figure 5.11) in addition to an already rough surface (Figure 5.1). By contrast, the AZO film did not exhibit much additional damage, as evidenced in Figure 5.27. The AFM scan was not markedly different to Figure 5.16, which showed a different region of the same substrate before the device was produced.

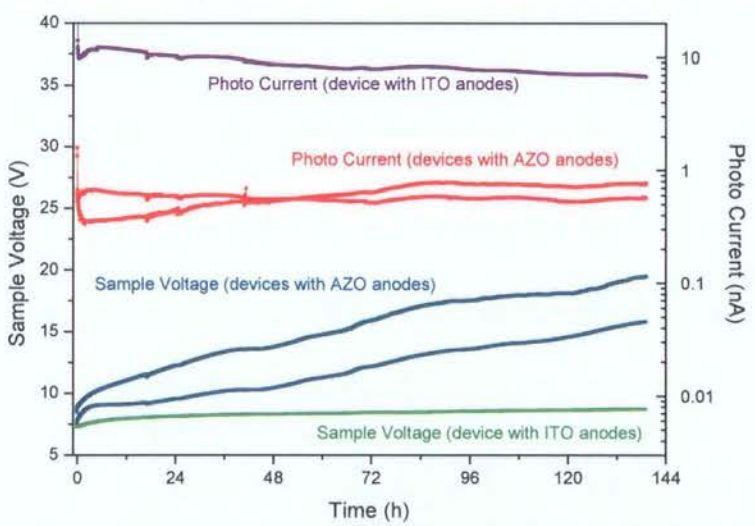

Figure 5.26 Stability characteristics for MEH-PPV : PDPyDP (80 : 20) aluminium-cathode devices with AZO or ITO anodes and a layer of PEDOT

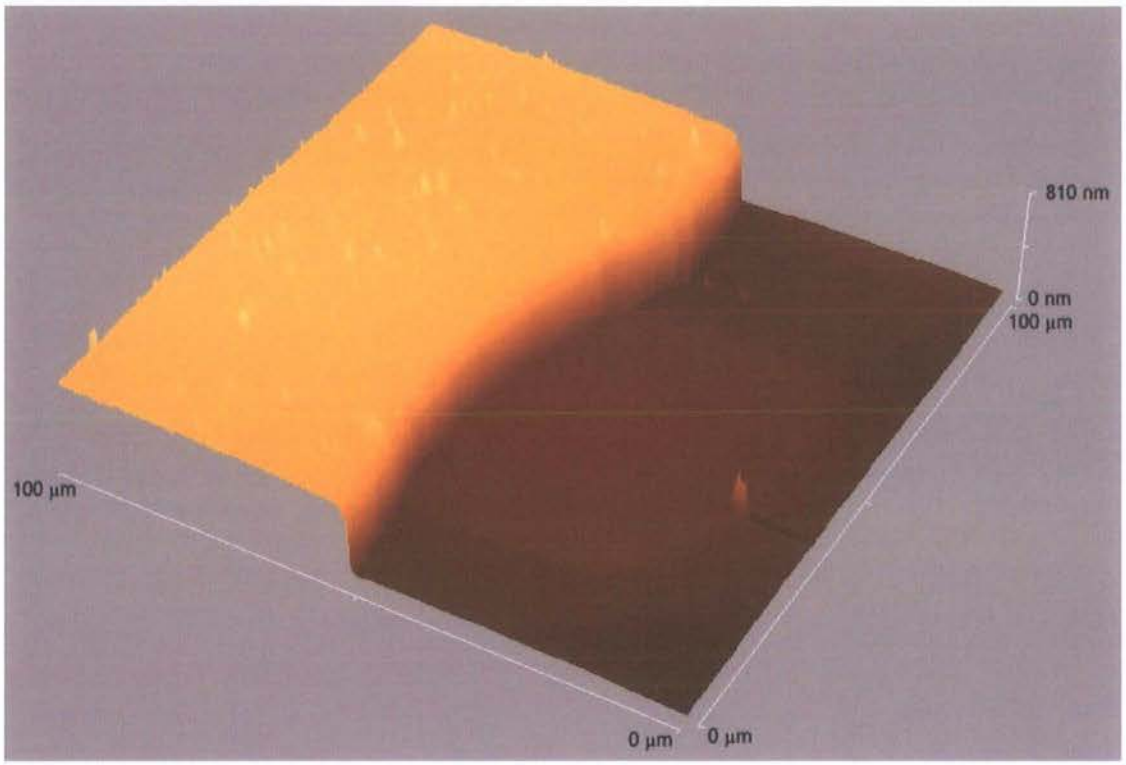

Figure 5.27 AFM image of the AZO-glass step for an operated MEH-PPV : PDPyDP (80 : 20) aluminium-cathode device after the upper layers have been removed

5.4 Comparison of PEDOT and AZO data

Following the previous studies, the data for AZO devices with PEDOT were plotted together with the data for ITO devices with and without PEDOT. The I-V characteristics are given in Figure 5.28 and estimates of the QE are shown in Figure 5.29. Devices with AZO anodes and without PEDOT did not emit any light and the data are not plotted.

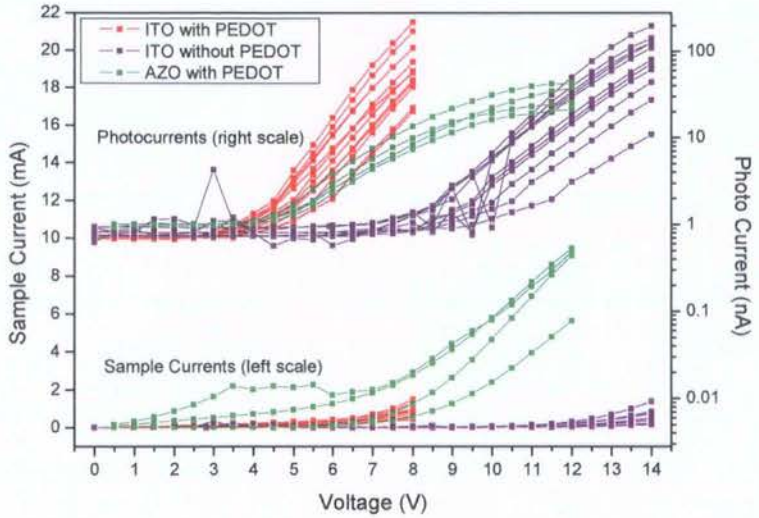

Figure 5.28 I-V and light-voltage characteristics for MEH-PPV : PDPyDP (80 : 20) aluminium-cathode devices with AZO or ITO anodes each with and without a layer of PEDOT

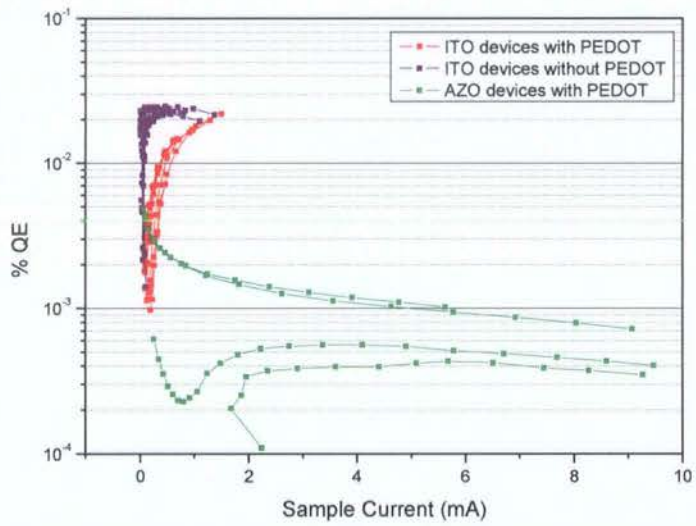

Figure 5.29 QE characteristics for MEH-PPV : PDPyDP (80 : 20) aluminium-cathode devices with AZO or ITO anodes each with and without a layer of PEDOT

From these data it is clear that, of the three types of device, those with ITO anodes and a layer of PEDOT had the best overall characteristics, combining a low turn-on voltage with high light output and high efficiency. The high sample current in the AZO devices coupled with relatively low light output meant that the efficiency of these devices was poor.

The choice of anode material was, therefore, more significant than the influence of PEDOT. The most attractive characteristic of the AZO was the fact that it appeared not to migrate into the polymer as readily as ITO. It is possible that, by combining the two anode materials in a bi-layer structure, anode migration could be minimised while maximising light output and quantum efficiency.

5.5 Conclusion

The composition and preparation of the anode layer and presence or absence of PEDOT had a significant influence on the morphological and operational device characteristics.

By adding a layer of PEDOT (a) the roughness of the surface onto which the emissive layer was spun was significantly reduced and its wettability increased resulting in better film contact and adhesion; and (b) a physical barrier to ITO migration was introduced. These factors increased the stability of the device because better film adhesion reduced the likelihood of delamination and less ITO migration caused less damage to the emissive film.

Devices produced using an AZO anode exhibited poorer performance when compared with ITO anode devices. In particular, the light output and quantum efficiency were far inferior. This could be attributed partly to the fact that the AZO had a higher sheet resistance than the ITO.

As a result of the evidence given in this chapter, the devices described in the following chapters were all made with ITO anodes and a layer of PEDOT.

5.6 References

1 G. Wantz, L. Hirsch, N. Huby, L. Vignau, J.F. Silvain, A.S. Barriére and J.P. Parneix, *Correlation between the Indium Tin Oxide morphology and the performances of polymer light-emitting diodes.* Thin Solid Films, 485, 247 (2005).

2 J.-S. Kim, R.H. Friend and F. Cacialli, *Improved operational stability of polyfluorene-based organic light-emitting diodes with plasma-treated indium–tin–oxide anodes.* Applied Physics Letters, 74, 3084 (1999).

3 J.-S. Kim, F. Cacialli and R.H. Friend, *Surface conditioning of indium-tin oxide anodes for organic light-emitting diodes.* Thin Solid Films, 445, 358 (2003).

4 S.A. Carter, M. Angelopoulos, S. Karg, P.J. Brock and J.C. Scott, *Polymeric anodes for improved polymer light-emitting diode performance.* Applied Physics Letters, 70, 2067 (1997).

5 J.C. Scott, S.A. Carter, S. Karg and M. Angelopoulos, *Polymeric anodes for organic light-emitting diodes.* Synthetic Metals, 85, 1197 (1997).

6 A.R. Schlatmann, D. Wilms Floet, A. Hilberer, F. Garten, P.J.M. Smulders, J.M. Klapwijk and G. Hadziioannou, *Indium contamination from the indium–tin–oxide electrode in polymer light-emitting diodes.* Applied Physics Letters, 69, 1764 (1996).

7 J.C. Scott, J.H. Kaufman, P.J. Brock, R. DiPietro, J. Salem and J.A. Goitia, *Degradation and failure of MEH-PPV light-emitting diodes.* Journal of Applied Physics, 79, 2745, (1996).

8 Y. Cao, G. Yu, C. Zhang, R. Menon, A.J. Heeger, *Polymer light-emitting diodes with polyethylene dioxythiophene–polystyrene sulfonate as the transparent anode.* Synthetic Metals, 87, 171 (1997).

9 L. Groenendaal , F. Jonas, D. Freitag, H. Pielartzik and J. Reynolds, *Poly(3,4-ethylenedioxythiophene) and its derivatives: past, present, and future.* Advanced Materials, 12, 481 (2000).

10 Z.Y. Zhong, Y.X. Zhong, C. Liu, S. Yin, W.X. Zhang and D.F. Shi, *Study on the surface wetting properties of treated indium-tin-oxide anodes for polymer electroluminescent devices.* Physica Status Solidi (a), 198, 197 (2003).

11 I.D. Parker, *Carrier tunneling and device characteristics in polymer light-emitting devices.* Journal of Applied Physics, 75, 1656 (1994).

12 A.J. Campbell, D.D.C. Bradley and D.G. Lidzey, *Space-charge limited conduction with traps in poly(phenylene vinylene) light emitting diodes.* Journal of Applied Physics, 82, 6326 (1997).

13 A. van Dijken, A. Perro, E.A. Meulenkamp and K. Brunner, *The influence of a PEDOT:PSS layer on the efficiency of a polymer light-emitting diode.* Organic Electronics, 4, 131 (2003).

14 N. Koch, A. Kahn, J. Ghijsen, J.-J. Pireaux, J. Schwartz, R.L. Johnson and A. Elschner, *Conjugated organic molecules on metal versus polymer electrodes: Demonstration of a key energy level alignment mechanism.* Applied Physics Letters, 82, 70 (2003).

15 S. Dunn and R.W. Whatmore, *Transformation dependence of lead zirconate titanate (PZT) as shown by piezoAFM surface mapping of sol-get produced PZT on various substrates.* Integrated Ferroelectrics, 38, 39 (2001). Followed by personal communication with S. Dunn.

16 G. Liu, J.B. Kerr and S. Johnson, *Dark spot formation relative to ITO surface roughness for polyfluorene devices.* Synthetic Metals, 144, 1 (2004).

17 S.T. Lee, Z.Q. Gao and L.S. Hung, *Metal diffusion from electrodes in organic light-emitting diodes.* Applied Physics Letters, 75, 1404 (1999).

18 J. Cui, A. Wang, N.L. Edleman, J. Ni, P. Lee, N.R. Armstrong and T.J. Marks, *Indium tin oxide alternatives - high work function transparent conducting oxides as anodes for organic light-emitting diodes.* Advanced Materials, 13, 1476 (2001).

19 V. Adamovich, A. Shoustikov and M.E. Thompson, *TiN as an Anode Material for Organic Light-Emitting Diodes.* Advanced Materials, 11, 727 (1999).

20 L. Zugangy, Z. Weimingy, J. Rongbiny, Z. Zhiliny, J. Xueyiny, X. Minzhaoz and F. Binz, *Organic thin film electroluminescent devices with ZnO:Al as the anode.* Journal of Physics: Condensed Matter, 8, 3221 (1996).

21 H. Kim, C.M. Gilmore, J.S. Horwitz, A. Piqué, H. Murata, G.P. Kushto, R. Schlaf, Z.H. Kafafi, and D.B. Chrisey, *Transparent conducting aluminum-doped zinc oxide thin films for organic light-emitting devices.* Applied Physics Letters, 76, 259 (2000).

22 I.D. Parker, *Carrier tunneling and device characteristics in polymer light-emitting diodes.* Journal of Applied Physics, 75, 1656 (1994).

23 G.G. Malliaras and J.C. Scott, *The roles of injection and mobility in organic light emitting diodes.* Journal of Applied Physics, 83, 5399 (1998).

24 J.C. Scott, G.G. Malliaras, W.D. Chen, J.-C. Breach, J.R. Salem, P.J. Brock, S.B. Sachs and C.E.D. Chidsey, *Hole limited recombination in polymer light-emitting diodes.* Applied Physics Letters, 74, 1510 (1999).

25 Y. Shi, J. Liu and Y. Yang, *Device performance and polymer morphology in polymer light emitting diodes: The control of thin film morphology and device quantum efficiency.* Journal of Applied Physics, 87, 4254 (2000).

Chapter Six

Organic LEDs derived from blends of the electroluminescent polymer MEH-PPV and the electron transporting molecule PDPyDP

6.1 Introduction

Light emitting polymers are generally more effective in transporting one charge carrier over the other. In particular, MEH-PPV transports holes better than electrons [1]. The efficiency of a device can be improved by balancing injection and transport of electrons and holes. One way to achieve this is by using an electron transporting material, either as an additional layer between the MEH-PPV and the cathode, or by blending it with the MEH-PPV in a single film [2-4]. Using a blended film rather than multiple discrete layers reduces both the number of film interfaces, which has advantages in terms of device stability, and the cost and complexity of manufacture.

The devices described in this chapter were formed with blends of MEH-PPV and the electron transporting material PDPyDP. A range of blend ratios was investigated and the electrical, stability and degradation characteristics are presented and discussed below.

6.2 MEH-PPV chemical structure and properties

MEH-PPV, more fully known as poly(2-methoxy-5-(5'-ethylhexyloxy)-p-phenylenevinylene), was the first soluble derivative of PPV [5] and the first electroluminescent polymer to be applied from solution [6]. Its chemical structure is shown in Figure 6.1.

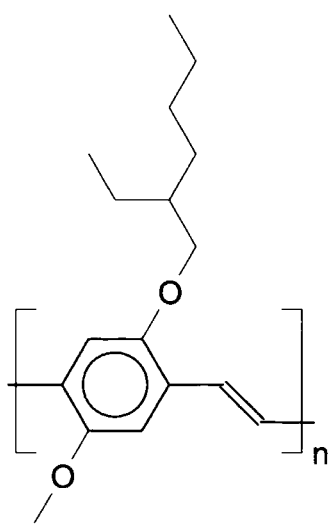

MEH-PPV

Figure 6.1 Chemical structure of MEH-PPV

The side groups facilitate good solubility of the conjugated polymer. Without the side groups the material could not be deposited from solution which is one of its greatest benefits.

This material was purchased from Sigma Aldrich (product code: 541443; batch number: 09808MA) with average molecular weight (M_n) in the range 70,000 to 100,000. The manufacturer was unable to supply purity information.

The HOMO and LUMO levels for MEH-PPV are most often quoted as -5.0 eV and -2.8 eV, respectively. However, a review of the literature revealed a range of values between -4.9 eV [7] and -5.4 eV [8] for the HOMO, and -2.8 eV [7] and -3.0 eV [9] for the LUMO. There are two likely reasons for these large variations. First, published papers rarely specify whether the data were calculated or measured. Calculations are generally for a single molecule in the gas phase because this involves the fewest variables and the lowest computation time. Measured values are most often for a cluster of molecules in the solid phase or in solution. It is likely, therefore, that the calculated and measured values differ. Also, HOMO and LUMO levels are influenced by molecular weight. The molecular weight of the MEH-PPV used in a particular investigation is not often quoted in the literature. However, values for molecular weight of commercially available MEH-PPV range from 40,000 to 250,000.

A difference in HOMO or LUMO values of just 0.1 eV, is known to influence device behaviour [10].

6.3 PDPyDP chemical structure and properties

PDPyDP (2,5-bis[5-(4-tert-butylphenyl)-2-pyridyl]-1,3,4-oxadiazole) was synthesised in the Chemistry Department at Durham University [11]. The molecule includes two electron-deficient oxadiazol groups which provide the electron transporting ability and are known for their chemical and thermal stability [12]. The structure of the molecule is shown in Figure 6.2.

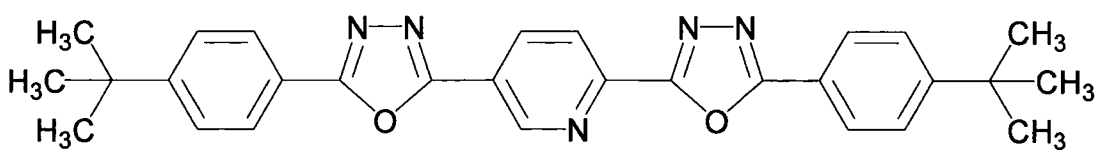

Figure 6.2 Chemical structure of PDPyDP

The purity of the material was assessed by elemental analysis. A small quantity of PDPyDP was burnt and the resulting gases of carbon, hydrogen and nitrogen were measured to determine the proportions of these materials. The analysis in terms of molecular weight gave C: 72.52 %; H: 6.08 %; N: 14.58 %. The calculated values for PDPyDP were C: 72.63 %; H: 6.10 %; N: 14.60 %. Therefore, the errors for each element were: C: 0.11 %; H: 0.02 %; and N: 0.02 %. Each value is within 0.3 % of the calculated value, the maximum set for publication by most journals.

A molecular modelling program called GAUSSIAN 03, was used to predict the energy levels for PDPyDP. More specifically, the density functional theory approach was used to calculate the electronic structure of a single molecule in the gas phase using the principles of quantum mechanics. The estimates provided for the HOMO and LUMO levels were -6.2 eV and -2.5 eV, respectively. The accuracy of such predictions depends on the level of computation and the number of iterations. The same calculation was used to estimate the levels for all the small molecules studied in this thesis. Therefore, even though the values may not be accurate in absolute terms, they provide an accurate comparison between the HOMO and LUMO levels of the different molecules.

In order to identify the likely accuracy of the calculations, the same computations were used to estimate the energy levels of the widely known organic molecule OXD-7, for which the energy levels were obtained experimentally by considering the optical gap energy. The calculated and measured values for HOMO were consistent. However, the calculated value for LUMO (-2.0 eV) was 0.8 eV higher than that found experimentally (-2.8 eV). Oyston *et al.* argue that there is a similar error in the calculated LUMO values for PDPyDP and other materials [13, 14].

6.4 Energy levels in the blended devices

The energy levels of MEH-PPV and PDPyDP are shown schematically in Figure 6.3 alongside those of PEDOT and the Fermi levels of the electrode materials. A step in energy level between adjacent layers influences the injection of charge carriers between the layers [10].

There are two reasons to be cautious when considering energy levels. As noted above, there may be errors in the quoted values as they are difficult to measure and calculate accurately. A second problem arises from an argument that the energy barrier is not simply equal to the difference between the two adjacent energy levels [15]. The difference in

height between neighbouring energy levels in Figure 6.3 represents the intrinsic contribution to the energy barrier between the materials. There is also a contact dependent contribution that arises at each film interface (see earlier discussion at Section 5.3.3). Where metal cathodes are deposited onto the polymer by evaporation, some of the metal diffuses into the polymer by up to 5 nm. Therefore, the energy barrier contribution arising at the metal / polymer interface is likely to be small. In contrast, where the polymer is spin coated onto the anode no diffusion is possible, and the evaporation of solvent results in empty space at the interface [16]. Hence, the contact dependent contribution to the energy barrier at the polymer / anode interface is likely to be larger.

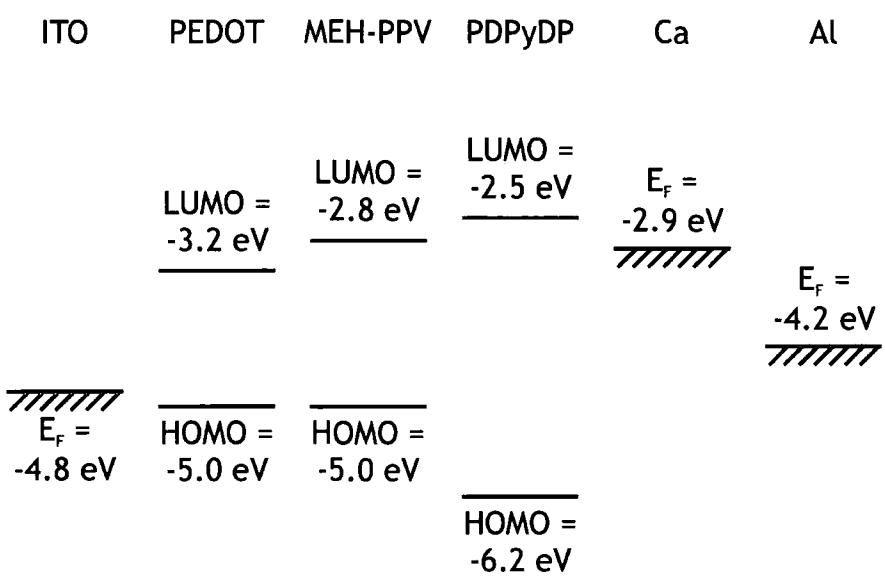

Figure 6.3 Energy diagram showing the HOMO and LUMO levels of the organic materials and the Fermi levels of the electrode materials

One of the main benefits of using blended and additional layers is to provide an intermediate energy level between the Fermi level of the electrodes and the HOMO and LUMO levels of the electroluminescent material.

6.5 Device fabrication

Devices were fabricated using the techniques described in Chapter 3. The anode material employed in all the OLEDs described in this chapter was ITO with an approximate sheet resistance of 7.8 $\Omega\ \square^{-1}$.

All the devices in this chapter included a layer of PEDOT between the ITO and the polymer blend. The PEDOT dispersion was diluted with water (1:1) and 200 µl was dispensed onto each substrate before spinning at 1500 rpm for 60 s. The devices were

placed in a vacuum for 1 h to remove residual water vapour before applying the blended polymer layer.

The device cathodes were formed either by evaporating a 100 nm layer of aluminium, or by evaporating a 15 nm layer of calcium followed by a 100 nm layer of aluminium. The single layer aluminium cathode devices are described in 6.7 and those with calcium and aluminium double layer cathodes in 6.8.

6.5.1 Blended layers

The electroluminescent layer of each device was formed from a blend of PDPyDP with MEH-PPV [17]. For each blend, the specified masses of solid MEH-PPV and solid PDPyDP were placed into a glass vial and a specified volume of chloroform was added to produce a blended solution. Chloroform solutions of pure PDPyDP and pure MEH-PPV were also produced. 12 h of stirring with a magnetic bead ensured that the full quantity of solid dissolved. The electroluminescent films were produced by spin coating the relevant solution on top of the PEDOT layer. The solution ratios, concentrations and spin speeds for each of the PDPyDP : MEH-PPV blends are listed in Table 6.1.

Ratio of PDPyDP : MEH:PPV by weight	Solution concentration	Spin speed
0 : 100	6.67 mg ml^{-1}	1000 rpm
20 : 80	8.75 mg ml^{-1}	1000 rpm
50 : 50	12 mg ml^{-1}	1000 rpm
70 : 30	13.33 mg ml^{-1}	750 rpm
95 : 5	15 mg ml^{-1}	750 rpm
100 : 0	16 mg ml^{-1}	750 rpm

Table 6.1 Solution ratios, concentrations and spin speeds for blends of MEH-PPV and PDPyDP

The parameters used for each blend ratio were deduced by iterative experimental testing in order to produce similar film thicknesses and qualities for all blends. Thicknesses were measured using an Alpha step profilometer. The quality of each film was qualitatively assessed by a visual inspection. Film quality was judged to be poor if it was uneven and included streaks of different thicknesses due to differential evaporation of the solvent. By using the parameters listed in Table 6.1, the quality of the films appeared similar, without morphological defects, and the average thickness was 100 nm for all the blend ratios. This

was important to achieve the same magnitude of electric field in all devices. A photograph of the solutions is shown in Figure 6.4, and a photograph of a batch of devices taken immediately after fabrication is given in Figure 6.5.

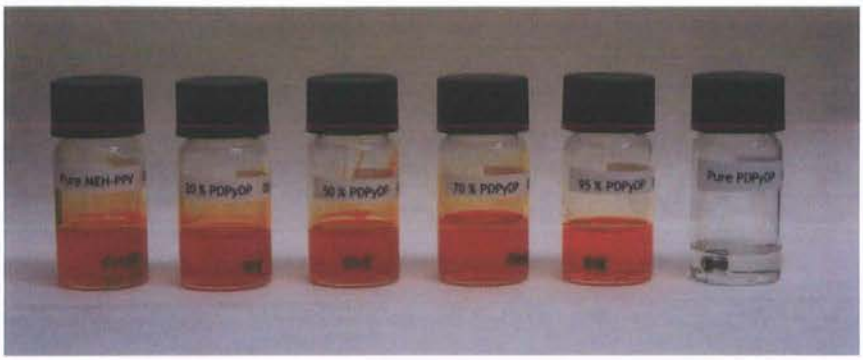

Figure 6.4 Photograph of blended solutions in chloroform

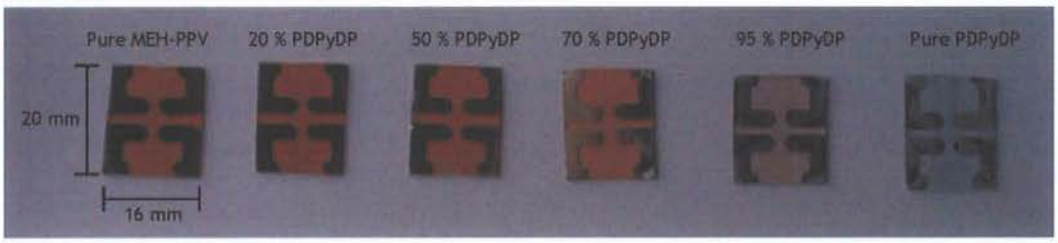

Figure 6.5 Photograph of devices taken immediately after fabrication

6.6 Occasional anomalous device characteristics

Some current-voltage scans exhibited a peak in the sample current often without a corresponding peak in the light output. A typical example of this phenomenon is illustrated in Figure 6.6.

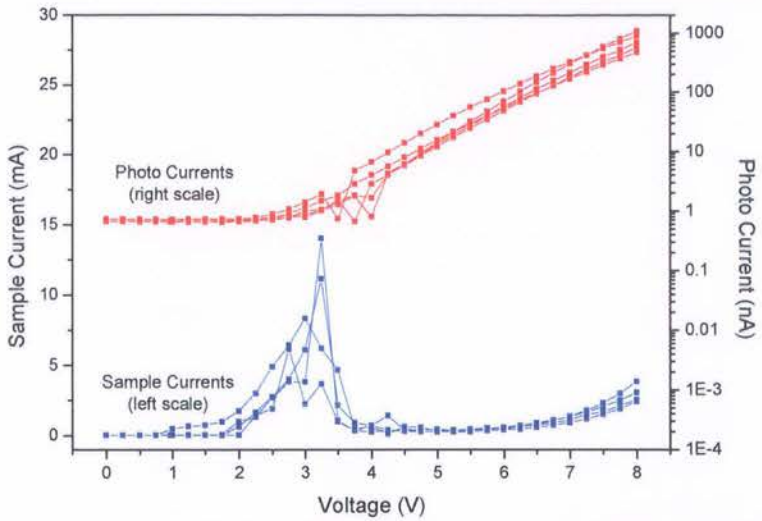

Figure 6.6 I-V and light-voltage characteristics for MEH-PPV : PDPyDP (80 : 20) aluminium-cathode devices showing the peak in sample current at low voltages as an example of that occasionally observed in blended devices

The peaks were unpredictable and not often repeatable from one batch of apparently identically produced devices to the next. Many of the scans exhibited no peak at all. They were observed in a proportion of the devices with ITO anodes, but never in devices with AZO anodes. The data for some blends had a higher proportion of devices showing the characteristic peak than others, but there was no obvious correlation between blend composition and likelihood of peak occurrence. The amplitude of the peak decreased with each repetition of the I-V scan, to the extent that it was rarely observed on the third or subsequent scans. This suggested that the peak was removed by an annealing mechanism that occurred during device operation. Given the discussions on anode morphology in Chapter 5 and the absence of apparent links with the blend composition, it was probable that the current peaks were caused where ITO spikes punctured the polymer film and made direct contact with the cathode, rendering a short circuit. The short circuits were not permanent and were most likely removed through a process initiated by the high electric field in the region of the ITO spike. This caused the surrounding polymer film to degenerate and so lose its semi-conducting properties, which effectively isolated the region. Once isolated, the short circuit was removed so eliminating the cause of the sample current peaks. The fact that the anomalous current peaks were not observed for devices with AZO anodes correlates with the observation that there were very few spikes in the AZO films of operated devices (see Figure 5.27).

Kim *et al.* have observed similar peaks in the current behaviour during the first two I-V scans when leaving their devices in air for two days between fabrication and testing [18].

Rather than damaging the anode material, they suggest that the high current density at the location of a cathode pin hole resulted in degradation and delamination in the surrounding material. This was probably caused by the ingress of oxygen and water vapour through pin holes during the two day storage period. Such a process seems less likely in the devices considered here because they were tested immediately after fabrication and no cathode delamination was observed. Kim and co-workers do not mention anode degradation, yet observations of ITO morphology and degradation seen in Chapter 5 suggest that anode degradation was more prevalent in these devices. In the case of either anode- or cathode-degradation, the result was a non-emitting region which subsequently became electrically isolated from the rest of the device, meaning that the effect on the current was not permanent.

6.7 PDPyDP blends with aluminium cathodes

The devices discussed in this section were fabricated with a single cathode layer of 100 nm of thermally evaporated aluminium.

6.7.1 Current-voltage and light-voltage characteristics

Current-voltage and light-voltage characteristics for the as-produced devices are shown in Figure 6.7. Readings were taken at 0.25 V intervals, but for the sake of clarity the individual data points are not shown. Instead the data are plotted as one continuous line for each device.

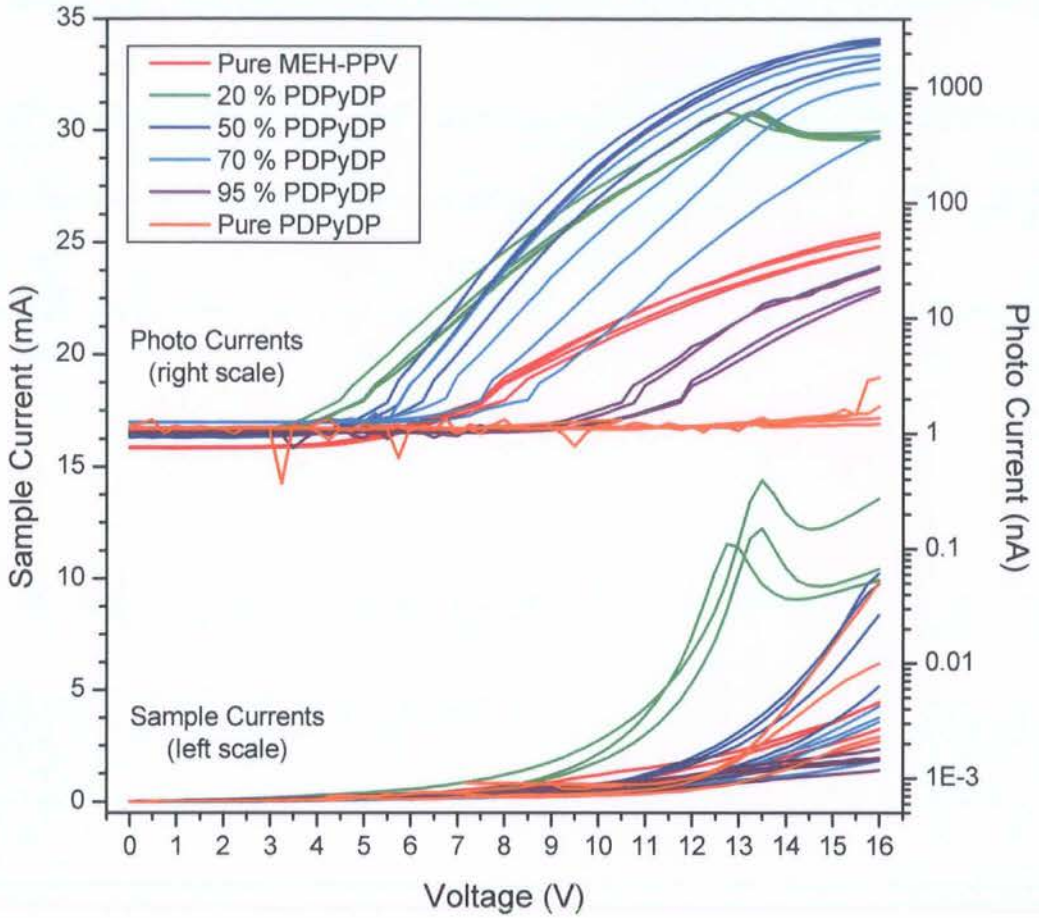

Figure 6.7 I-V and light-voltage characteristics for aluminium-cathode devices with varying ratios of PDPyDP : MEH-PPV

Both light output and current were influenced by blend composition. An increase in light emission is just one of the benefits achievable through blending MEH-PPV with an additional electron transporting material. The 50% PDPyDP devices emitted the most light (an average of 2,500 nA), which was more than 40 times that produced by the pure MEH-PPV devices. In theory, the maximum light emission occurs when the numbers of electrons and holes in the emissive polymer are balanced. The data suggest that, of the blend ratios tested, the 50 % blend was most balanced. Only the 95 % blend and pure PDPyDP devices emitted less light than the pure MEH-PPV devices. This was because, in blended films consisting predominantly of PDPyDP, the current was dominated by electron flow which limited the possibility of electron-hole recombination. The devices with 70 % PDPyDP averaged a light output equating to 900 nA, 15 times that of the pure MEH-PPV. So, despite the light emitting component constituting only 30 % of the blend, the light emission from this device was increased by the improved electron transporting capability.

An imprecise estimate suggested that the length of an average MEH-PPV polymer chain was approximately 80 times the length of a PDPyDP molecule. (This was based on the assumption that the molecular weight of PDPyDP is similar to that of four repeat units of MEH-PPV.) Therefore, for the device with the highest light emission (the 50 % blend) there were approximately 80 times more PDPyDP molecules than MEH-PPV chains.

The 95 % blend emitted minimal light, suggesting a poor balance of electrons and holes. Given that the MEH-PPV contributed just 5 % of the blend by weight and was 80 times longer than the PDPyDP, there were approximately 1500 times $((95 \div 5) \times 80)$ as many molecules as polymer chains. It was therefore statistically probable that most MEH-PPV chains were completely surrounded by PDPyDP and so isolated from one another. This limited the hole-transport in the film. The device current was of the same order as for the other blend ratios, and was attributed to electrons being transported through the film without recombination.

In the 70 % blend film, there were approximately 190 times $((70 \div 30) \times 80)$ more PDPyDP molecules than MEH-PPV chains. Compared with the 95 % blend, the chance of MEH-PPV chains interacting with one other at some point along their length was much increased. Inter-chain contact of MEH-PPV preserved hole-transport in the film, while the PDPyDP content improved electron-transport.

Another advantage of the blended devices was the lower turn-on voltage for both current flow and light emission. The lowest value for light emission, of 3.5 V, was for the 20 % blend device, while the equivalent value for the pure MEH-PPV device was 6 V. The turn-on voltage of a device can be lowered by reducing the barrier to injection of the minority carriers (which, in the case of MEH-PPV, are electrons) [10]. According to the estimated energy levels (shown in Figure 6.3), PDPyDP actually increased the energy barrier for electrons: the barrier between aluminium and PDPyDP was 1.9 eV and between aluminium and MEH-PPV it was 1.4 eV. However, as was discussed previously (in sections 6.3 and 6.4), there is an error in the LUMO value calculated by GAUSSIAN 03 of approximately 0.8 eV. The actual LUMO value is likely to be closer to 3.3 eV. If this is the case then, the PDPyDP provided an intermediate energy level between the LUMO of MEH-PPV (-2.8 eV) and the Fermi level of aluminium (-4.2 eV), which improved the electron injection into the device.

There was a peak in the current and light emission characteristics for all of the 20 % blend devices, which occurred at approximately 13 V. For voltages between 13 V and 14 V a pronounced voltage-controlled, negative resistance region was observed that did not feature in any of the other blend compositions. A similar phenomenon was observed in thin insulating films by Simmons and Verderber in 1967 [19]. Certain conditions relating to the nature of the layer and the applied voltage can lead to electrons becoming trapped at high energy defect levels within the film. Once the electrons have been trapped, small increases in voltage are not sufficient to move the trapped electrons so the current drops. This might provide the explanation for the drop in current (and hence light emission) at voltages between approximately 13 V and 14 V.

6.7.2 Quantum efficiency

Figure 6.8 shows quantum efficiency data plotted against sample current.

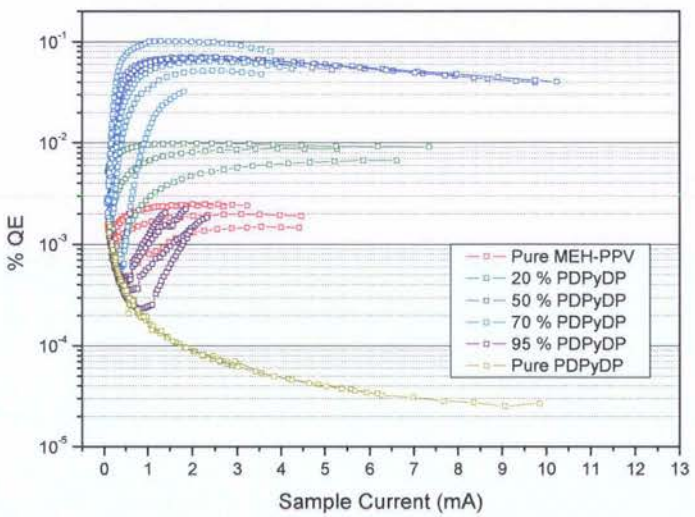

Figure 6.8 QE characteristics for aluminium-cathode devices with varying ratios of PDPyDP : MEH-PPV

The pure MEH-PPV devices gave quantum efficiencies averaging 2×10^{-3} % while the most efficient (50 %) blend devices averaged 7×10^{-2} %, representing a 35-fold increase. The average currents in these two sets of devices were similar, but the light emission from the 50 % blend devices was an order of magnitude greater. This confirms that the blended devices were more effective in balanced charge flow. Improvements in efficiency of a similar order of magnitude have previously been observed by employing blended electroluminescent layers [20].

Only the 95 % and pure PDPyDP devices had lower quantum efficiencies than the pure MEH-PPV devices. This was because the high PDPyDP content resulted in current being dominated by electron flow. In addition, with the small proportion of MEH-PPV most of the charge carriers were injected into the electroluminescent blended film via PDPyDP. The barriers to injection into PDPyDP were greater than into MEH-PPV so more energy was required, which also had a negative impact on the efficiency.

6.7.3 Stability

The device stability was measured at a constant current of 0.56 mA over 18 days. The photo-currents (proportional to light emission) and voltages are shown against time in Figure 6.9 (a) and (b), respectively.

As well as having the highest light output and quantum efficiency, the 50 % blend devices were the only ones to emit light for the full 18 day period. The 70 % blend device emitted light for more than two weeks. The remainder of the OLEDs ceased to emit light after a very short period, usually measured in hours or less.

The most common method for evaluating the stability of devices is by comparing half-lives. Such a comparison with these data would, however, invite questionable conclusions for two reasons. First, the initial light emission for devices was different for each blend. Some devices began emitting at a meaninglessly low level and dropped to half that level only over a much extended period. This was the case for the 95 % PDPyDP device which had the longest half-life. However, emission at its half-life was below the threshold for visibility. Secondly, some devices, including the 95 % blend device, dropped to half their initial light emission once the voltage has already reached the 25 V threshold imposed by the measurement equipment. This indicates that the device was no longer operating in constant current mode so any comparison would be invalid. The 50 % and 70 % devices settled rapidly at an emission level which, although less that half of the initial level, was still visible for a matter of weeks. Also, these blends did not reach the 25 V threshold. For these reasons, the 50 % and 70 % devices were considered the most stable.

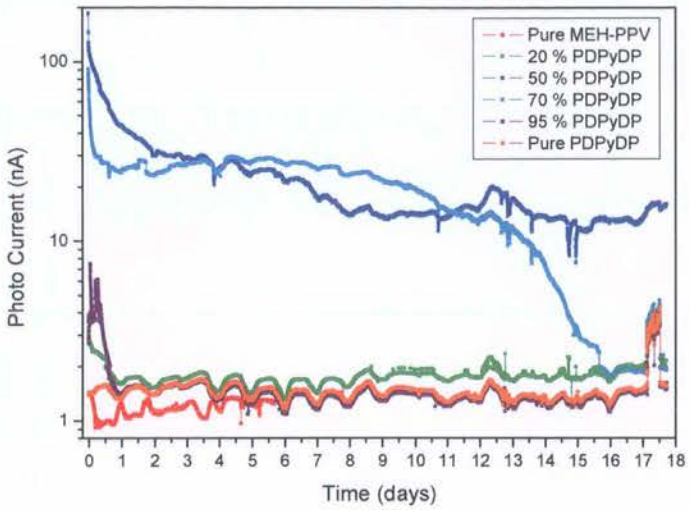

(a)

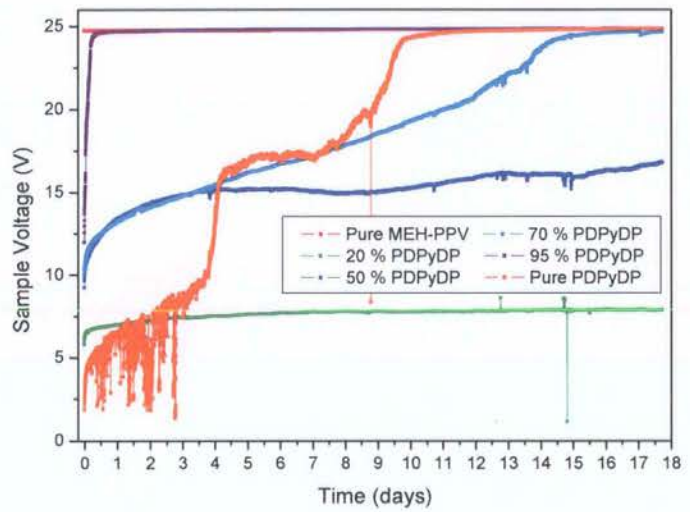

(b)

Figure 6.9 Stability characteristics for aluminium-cathode devices with varying ratios of PDPyDP : MEH-PPV: (a) photo-current against time; and (b) sample voltage against time

The evidence suggests that stability was related to the percentage of PDPyDP. Devices which incorporated higher proportions of PDPyDP were more stable. This was most obvious when comparing the stability of the 70 % and 50 % devices with the 20 % and pure MEH-PPV devices. The relationship between percentage PDPyDP and stability suggested, not only that PDPyDP was more stable than MEH-PPV, but also that the molecule actively protected the polymer within the blend. It is well known that MEH-PPV is vulnerable to attack from oxygen and water vapour [21-23] and for this reason it is common to encapsulate MEH-PPV devices. Various techniques have been devised for protecting PLEDs with an inert encapsulation [24-26]. The data suggest that the presence

of the less reactive PDPyDP in the blended devices provided a form of encapsulation for the MEH-PPV, protecting the polymer from the effects of contaminants such as oxygen and water vapour. Further, given that the two materials were blended in a single layer this suggests that the PDPyDP encapsulation functioned at the scale of individual polymer chains, or clusters of chains. The notion of nano-encapsulation was therefore introduced.

As well as the degradation mechanisms related to the emissive material, it is clear from the literature that the choice of cathode material can significantly influence device stability [27]. The two cathode degradation mechanisms commonly linked with aluminium-cathode devices are electromigration of the aluminium [28] and delamination of the polymer film from the metal surface [29] both of which caused non-emissive dark spots. Dark spots and cathode delamination were observed in the devices discussed in this chapter. More detailed discussions of the degradation mechanisms common in pure and blended devices, including AFM images of anode damage in previously operated devices, are given in Chapter 7.

6.8 PDPyDP blends with calcium cathodes

The data discussed in the following section are for devices with a cathode which consisted of a 15 nm layer of calcium protected by a 100 nm layer of aluminium, both thermally evaporated.

6.8.1 Current-voltage and light-voltage characteristics

Current-voltage and light-voltage characteristics are shown in Figure 6.10.

This plot indicates that the benefit of blended layers was less significant in calcium-cathode devices than aluminium-cathode devices (Figure 6.7). The major advantage in using calcium cathodes was the improved match between the Fermi level of the cathode (-2.9 eV) and the LUMO of the MEH-PPV (-2.8 eV). This improved the balance of electrons and holes, making more pairs available for recombination. Other researchers suggested also that the calcium cathode doped the first few monolayers of the conjugated polymer such that the interface was no longer sensitive to the Fermi level of the metal [30, 31].

The pure MEH-PPV devices emitted more light than any of the other devices with calcium cathodes. As the proportion of PDPyDP increased, the conductivity and light emission reduced. The already small energy barrier (0.1 eV) for electron injection between calcium and MEH-PPV meant that the PDPyDP did not provide the intermediate energy level

which was so beneficial in aluminium-cathode devices. Furthermore, increasing the proportion of PDPyDP resulted in a corresponding reduction in the quantity of MEH-PPV, which in turn reduced both the hole transport capability and the number of sites for electron-hole recombination. All the blend ratios with more than 20 % PDPyDP emitted negligible quantities of light for this reason.

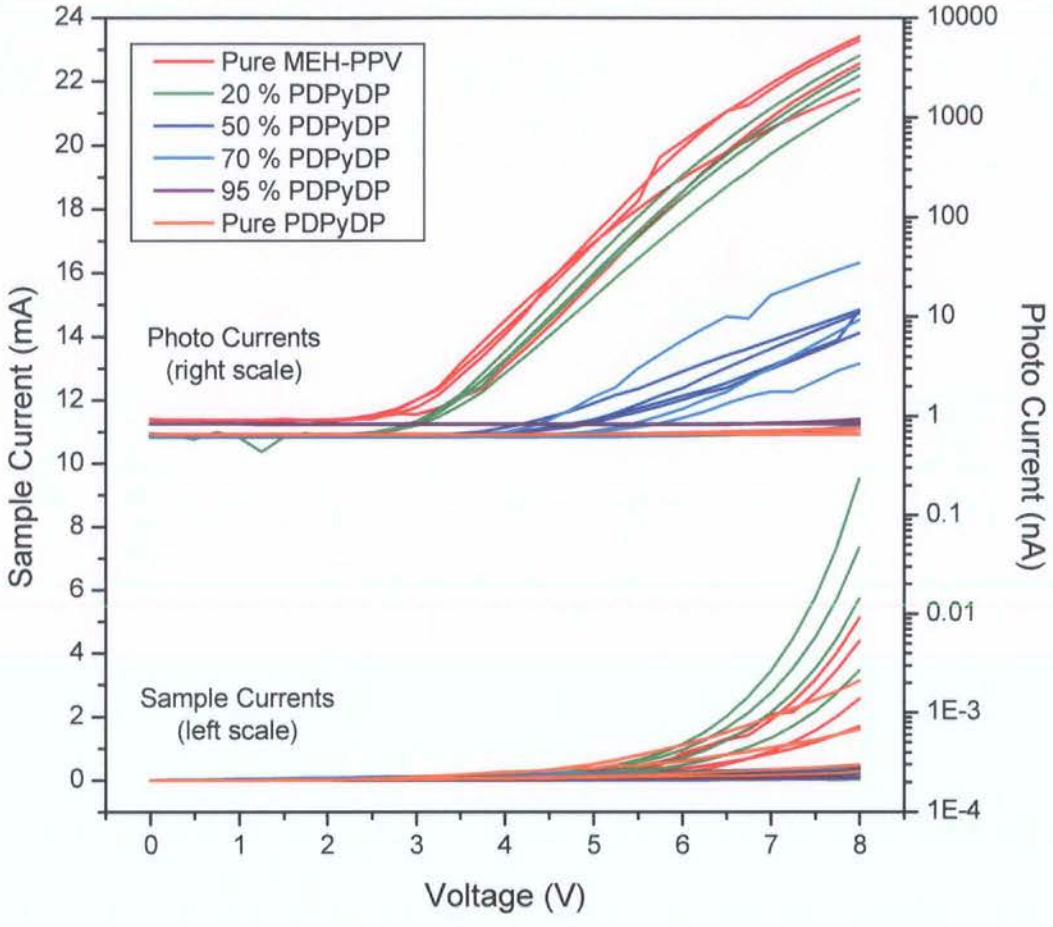

Figure 6.10 I-V and light-voltage characteristics for calcium-cathode devices with varying ratios of PDPyDP : MEH-PPV

6.8.2 Quantum efficiency

Estimates of quantum efficiency were made and are shown plotted against sample current in Figure 6.11. As the devices with higher percentages of PDPyDP produced little light, estimates for the quantum efficiency of these devices were very low.

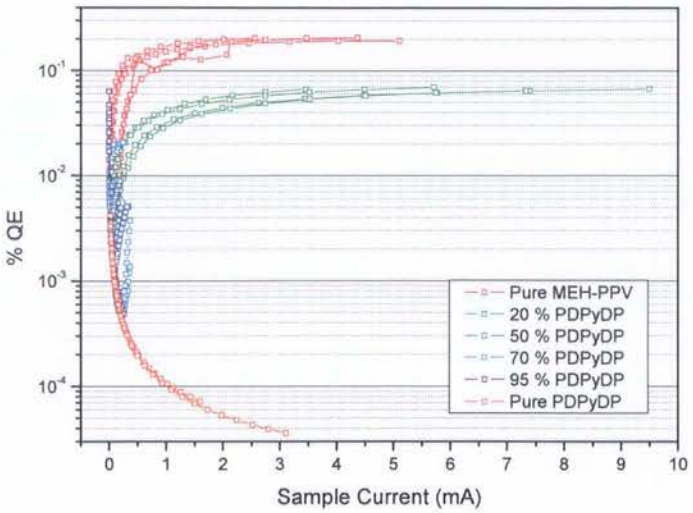

Figure 6.11 QE characteristics for calcium-cathode devices with varying ratios of PDPyDP : MEH-PPV

The quantum efficiency of the pure MEH-PPV devices with calcium cathodes was 2×10^{-1} %, which was 100 times greater than for the aluminium-cathode devices (2×10^{-3} %, Figure 6.8). The magnitude of the difference in quantum efficiency served as a clear illustration of the importance of improving the balance of charge carriers which was achieved through reducing the barriers to charge injection.

In calcium-cathode devices, for the reasons outlined above, the charge flow was most balanced in pure MEH-PPV devices. In aluminium-cathode devices, the balance was best achieved in the 50 % and 70 % blends.

It might have been assumed that a blended device with a calcium cathode would achieve the highest quantum efficiency, but this was not the case because with more than 20 % PDPyDP charge flow became dominated by electrons.

6.8.3 Luminous efficiency

The luminous current efficiency values, at a fixed luminance of 50 cd m^{-2}, are plotted in Figure 6.12. This luminance equates to approximately half of that emitted by a standard computer monitor. The voltage required to achieve a luminance of 50 cd m^{-2} in the 95 % blend and pure PDPyDP devices were so high as to cause total device failure. Hence, there were no data to plot for these devices.

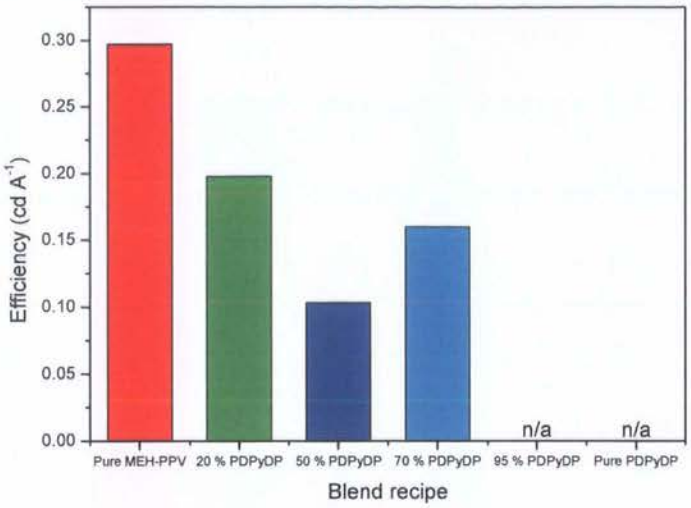

Figure 6.12 Luminous efficiency values at a fixed luminance of 50 cd m^{-2} for calcium-cathode devices with varying ratios of PDPyDP : MEH-PPV

As was discussed in section 3.5.4, quoting in terms of luminous efficiency is increasingly popular as a method for ensuring that values are universally comparable [32]. Though the quantum efficiency data plotted in Figure 6.11 were not assessed at a fixed luminance, they do correspond qualitatively, if not quantitatively, to the luminous efficiencies.

A comparison between these data and those of a commercial developer is made here for the sake of completeness. CDT and Sumation claim an efficiency of 11 cd A^{-1} at a constant luminance of 400 cd m^{-2} for their red phosphorescent devices [33]. Though these values differ considerably from the data obtained in this research, such a difference is to be expected given the multifaceted and highly resourced approaches undertaken in commercial development. By contrast, the data presented here have been obtained using a highly focused approach investigating the effect of blended electroluminescent layers.

On the basis of the evidence relating to light output and quantum efficiency, it would appear that the characteristics of pure MEH-PPV devices with a calcium cathode (sections 6.8.1 to 6.8.3) were similar to those of blended layer devices with an aluminium cathode (sections 6.7.1 and 6.7.2). However, the stability characteristics for these two sets of devices were not at all similar.

6.8.4 Stability

Stability data at a constant current of 0.56 mA are plotted in Figure 6.13. Note the difference in the time-scale between this (5 days) and the equivalent plot for aluminium cathode devices (18 days) shown in Figure 6.9.

Most of the calcium-cathode devices ceased to emit visible light after two days and one device (the 20 % blend) continued to emit light which was just visible after 5 days. These periods were much shorter than those seen for devices with aluminium cathodes. For example, one of the aluminium-cathode blended devices (70 % PDPyDP) emitted visible light continuously for two weeks and another (50 % PDPyDP) for 18 days. These data confirm what has been reported previously, that choice of appropriate cathode material (and thickness) is essential for improving the stability of PLEDs [27].

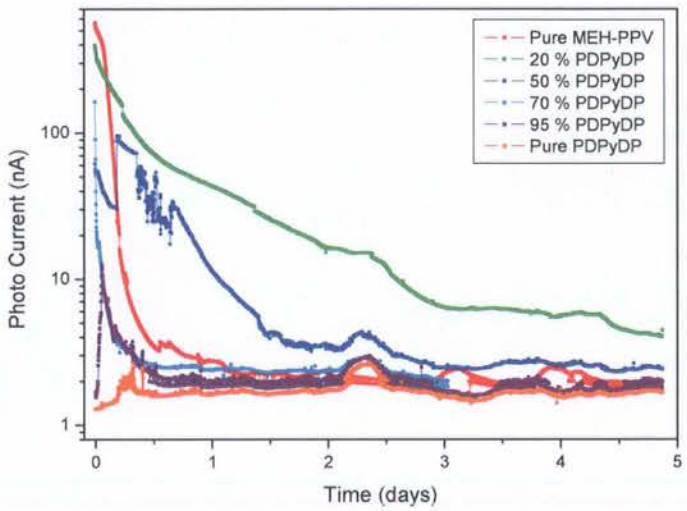

(a)

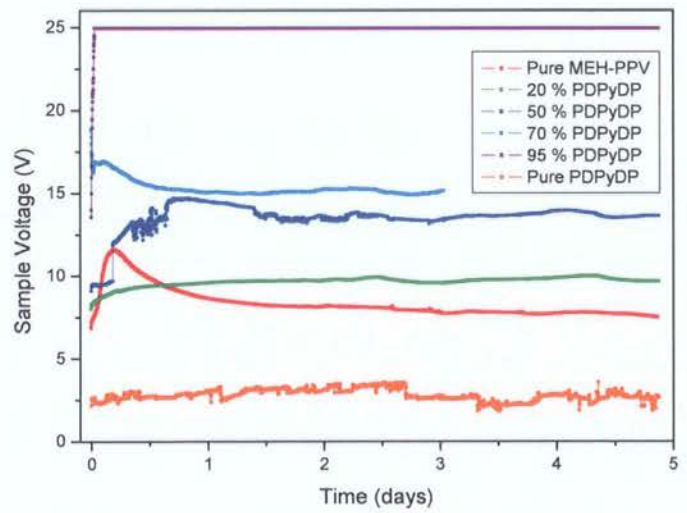

(b)

Figure 6.13 Stability characteristics for calcium-cathode devices with varying ratios of PDPyDP : MEH-PPV: (a) photo-current against time; and (b) sample voltage against time

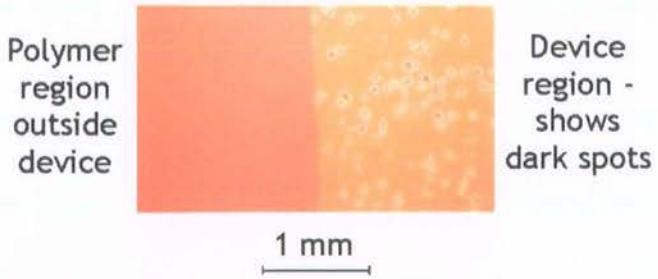

Figure 6.14 Micrograph of a device and the adjacent region taken after a period of continuous operation, which shows many examples of dark spots in the device region and no dark spots outside the device region

It has already been shown that the Fermi level of calcium makes it very suitable as a cathode material. Though it was highly efficient, the stability data reveal that the pure MEH-PPV device with calcium cathodes ceased to emit light after just 12 hours. Comparing Figure 6.9 (a) with Figure 6.13 (a) indicates clearly that the calcium cathode had a negative effect on the stability of the light emission. One reason for this was the diffusion of calcium into the organic film [34]. Also, in general, calcium tends to react with oxygen to produce calcium oxide (CaO), and with water to produce calcium hydroxide ($Ca(OH)_2$) [35]. Neither of these is electrically conductive so any region of the calcium cathode which reacted to form these compounds ceased to conduct. This resulted in a dark spot region from which no light was emitted. An example of a device with dark spots is shown in Figure 6.14. The formation of the metal oxide was not exclusive to the calcium-cathode devices. Aluminium also oxidised (and more rapidly than calcium) but this tended to happen solely at the surface of the film which meant that the effect was less detrimental to the device performance.

6.9 The influence of blends on EL emission spectrum

The electroluminescent spectra for a range of MEH-PPV : PDPyDP blend concentrations are shown in Figure 6.15. Though these are for devices with aluminium cathodes, the cathode material was not seen to influence the device spectra.

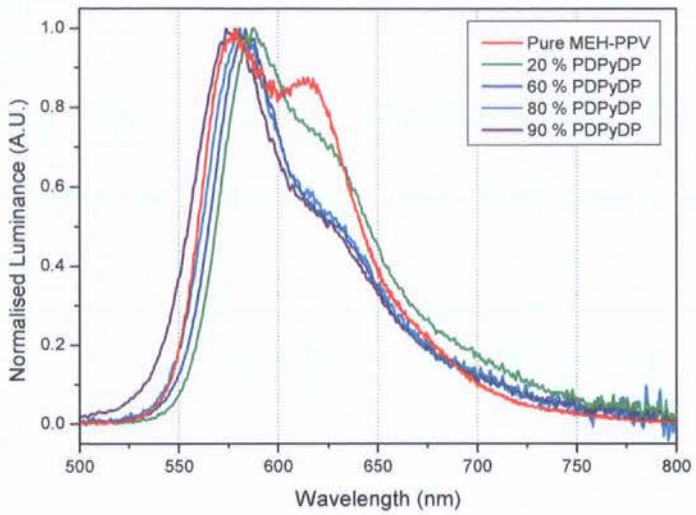

Figure 6.15 Electroluminescent spectra for aluminium-cathode devices with varying ratios of PDPyDP : MEH-PPV

The spectrum emitted by the pure MEH-PPV device is shown in red. Two peaks were present in the curve, the higher of which occurred at approximately 579 nm. The secondary 'shoulder' peak was present at approximately 615 nm and it was almost 0.88 the height of the taller peak. There were two main differences between the spectra emitted by pure MEH-PPV and the blended devices. One was that the spectra emitted by almost all the blended devices were red-shifted by comparison with the pure MEH-PPV. The furthest shift of 10 nm was seen in the 20 % blend, which peaked at 589 nm. The only exception to this was the spectrum from the blend with the highest proportion of PDPyDP (purple curve) which was blue-shifted by 5 nm to peak at 574 nm. The other difference was a change in the shape and relative height of the shoulder. In terms of shape, the pure MEH-PPV had a clear minimum between the main and secondary peaks. In contrast, the shoulders in the spectra for the blended devices were identified only by a change in the gradient of the curve in that region. In terms of height, the shoulders for the blend devices were lower than for the MEH-PPV device, though because of the absence of a clear minimum it was difficult to identify the exact location and height of each shoulder peak. Depending on definition, the shoulder height for the blend devices occurred in the range 0.5 to 0.6 of the spectral peak height.

It has been argued that that the optical (and electrical) properties of MEH-PPV films are influenced by adjusting the morphology or aggregation of the polymer chains [36, 37]. For the devices presented in Figure 6.15, polymer aggregation was influenced by varying the spin speeds and solution densities. A variety of characteristics was observed depending on whether the polymer backbone or side chains were exposed and how the polymer chains

interacted with each other. Different quantities of PDPyDP in electroluminescent blends may also affect the aggregation of MEH-PPV, and therefore the optical properties of the film.

Shi *et al.* proposed a range of factors which had specific influences on the electromagnetic spectra of MEH-PPV films [38]. Two of these provide a convincing explanation of the differences between the spectra shown in Figure 6.15.

One of Shi's arguments was that interchain species (resulting from high aggregation) were more likely to emit in the red region (~ 615 nm). It would therefore be expected that increasing the proportion of PDPyDP, which reduced the polymer aggregation, would reduce the red emission. This was the case. Figure 6.15 shows that the pure MEH-PPV, being the film with the highest aggregation, had the greatest red emission. Conversely, the device with the highest proportion of PDPyDP, and hence the lowest aggregation, had the least red emission.

The second of Shi's observations was that films spun at lower speeds had yellow dominated emission. For the sake of experimental consistency, it was considered important to maintain the same film thicknesses across the range of blended devices investigated in this thesis. The solutions with higher proportions of PDPyDP had lower viscosity and, therefore, required slower spin speeds. The peak at the yellow end of each spectrum (occurring in the range 574 nm to 579 nm) was increasingly yellow-shifted with higher proportions of PDPyDP. It was least yellow for the 20 % PDPyDP blend device and most yellow for the 90 % blend device. This concurs with Shi's relationship between spin speed and yellow emission. It was not obvious why the pure MEH-PPV device was more yellow than almost all the blend devices, but this might be attributed to the much greater polymer aggregation (*vide supra*).

6.10 Conclusions

The most obvious benefit of employing blended electroluminescent layers was the ability to influence the light output, efficiency and stability of light emission. Calcium rather than aluminium cathodes were seen to provide similar benefits to blends in terms of light output and efficiency. However, calcium-cathode devices were shown to have less stability of light emission than blended devices with aluminium cathodes. Of the devices considered in this Chapter, the 50 % PDPyDP blend device with an aluminium cathode gave the best combination of light output, efficiency and stability of light emission. Compared with the

equivalent unblended device, the 50 % blend had 40 times greater light emission, 35 times higher efficiency, and it emitted light for more than two weeks as opposed to tens of minutes. The benefits of blending are therefore shown to be significant across the three most widely compared characteristics.

6.11 References

1 P.W.M. Blom, M.J.M. de Jong, C.T.H.F. Liedenbaum and J.J.M. Vleggaar, *Device characteristics of polymer light-emitting diodes.* Synthetic Metals, 85, 1287 (1997).

2 S. Naka, K. Shinno, H. Okada, H. Onnagawa, and K. Miyasita, *Organic electroluminescent devices using a mixed single layer.* Japanese Journal of Applied Physics, Part 2, 33, L1772 (1994).

3 Y. Cao, I.D. Parker, G. Yu, C. Zhang and A.J. Heeger, *Improved quantum efficiency for electroluminescence in semiconducting polymers.* Nature 397, 414 (1999).

4 I.N. Kang, D.H. Hwang, H.K. Shim, T. Zyung and J.J. Kim, *Highly improved quantum efficiency in blend polymer LEDs.* Macromolecules, 29, 165 (1996).

5 J.H. Burroughes, D.D.C. Bradley, A.R. Brown, R.N. Marks, K. Mackay, R.H. Friend, P.L. Burns and A.B. Holmes, *Light-emitting diodes based on conjugated polymers.* Nature 347, 539 (1990).

6 D. Braun and A.J. Heeger, *Visible light emission from semiconducting polymer diodes.* Applied Physics Letters, 58, 1982 (1991).

7 F.Z. Shen, F. He, D. Lu, Z.Q. Xie, W.J. Xie, Y.G. Ma and B. Hu, *Bright and colour stable white polymer light-emitting diodes.* Semiconductor Science and Technology, 21, L16 (2006).

8 L. Bozano, S.A. Carter, J.C. Scott, G.G. Malliaras and P.J. Brock, *Temperature- and field-dependent electron and hole mobilities in polymer light-emitting diodes.* Applied Physics Letters, 74, 1132 (1999).

9 I.H. Campbell, T.W. Hagler, D.L. Smith and J.P. Ferraris, *Direct measurement of conjugated polymer electronic excitation energies using metal/polymer/metal structures.* Physical Review Letters, 76, 1900 (1996).

10 I.D. Parker, *Carrier tunneling and device characteristics in polymer light-emitting diodes.* Journal of Applied Physics, 75, 1656 (1994).

11 C.S. Wang, G.Y. Jung, Y.L. Hua, C. Pearson, M.R. Bryce, M.C. Petty, A.S. Batsanov, A.E. Goeta and J.A.K. Howard, *An efficient pyridine- and oxadiazole-containing hole-blocking material for organic light-emitting diodes: synthesis, crystal structure, and device performance.* Chemistry of Materials, 13, 1167 (2001).

12 G. Hughes, M.R. Bryce, *Electron-transporting materials for organic electroluminescent and electrophosphorescent devices.* Journal of Materials Chemistry, 15, 94 (2005).

13 S. Oyston, C. Wang, G. Hughes, A.S. Batsanov, I.F. Perepichka, M.R. Bryce, J.H. Ahn, C. Pearson and M.C. Petty, *New 2,5-diaryl-1,3,4-oxadiazole–fluorene hybrids as electron transporting materials for blended-layer organic light emitting diodes.* Journal of Materials Chemistry, 15, 194 (2005).

14 I.F. Perepichka, personal communication, 7th July 2006.

15 G.G. Malliaras, J.R. Salem, P.J. Brock, and J.C. Scott, *Electrical characteristics and efficiency of single-layer organic light-emitting diodes.* Physical Review B, 58, 13411 (1998).

16 Y. Shi, J. Liu and Y. Yang, Organic-light emitting devices, A survey, Springer-Verlag New York, page 168 (2004).

17 P. Cea, Y. Hua, C. Pearson, C. Wang, M.R. Bryce, M.C. Lopez, and M.C. Petty, *A blended layer MEH-PPV electroluminiscent device incorporating a new electron transport material.* Materials Science and Engineering C, 22, 87 (2002).

18 S.H. Kim, H.Y. Chu, T. Zyung, L.-M. Do, D.-H. Hwang, *The growth mechanism of black spots in polymer EL device.* Synthetic Metals 111–112, 253 (2000).

19 J.G. Simmons and R.R. Verderber, *New conduction and reversible memory phenomena in thin insulating films.* Proceedings of the Royal Society of London Series A - Mathematical and Physical Sciences 301, 77 (1967).

20 I.N. Kang, D.H. Hwang, H. K. Shim, T. Zyung and J.J. Kim, *Highly improved quantum efficiency in blend polymer LEDs.* Macromolecules, 29, 165 (1996).

21 B.H. Cumpston and K.F. Jensen, *Photo-oxidation of polymers used in electroluminescent devices.* Synthetic Metals, 73, 195 (1995).

22 B.H. Cumpston, I.D. Parker and K.F. Jensen, *In situ characterization of the oxidative degradation of a polymeric light emitting device.* Journal of Applied Physics, 81, 3716 (1997).

23 M. Atreya, S. Li, E.T. Kang, K.G. Neoh, Z.H. Ma, K.L. Tan and W. Huang, *Stability studies of poly(2-methoxy-5-(2'-ethyl hexyloxy)-p- (phenylene vinylene) [MEH-PPV].* Polymer Degradation and Stability, 65, 287 (1999).

24 S.H. Kwon, S.Y. Paik, O.J. Kwon and J.S. Yoo, *Triple-layer passivation for longevity of polymer light-emitting diodes.* Applied Physics Letters, 79, 4450 (2001).

25 G.H. Kim, J. Oh, Y.S. Yang, L.M. Do and K.S. Suh, *Encapsulation of organic light-emitting devices by means of photopolymerized polyacrylate films.* Polymer, 45, 1879 (2004).

26 M.S. Weaver, L.A. Michalski, K. Rajan, M.A. Rothman, J.A. Silvernail, J.J. Brown, P.E. Burrows, G.L. Graff, M.E. Gross, P.M. Martin, M. Hall, E. Mast, C. Bonham, W. Bennett and M. Zumhoff, *Organic light-emitting devices with extended operating lifetimes on plastic substrates.* Applied Physics Letters, 81, 2929 (2002).

27 Y. Cao, G. Yu, I.D. Parker and A.J. Heeger, *Ultrathin layer alkaline earth metals as stable electron-injecting electrodes for polymer light emitting diodes.* Journal of Applied Physics, 88, 3618 (2000).

28 B.H. Cumpston and K.F. Jensen, *Electromigration of aluminum cathodes in polymer-based electroluminescent devices.* Applied Physics Letters, 69, 3941 (1996).

29 V.N. Savvate'ev, A.V. Yakimov, D. Davidov, R.M. Pogreb, R. Neumann and Y. Avny, *Degradation of nonencapsulated polymer-based light-emitting diodes: Noise and morphology.* Applied Physics Letters, 71, 3344 (1997).

30 Y. Park, V. Choong, E. Ettedgui, Y. Gao, B.R. Hsieh, T. Wehrmeister and K. Müllen, *Degradation of nonencapsulated polymer-based light-emitting diodes: Noise and morphology.* Applied Physics Letters, 69, 1080 (1996).

31 J.M. Bharathan and Y. Yang, *Polymer/metal interfaces and the performance of polymer light-emitting diodes.* Journal of Applied Physics, 84, 3207 (1998).

32 S.R. Forrest, D.D.C. Bradley and M.E. Thompson, *Measuring the Efficiency of Organic Light-Emitting Devices.* Advanced Materials, 15, 1043 (2003).

33 Cambridge Display Technology Press Release, *CDT Sees Further Rapid Progress In Polymer Lifetime Development*, 13th March 2006.

34 M.C. Suha, H.K. Chung, S.Y. Kimb, J.H. Kwonc and B.D. Chin, *Cathode diffusion and degradation mechanism of polymeric light emitting devices.* Chemical Physics Letters, 413, 205 (2005).

35 K.K. Lin, S.J. Chua, W. Wang and S.F. Lim, *Influence of electrical stress voltage on cathode degradation of organic light-emitting devices.* Journal of Applied Physics, 90, 976 (2001).

36 Y. Shi, J. Liu, and Y. Yang, *Device performance and polymer morphology in polymer light emitting diodes: The control of thin film morphology and device quantum efficiency.* Journal of Applied Physics, 87, 4254 (2000).

37 J.W. Blatchford, S.W. Jessen, L.B. Lin, T.L. Gustafson, D.K. Fu, H.L. Wang, T.M. Swager, A.G. MacDiarmid, and A.J. Epstein, *Photoluminescence in pyridine-based polymers: Role of aggregates.* Physical Review B, 54, 9180 (1996).

38 Y. Shi, J. Liu and Y. Yang, Organic-light emitting devices, A survey, Springer-Verlag New York, pages 177-180 (2004).

Chapter Seven

Organic LEDs derived from blends of the electroluminescent polymer MEH-PPV and the electron transporting molecule KTK34

7.1 Introduction

Following the experiments on blended PDPyDP : MEH-PPV devices a new material, KTK34, was developed for use in MEH-PPV blends. Experiments were carried out to investigate the electrical, light emission, efficiency and stability characteristics of each device. The devices are compared with the MEH-PPV : PDPyDP blend devices presented in Chapter 6. A short summary of common degradation mechanisms is given. It is proposed that there are preferential degradation mechanisms for different blend ratios. Although devices with high proportions of KTK34 potentially benefited from nano-encapsulation of the emissive polymer, these devices suffered more from electromigration of the ITO into the polymer blend.

7.2 KTK34 chemical structure

KTK34 is a blue-emitting electron transport material with the chemical structure shown in Figure 7.1. Its electron transporting ability is derived from the electron-deficient 1,3,4-oxadiazol unit, at the centre of the molecule, which is known for its high chemical and thermal stability [1]. Fluorene is also known for its high chemical and thermal stability as well as for its high photoluminescent quantum yields. The molecule includes two fluorene units, which are represented in the structure diagram by the three conjoined polygons at both ends. KTK34 was synthesised in the Chemistry Department at Durham University from commercially available starting materials in five steps.

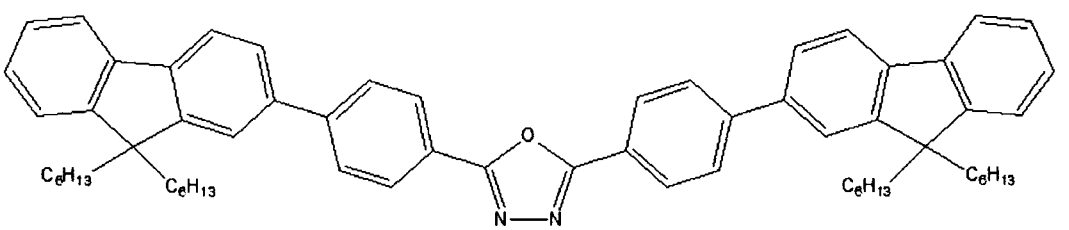

Figure 7.1 Chemical structure of KTK34

Analysis revealed that the HOMO occurred at -5.9 eV and the LUMO occurred at -2.8 eV. When analysed by the same method, the equivalent levels for PDPyDP were -6.2 eV and -2.5 eV, respectively. Therefore, the HOMO and LUMO of KTK34 are better aligned than those of PDPyDP to the Fermi levels of the electrode materials and to the HOMO and LUMO levels of MEH-PPV.

The purity of KTK34 was assessed by elemental analysis which showed the following proportions: C: 86.86 %; H: 8.46 %; and N: 3.20 %. The calculated values were

C: 86.63 %; H: 8.41 %; and N: 3.16 %. Therefore the errors for each element (C: 0.23 %; H: 0.05 %; and N: 0.04 %) were within the maximum permitted for publication (0.3 %).

7.3 Energy levels

Figure 7.2 shows the energy levels of the KTK34 together with those of other materials used in the devices described in this chapter. KTK34 was selected as the electron transport material to replace PDPyDP because its estimated HOMO and LUMO levels are closer to the Fermi levels of the electrodes. (The HOMO and LUMO of PDPyDP were -6.2 eV and -2.5 eV, respectively.)

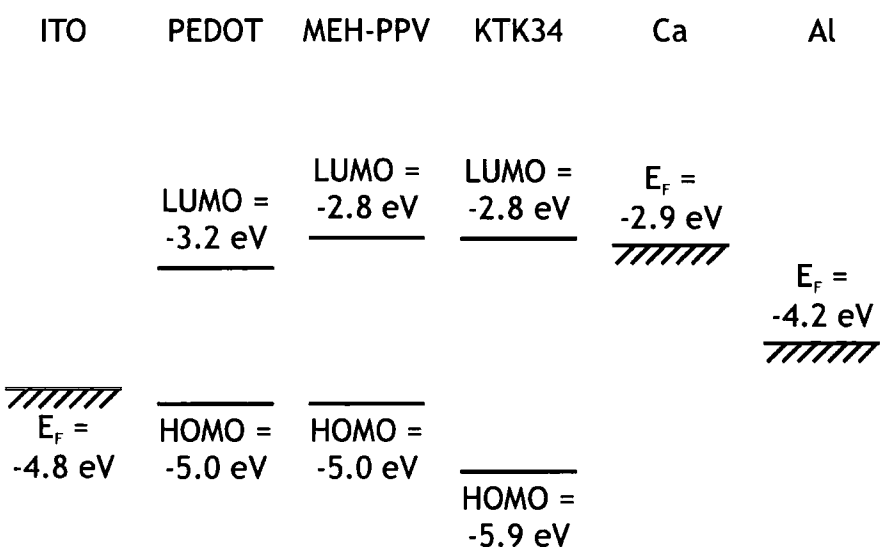

Figure 7.2 Energy level diagram

7.4 Device fabrication

Devices were fabricated using the techniques described in Chapter 3. The anode material was ITO with approximate sheet resistance of 7.8 Ω □ $^{-1}$.

A layer of PEDOT:PSS was used between the ITO and the polymer blend layer in all devices. 200 μl of PEDOT:PSS solution diluted with 50 % pure water was applied to each substrate and spun at 1500 rpm for 60 s. The devices were placed in a vacuum at 10^{-1} mbar for 1 h to remove residual water vapour before applying the blended polymer layer.

Device cathodes were formed either by evaporating a 100 nm layer of aluminium or by evaporating a 15 nm layer of calcium followed by a 100 nm layer of aluminium.

7.4.1 Blended layers

The electroluminescent layer of each device was formed from a mixture of KTK34 and MEH-PPV. The proportion of each material was measured by weight when solid. Solutions were formed in chloroform and spin coated to form the electroluminescent film on top of the PEDOT:PSS layer.

The solution ratios, concentrations and spin speeds for each of the KTK34 : MEH-PPV blends are listed in full in Table 7.1. The solution concentration and spin speed for each blend ratio were deduced by iterative experimental testing so as to achieve similar film thicknesses and qualities across the range of blends. The average film thickness was 100 nm. A photograph showing devices incorporating the full range of electroluminescent films is shown in Figure 7.3.

Ratio of KTK34 : MEH:PPV by weight	Solution concentration	Spin speed
0 : 100	6.67 mg ml^{-1}	1000 rpm
20 : 80	8.75 mg ml^{-1}	1000 rpm
50 : 50	12 mg ml^{-1}	1000 rpm
70 : 30	13.33 mg ml^{-1}	750 rpm
95 : 5	15 mg ml^{-1}	750 rpm
100 : 0	16 mg ml^{-1}	750 rpm

Table 7.1 Solution ratios, concentrations and spin speeds for blends of MEH-PPV and KTK34

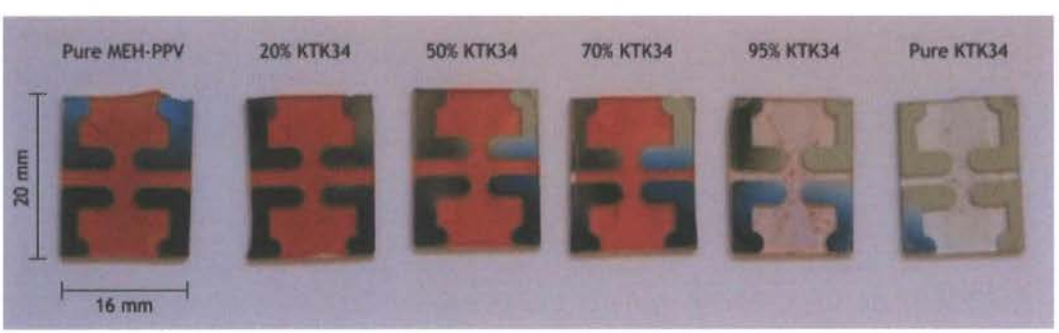

Figure 7.3 Photograph showing the range of pure and blended electroluminescent layer devices

(The faint circular marks on the 95 % KTK34 device were not defects in the film but were small regions of polymer material on the underside of the substrate caused where the substrate was fastened to the vacuum chuck of the spin-coater.)

7.5 KTK34 blends with aluminium cathodes

For the devices described in this section, each electroluminescent layer was produced by spin coating one of the blended solutions described above. The cathode layer was formed from a single 100 nm layer of thermally evaporated aluminium.

7.5.1 Current-voltage and light-voltage characteristics

Current-voltage (I-V) and light-voltage characteristics were measured between 0 V and 20 V and data are plotted in Figure 7.4. As with some of the earlier plots, the individual data points (taken at 0.25 V intervals) are not shown for the sake of clarity.

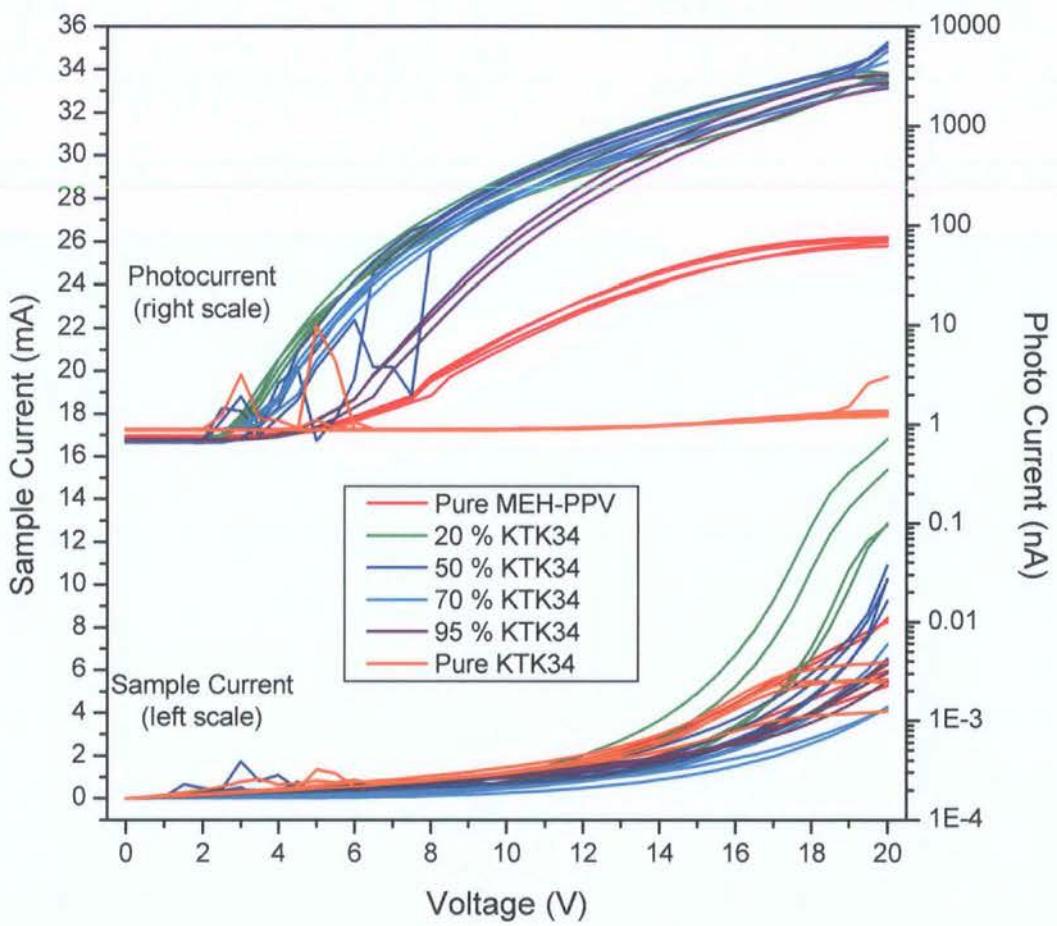

Figure 7.4 I-V and light-voltage characteristics for aluminium-cathode devices with varying ratios of KTK34 : MEH-PPV

These data follow the same trends as those for the equivalent blended PDPyDP devices with some minor differences. As with the PDPyDP blends, the greatest benefit of the KTK34 blends over pure MEH-PPV was the increase in light emission by up to two orders of magnitude. This was due to an improved balance of electrons and holes in the emissive layer, which resulted in more electron-hole pairs for recombination and light emission. At 20 V, the pure MEH-PPV devices generated an average photo-current of approximately 80 nA. The most light emission came from the 50 % blend devices which generated an average photo-current of 8,000 nA. Therefore, the best blends provided a 100-fold improvement over the pure MEH-PPV devices. By comparison, the variation between the least and most emissive blend devices was a factor of just three.

As well as the light emission, the current was also influenced by the blending of the polymer layer. At maximum voltage the current was between 5 mA and 15 mA across the range of blends. This was the same range of currents as in the PDPyDP blend devices.

As to the differences between KTK34 and PDPyDP blended devices, the proportion of KTK34 seemed to have less of an effect on light emission than the proportion of PDPyDP. In particular, the 95 % PDPyDP device emitted two orders of magnitude less than the other PDPyDP blends, but the 95 % KTK34 was a similar brightness to the other KTK34 blends. This suggests that varying the proportion of KTK34 in aluminium cathode devices did not significantly influence the electron-hole balance. This may be because, with the energy levels of KTK34 being better aligned to MEH-PPV, any proportion of KTK34 was enough to cause relatively balanced flow of electrons and holes.

The pure KTK34 devices were electrically conductive but did not emit visible light, which suggests that the current in these devices was exclusively through the flow of electrons.

By blending MEH-PPV with KTK34 the minimum voltage to achieve light output was reduced. The turn-on voltage for the 20 %, 50 % and 70 % blends was between 2.5 V and 3.5 V but the pure MEH-PPV devices did not emit light below 6 V. The turn-on voltage was most likely influenced by charge carrier injection [2]. Though the LUMO levels of MEH-PPV and KTK34 are both estimated as -2.8 eV, these values are approximate. (For more detailed information see the discussion in section 6.2.) The LUMO level of KTK34 may be below that of MEH-PPV. This would be consistent with the presence of KTK34 lowering the turn-on voltage of the device by reducing the effective barrier to injection of electrons.

7.5.2 Quantum efficiency characteristics

The I-V and light-voltage data were used to estimate values for quantum efficiency which are plotted against sample current in Figure 7.5.

The 50% and 70% blends gave the highest quantum efficiencies of approximately 10^{-1} %. This represented a 65-fold increase on the pure MEH-PPV devices. The equivalent improvement factor for PDPyDP blend devices was 35 times. Both KTK34 and PDPyDP provided increased electron transport compared with pure MEH-PPV. However, unlike the PDPyDP, the energy levels of the KTK34 were well matched to the adjacent layers. Therefore, much less energy was required to inject carriers into the KTK34 blend devices.

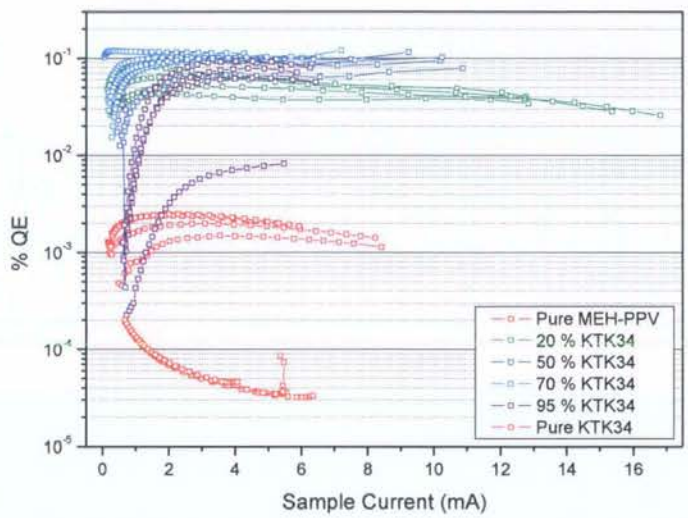

Figure 7.5 QE characteristics for aluminium-cathode devices with varying ratios of KTK34 : MEH-PPV

Compared to the PDPyDP devices, there was less spread in the QE values across the range of blends. This was also attributed to the better energy level matching of the KTK34 to the electrodes (which was similar regardless of blend ratio) rather than to the improved electron transport (which was proportional to the ratio of KTK34 in the blend).

7.5.3 Stability characteristics

Stability tests were performed at a constant current of 0.56 mA. The photo-currents (proportional to light emission) and voltages are shown against time in Figure 7.6 (a) and (b), respectively. The 50 % device was the most stable, as was the 50 % PDPyDP device with aluminium cathodes shown in Figure 6.9. (Note that Figure 7.6 and Figure 6.9 have different time scales.)

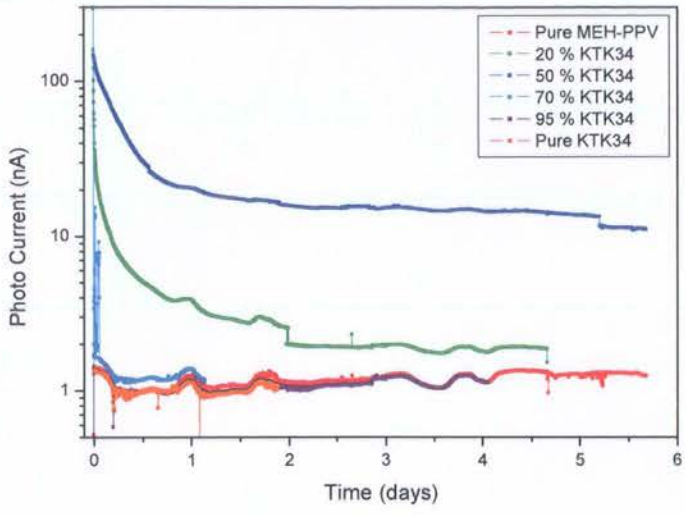

(a)

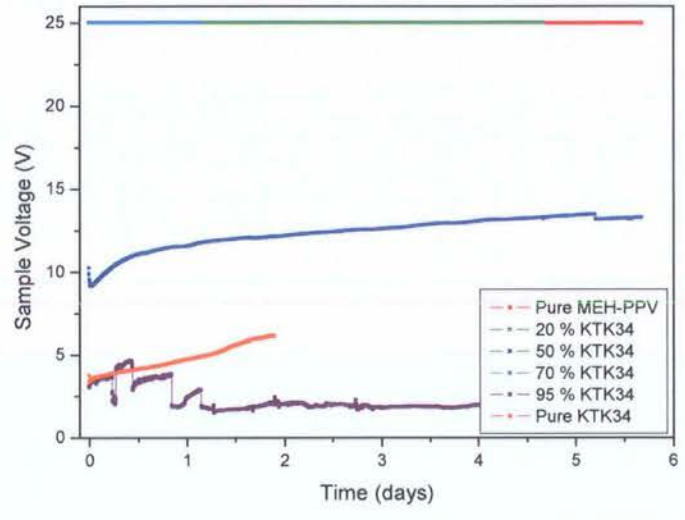

(b)

Figure 7.6 Stability characteristics for aluminium-cathode devices with varying ratios of KTK34 : MEH-PPV: (a) photo-current against time; and (b) sample voltage against time

Of all the KTK34 blends with aluminium cathodes, the 50 % KTK34 blend was the only device with visible light emission not to reach the 25 V threshold immediately. The constant current feedback circuit in the measurement apparatus increased the voltage across the 20 % and 70 % blend devices to 25 V within the first few minutes of the stability test. Once the threshold was reached, it was unlikely that the 0.56 mA current was maintained. The devices degraded with time, which increased their resistance. Higher resistance at fixed voltage meant lower current, which provided less likelihood of light emission.

A higher proportion of KTK34 or PDPyDP in the blend resulted in an increased probability of surrounding the MEH-PPV polymer chains within the film. The relationship between stability and proportion of the dopant molecule did not hold for high proportions of KTK34 and aluminium cathodes. This may be because any degradation which affected the small proportions of MEH-PPV in the blend caused a sudden and significant imbalance between the flow of holes and electrons, resulting in few opportunities for electron-hole recombination. Although unbalanced charge flow meant that the light emission rapidly became insignificant, the voltage required to maintain the constant current remained relatively low and stable.

In summary, increased light outputs, lower turn-on voltages, and higher quantum efficiencies were achieved by blending MEH-PPV with KTK34 in devices with aluminium cathodes. The increases were attributed to a better electron transport, and a more balanced distribution of electrons and holes.

7.6 KTK34 blends with calcium cathodes

New devices were fabricated with the same blend solutions as those described above but they included a 15 nm layer of calcium between the polymer and the aluminium.

7.6.1 Current-voltage and light-voltage characteristics

The light emission and sample currents for calcium-cathode devices are plotted in Figure 7.7. On average, the pure MEH-PPV devices emitted more light than all of the KTK34 blends. This was opposite to what was seen in the devices with aluminium cathodes (Figure 7.4), where all the blended devices emitted more light than the pure MEH-PPV devices. In addition, the voltages and currents required to provide a particular level of light emission were much less in calcium cathode than aluminium cathode devices. For example, to achieve a photo-current of 1,000 nA in the 50 % KTK34 calcium-cathode device required 7.5 V and 0.5 mA. The same device with an aluminium cathode required 14 V and 2 mA. The currents in Figure 7.7 were the lowest seen in this thesis. This had a positive effect on device stability (*vide infra*).

Another difference between the devices with aluminium and calcium cathodes was the variation in light outputs for the different blend ratios. The blended devices with an aluminium cathode all emitted similar quantities of light (as discussed in Section 7.5.1), but there was considerable variation in light outputs between the different blend ratios when combined with a calcium cathode. The 70 % KTK34 calcium cathode-devices emitted

light averaging 25 nA while the 20 % blend devices emitted light averaging 2,500 nA. Increasing the proportion of KTK34 caused the light emission and current to drop. This was the same relationship as that observed in the PDPyDP blends with calcium cathodes. It was again attributed to the electrons outnumbering the holes because of increased electron injection (calcium cathode) and increased electron transport (KTK34). Higher proportions of KTK34 meant that the current became increasingly dominated by electron flow, which reduced light emission due to the small number of available holes.

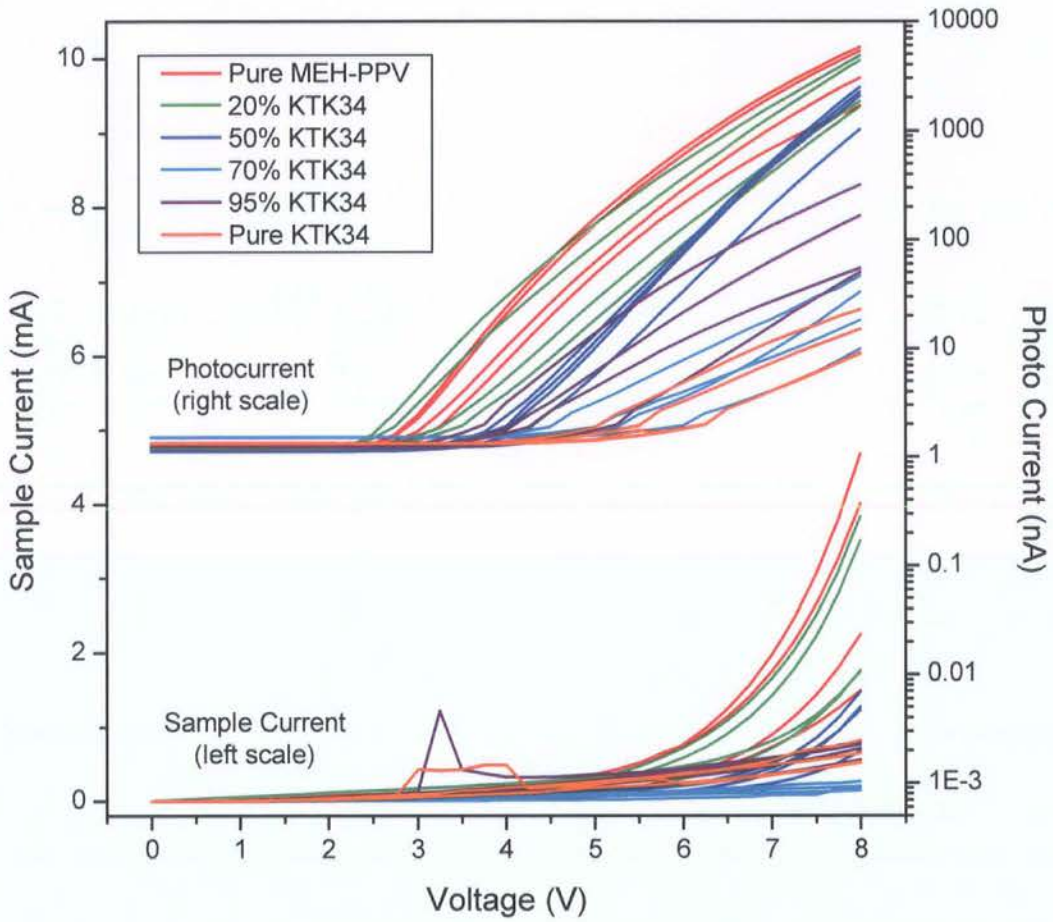

Figure 7.7 I-V and light-voltage characteristics for calcium-cathode devices with varying ratios of KTK34 : MEH-PPV

7.6.2 Quantum efficiency characteristics

Quantum efficiency estimates for calcium cathode devices are plotted in Figure 7.8. The 50 % KTK34 blend devices gave the highest average quantum efficiency of 0.25 %. This was, however, only slightly greater than that for the pure MEH-PPV devices (0.20 %). There was relatively little variation between the quantum efficiency values for pure MEH-PPV devices and the 20 % and 50 % blends. This suggests that the balance of holes and electrons was fairly similar for these emissive layers. By increasing the content of

KTK34 beyond 50 % there was an imbalance of carriers, as indicated by the reductions in quantum efficiency and light emission.

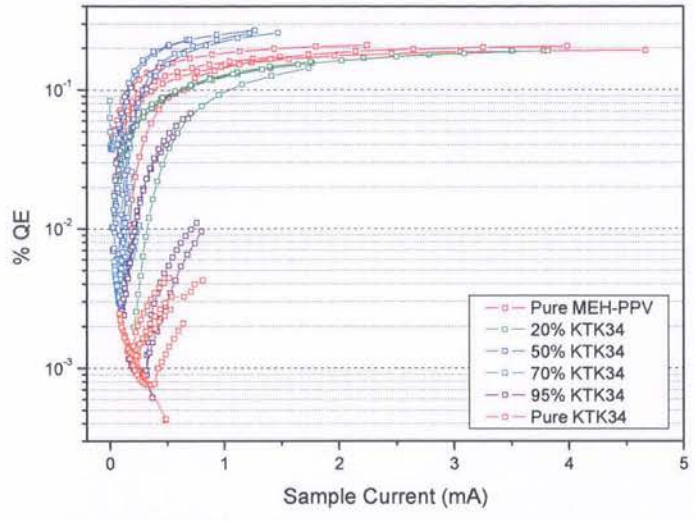

Figure 7.8 QE characteristics for calcium-cathode devices with varying ratios of KTK34 : MEH-PPV

7.6.3 Stability characteristics

The light output and voltage data obtained from constant current (0.56 mA) stability tests of calcium-cathode devices are shown in Figure 7.9 (a) and (b), respectively. (These graphs have different scales to the equivalent plots for KTK34 blends with aluminium cathodes which are shown in Figure 7.6.)

In general, the calcium-cathode devices were more stable than their aluminium-cathode counterparts. This suggested that there was a more significant factor influencing lifetime than the susceptibility of calcium to form insulating compounds. The data also indicated that the increased stability was related to the lower voltages and currents. Of all the KTK34 blends with calcium cathodes only one reached the voltage limit during the 11 day period. In contrast, three of the aluminium-cathode devices reached the maximum within a matter of minutes. Furthermore, after six days all except one of the aluminium-cathode devices had ceased emitting a visible light output, but three of the calcium-cathode devices continued emitting after the same length of time.

The I-V and light-voltage curves for aluminium- and calcium-cathode devices (Figure 7.4 and Figure 7.7, respectively) show that the calcium-cathode devices gave greater light emission at lower voltages and lower currents. Therefore the calcium-cathode devices experience smaller electric fields and current densities. As these factors are known to

accelerate device degradation, the fact that they were smaller explains the relatively high stability of the devices with calcium cathodes.

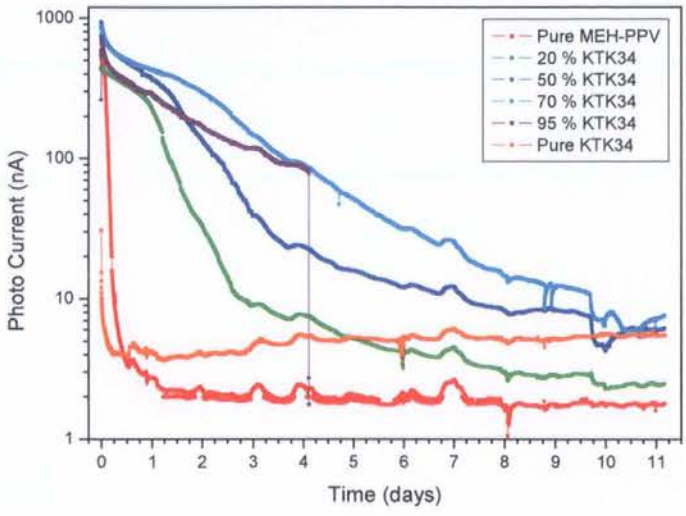

(a)

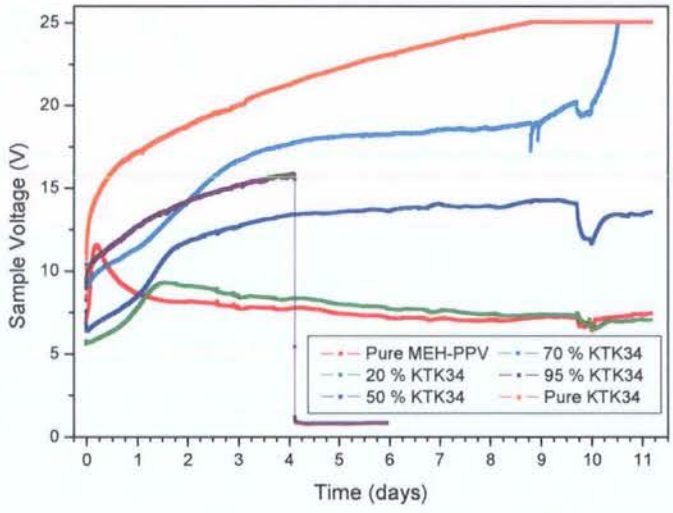

(b)

Figure 7.9 Stability characteristics for calcium-cathode devices with varying ratios of KTK34 : MEH-PPV: (a) photo-current against time; and (b) sample voltage against time

For devices presented up to this point in the thesis it was considered misleading to compare half-life values (see discussion in Section 6.7.3). In the case of KTK34 blend devices with calcium cathodes it is legitimate and meaningful to consider half-lives because: (a) the devices all emitted a visible quantity of light at the half-life stage; (b) they began emitting light at approximately the same level; and (c) the voltage limit was not reached within the half-life period. Half-life data are plotted in Figure 7.10.

Half-life is the measure of stability which has been adopted most widely by commercial organisations. In March 2006, CDT and Sumation published data relating to their red phosphorescent devices in which they quoted a half-life of 50,000 h [3]. By contrast, the most stable KTK34 blend device had a half life of 63 h. Though, clearly, this indicates a difference in stability of orders of magnitude this is not unexpected since the approach adopted in this research is almost exclusively based on the effect of blended electroluminescent layers whereas the approach of commercial organisations is more wide-ranging.

More significant than the comparison with commercial devices is that the half-life data clearly indicate a relationship between increased proportion of KTK34 and increased stability. The 95 % KTK34 blend device with a calcium cathode had the longest half-life of 63 h which is more than an order of magnitude better than the comparable unblended device. Furthermore, the fact that greater proportions of KTK34 lead to longer half-lives gives additional weight to the concept of nano-encapsulation.

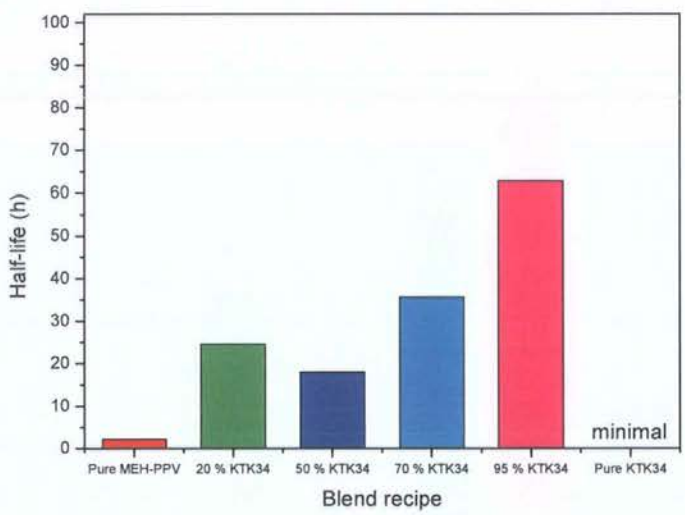

Figure 7.10 Half-life data for calcium-cathode devices with varying ratios of KTK34 : MEH-PPV

7.7 The influence of blends on EL emission spectrum

Figure 7.11 shows the electroluminescent spectra for the KTK34 pure and blend devices with aluminium cathodes. The cathode material made little discernable difference to the device spectra.

As discussed in Chapter 6, the standard MEH-PPV electroluminescent spectrum included two peaks. The larger one occurred at a wavelength of approximately 579 nm and a

smaller 'shoulder' peak appeared in the region of 615 nm. The spectra for all the blends followed the same basic shape with variation in the relative peak heights and in the width of the shoulder.

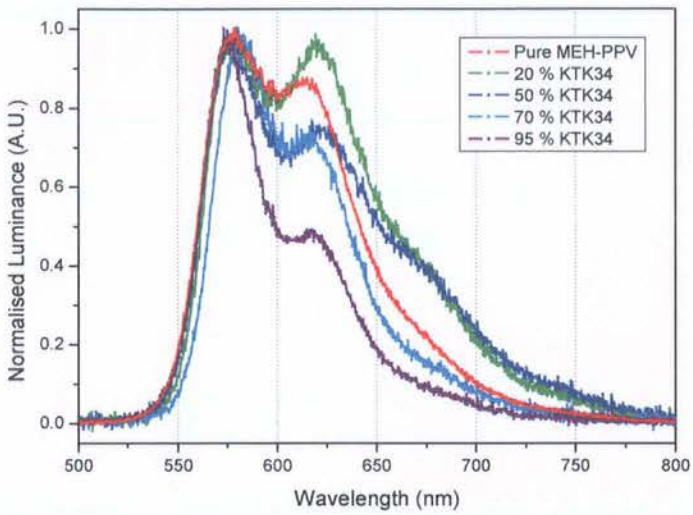

Figure 7.11 Electroluminescent spectra for aluminium-cathode devices with varying ratios of KTK34 : MEH-PPV

Also discussed in Chapter 6 were the findings of Shi *et al.* who suggest that the morphology or aggregation of polymer chains has a great effect on the emission spectrum [4, 5]. Compared with the electroluminescent spectra for PDPyDP blend devices (Figure 6.15) the secondary, or shoulder, peaks were more pronounced. This suggests that the aggregation of the MEH-PPV when blended with KTK34 was tighter than when blended with PDPyDP. The same fabrication conditions were applied for the equivalent KTK34 and PDPyDP blends, so the difference in aggregation could not be attributed to processing. This suggests that the difference was related to the direct influence of the two small molecules (KTK34 or PDPyDP) on the MEH-PPV. The tighter aggregation suggests that blends of MEH-PPV and KTK34 were formed of clusters of MEH-PPV and groups of KTK34 rather than an even distribution of both materials. Uneven blending may be beneficial for light output and carrier transport. A cluster of only one material promoted the flow of one charge carrier over another. The interface of a polymer cluster with a small molecule cluster provided a focal point for electron-hole recombination and photon emission. This theory has implications for the nano-encapsulation concept. Either the clusters were sufficiently small such that the nano-encapsulation occurred on the scale of clusters of polymer chains (rather than individual ones) or the clusters were large enough to mean that the nano-encapsulation effect was not as significant in these devices as in the PDPyDP blends.

Unlike for the PDPyDP blend devices, there was little variation in the location of the peak emission in the region of 580 nm. Shi's observation that lower spin speeds resulted in yellow dominated emission [5] does not appear to be replicated in these devices. This may be because the film properties were influenced more by the uneven mix of MEH-PPV with KTK34 than by the speed at which the film was spin coated.

7.8 Introduction to degradation in OLEDs

It is well known that OLEDs are prone to undergo a variety of physical and chemical changes which reduce their ability to produce light. Some of these changes occur during device operation and others take place even when the device is not in use.

Theories have been proposed to explain the nature of many of these degradation mechanisms. The very fact that OLEDs have been so long in coming to the market (particularly in applications where long lifetime is a critical requirement) suggests that the mechanisms are not sufficiently understood The number of variables involved in the fabrication of an OLED is very large. Also, there is often discrepancy in device behaviour even when every effort has been made to eliminate variation between devices. In combination, these factors make it a complex task to isolate individual causes for particular degradation mechanisms.

The individual degradation mechanisms proposed in the literature are many and varied. Some mechanisms are said to occur as a result of inherent instability of a material under certain conditions, and some are said to arise because of a defect such as a pin hole or a fragment of some contaminant material. Presented below is a summary of commonly reported degradation mechanisms.

- Chemical degradation of the organic emissive material is common. In PLEDs, photo-oxidation of the polymer, through exposure to light and oxygen, breaks the double bond, thereby destroying the extended conjugation in the polymer chain [6, 7]. Destruction of bonds reduces both the potential for carrier transport and the light generated. This mechanism is particularly rapid if the range of wavelengths in which the polymer is prone to photo-oxidation overlaps with the spectrum generated by the device [8]. Cross-linking of the polymer has also been observed independent of photo-oxidation, and has the effect of reducing conjugation length which limits the flow of charge carriers [9].

- Electromigration or diffusion of cathode materials including aluminium [10] and calcium [11] has been observed. This mechanism is more rapid than photo-oxidation and is thought to be induced by regions of high current density. As with much undesirable PLED behaviour, it is initiated by a defect in the polymer film such as an unduly thin region or pin hole. These defects influence the conductivity of the region resulting in high current densities which can be sufficient to induce electromigration of the cathode. Electromigrated metal can lead to short circuits, which may subsequently heal if electromigration is such that the region becomes electrically isolated. 'Healing' of these defects is well reported [12].

- Regions of high surface roughness in the ITO have been cited as initiators of non-emissive areas [13]. Spikes on the ITO surface cause regions of high field which could be responsible for initial local electrical shorts. The local high temperature could melt the polymer and form a channel for the indium to migrate.

- Regions which cease to emit light are known as 'dark spots' or 'black spots'. Studies have found that the nucleation points for these dark spots are particles of contaminant which give rise to pin holes in the polymer film [14]. Pin holes allow the penetration of oxygen and water vapour which can affect both the polymer and the cathode. Electrode metals react with these materials. As stated previously (Section 6.8.4), calcium reacts with oxygen and water [15]. As well as being electrically insulating, the resulting materials cause the polymers to corrode. Most often the black spots arise where, because of the chemical reactions, delamination occurs at the metal / polymer interface [16].

Methods suggested for reducing the prevalence of degradation mechanisms are many and more varied than the mechanisms themselves.

7.9 Anode degradation

After operating the devices, evidence was sought to establish the nature of the degradation mechanisms. On first inspection there was little damage to the cathode, therefore the anodes were inspected, which revealed prolific damage. This damage was studied by removing the upper layers of the device as described previously in Section 5.2.5.

Figure 7.12 shows a three-dimensional AFM image of the glass substrate which includes a damaged region of ITO.

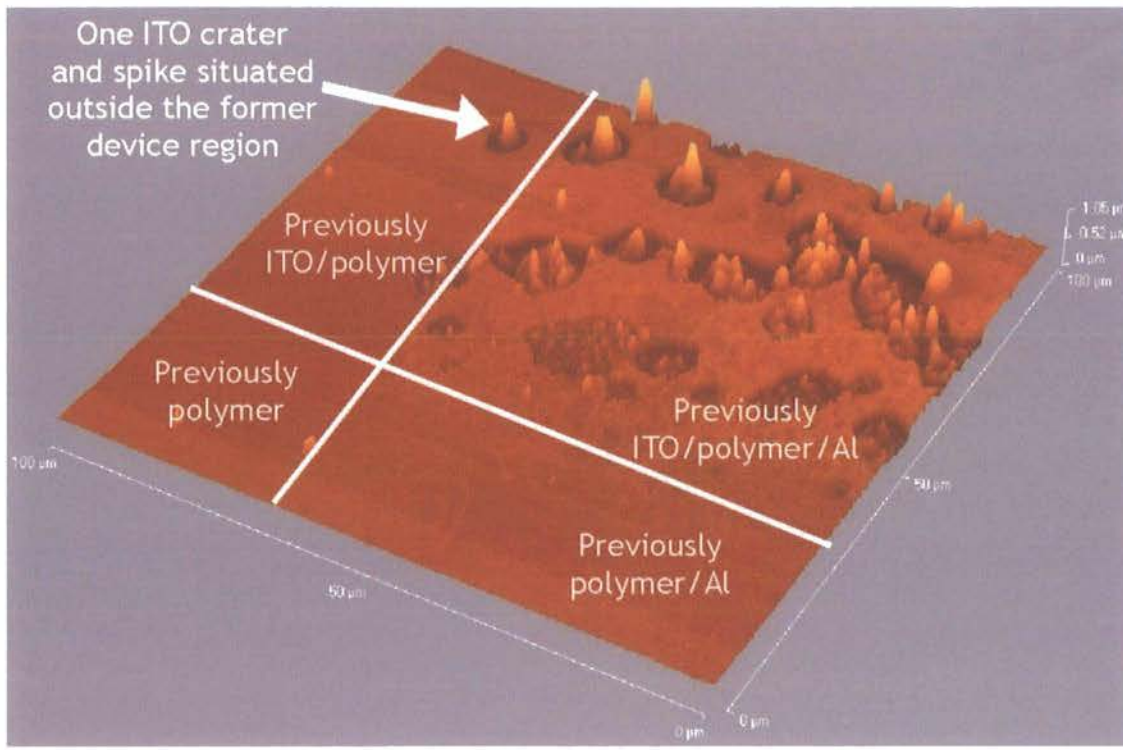

Figure 7.12 Three-dimensional AFM image illustrating the edge of a partially stripped device which previously included a pure KTK34 electroluminescent layer and an aluminium cathode

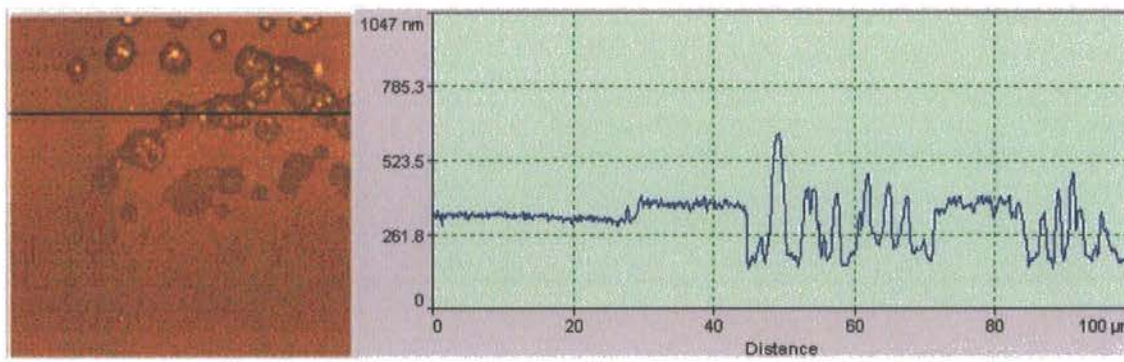

Figure 7.13 Surface profile of the substrate shown in Figure 7.12

This substrate was previously part of a device with a pure KTK34 organic layer and an aluminium cathode. The KTK34 and aluminium were stripped from the anode following operation. The location of the scan was such that it crossed both the ITO and the aluminium boundary. ITO in the region shown at the front of the image was removed during the early stages of device fabrication (process described in Section 3.2.2). Aluminium was present on the right side of the image until it was removed after two days of device operation. The device region was defined by where the ITO and aluminium overlapped, in the back right region of the scan. The image reveals a variety of anode

features which are commonly observed in highly degraded devices. In particular, there are a number of spikes surrounded by craters. Suggestions for the processes which generated these features were presented in Chapter 5.

The 2-dimensional surface profile of the AFM scan (Figure 7.13) shows that the highest spike extended approximately 250 nm above the surrounding ITO. Although this device ceased emitting visible light within minutes of the start of the test, the constant current through the device was maintained for almost two days. It is probable that the spikes and craters in the anode material increased in size over the two day period even after the light emission became negligible. One spike and crater is located in the ITO outside the device region beyond the bounds of the aluminium cathode. That there was only one such spike in this region was because the current path between ITO and aluminium was significantly longer.

The areas of ITO within the device region (top right of the scan) which did not constitute spikes and troughs rose on average by 60 nm compared with the ITO outside the device region (top left of the scan). Excepting the large spikes and craters there was no significant change to the surface roughness either side of the device boundary. This suggested that the ITO underwent largely uniform electromigration across most of the device region and underwent severe electromigration at the spike locations.

In contrast to the pure KTK34 device, the 50 % KTK34 blend was the most stable of all the aluminium-cathode devices. As expected, the AFM image of the anode, shown in Figure 7.14, revealed significantly less damage than the pure KTK34 device.

This scan shows two substrate regions, clearly identified in the insert to the figure. The front right region of the image shows the part of the substrate where the ITO was etched away in the early stages of device fabrication. The rest of the image shows the region where the ITO remains. There were only two apparent flaws in the ITO film. One was a narrow crater defect inside the main ITO film region with average depth of 80 nm. This was probably an imperfection in the commercially sputtered ITO. The other imperfections occurred along the edge of the ITO region and were probably caused by shortcomings in the patterning and etching process. No spike or crater was observed on this anode.

There was a clear correlation between shortness of lifetime and number of anode defects. The difference in the number of defects is demonstrated in Figure 7.12 and Figure 7.14, while the difference in lifetime between these two devices can be seen in Figure 7.9.

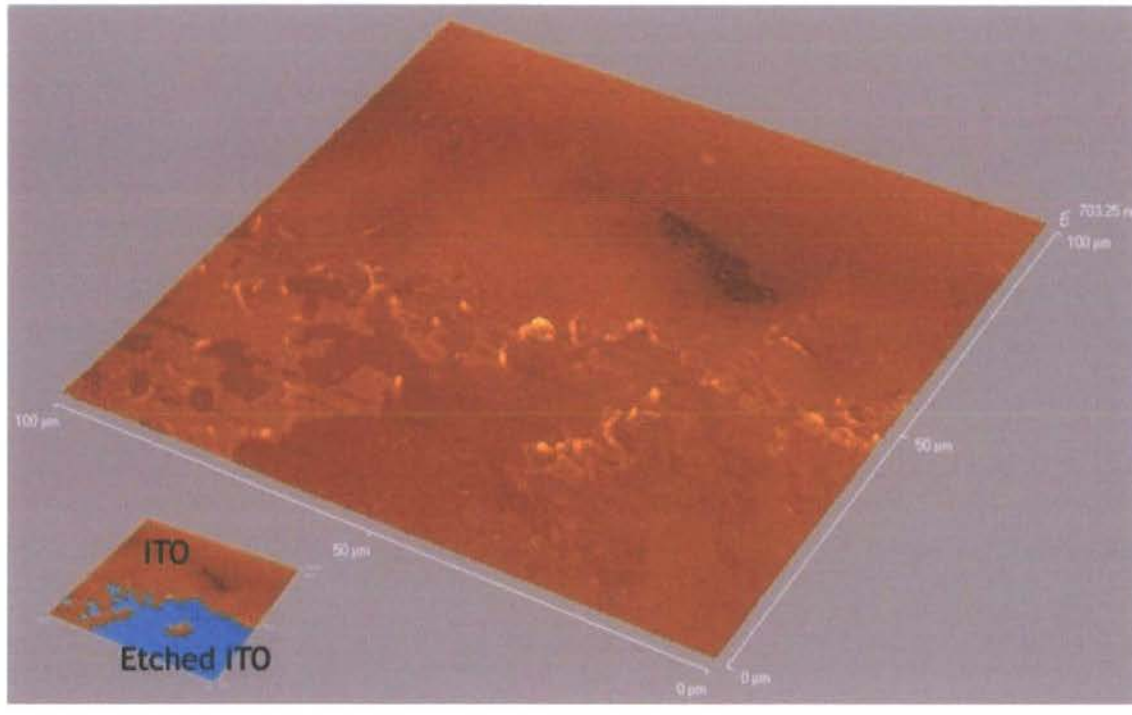

Figure 7.14 Three-dimensional AFM image illustrating the edge of a partially stripped device which previously included a 50 % KTK34 : MEH-PPV blended electroluminescent layer and an aluminium cathode. The front right corner of the image shows the region of the substrate where the ITO was etched away before fabrication.

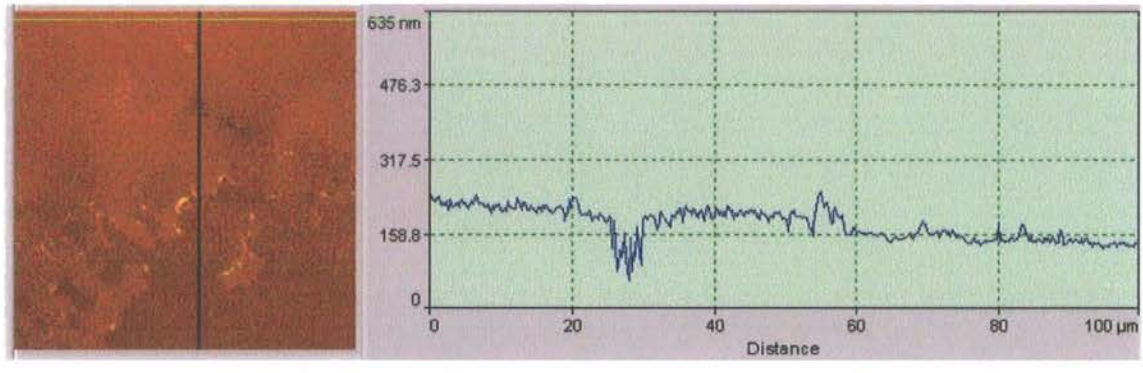

Figure 7.15 Surface profile of the substrate shown in Figure 7.14

The other commonly observed feature of devices operated over several days was the presence of an aluminium strip which was not removed by the solvent. Such strips of aluminium were only ever observed at the boundary of the device region. An example of this is shown in the AFM image in Figure 7.16. As in the case of Figure 7.12 the etched ITO region was at the front half of the image and the aluminium would have been present on the right side of the image. The ridge above the ITO at the edge of the region previously covered by aluminium was a residue of aluminium which was not successfully removed when the electroluminescent layer was dissolved. This stubborn strip of aluminium was observed at the equivalent location on a variety of substrates. This may be

because the adhesion of adjacent films increased at the edge of the device region as a result of the increased current density. Other edge effects, such as brighter emission close to the boundary of the device, were also attributed to increased current density.

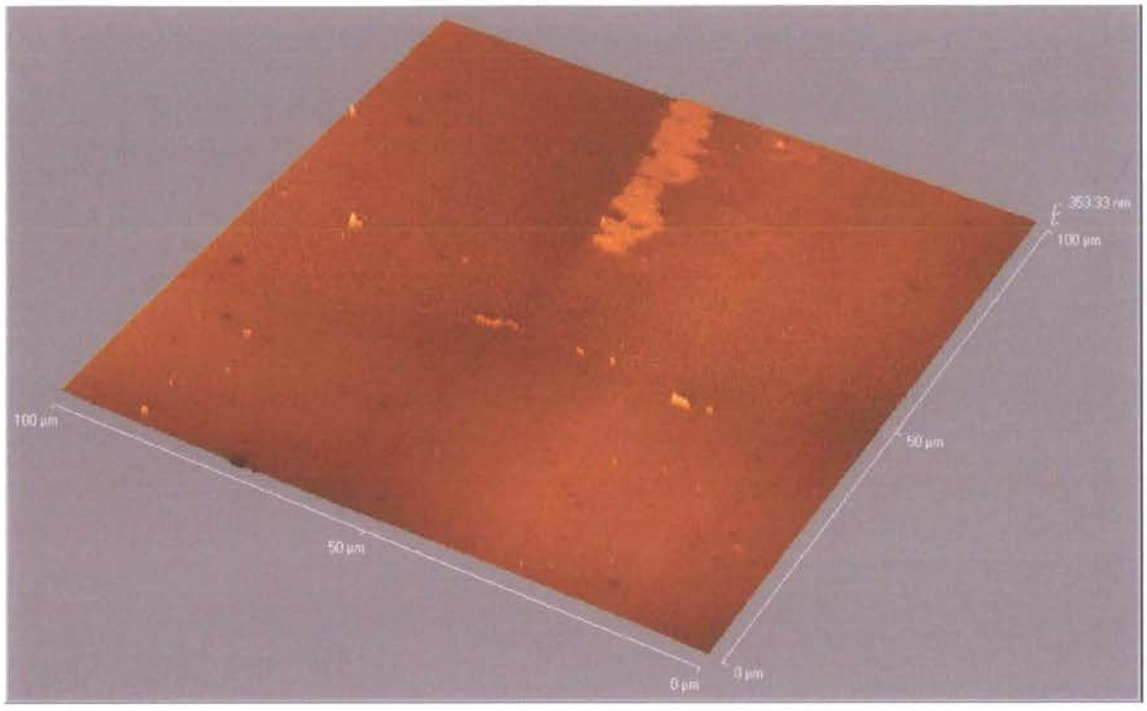

Figure 7.16 Three-dimensional AFM image illustrating the edge of a partially stripped device which previously included a pure MEH PPV electroluminescent layer and an aluminium cathode. The rear half of the image shows the ITO region and the right side of the image included aluminium before it was stripped off.

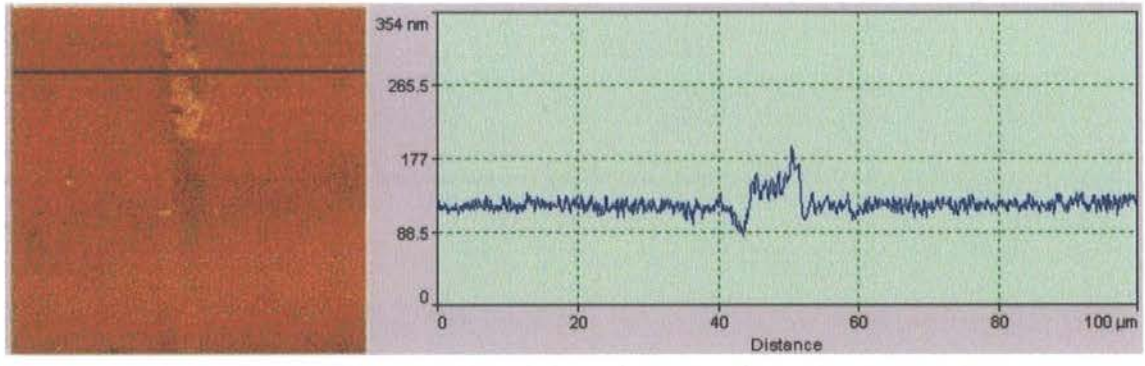

Figure 7.17 Surface profile of the substrate shown in Figure 7.16

Figure 7.17 shows the surface profile of a line across the substrate of the same device. The stubborn aluminium was approximately 50 nm above the unoperated ITO to the left and 45 nm above the operated ITO to the right. This equated to a rise in the ITO of 5 nm within the device region during operation.

7.9.1 Summary of observed degradation features

The AFM images provide evidence for significant anode degradation. There was correlation between the level of damage and the lifetime of the device. The least stable devices showed the greatest electromigration of ITO. In some cases the ITO spikes were tall enough to pierce through the polymer film and cause a short circuit. This was particularly apparent in pure KTK34 devices. ITO spikes were largely associated with craters from which the electromigrated ITO was sourced. Craters resulted in the ITO becoming delaminated from the polymer and preventing the flow of current. Any region without current flow did not emit light. As the area for light emission reduced so the device emitted less light.

7.10 Conclusion

It has been shown that the light output, quantum efficiency and stability characteristics of a device were influenced by blending MEH-PPV with KTK34 in a variety of ratios to produce the electroluminescent layer of a PLED. The use of blends in aluminium-cathode devices provided benefit in terms of light output and stability. Calcium-cathode devices were seen to be more stable than aluminium-cathode devices.

Maximum light output was achieved in a device with a pure MEH-PPV electroluminescent film and a calcium-cathode, but this device was among the most unstable. The quantum efficiency was highest in the 50 % KTK34 blend calcium-cathode devices. Half-life was longest for calcium-cathode devices produced with the 95 % KTK34 blend. Overall, the 50 % and 70 % blend devices with calcium cathodes had the best combination of light emission, quantum efficiency and stability.

Electromigration of ITO was the most obvious degradation mechanism. Even in the most stable devices, electromigration of ITO by at least 5 nm was observed. The number and size of electromigration defects increased with device instability. Devices with the shortest lifetimes, such as those employing pure KTK34 electroluminescent films, showed the greatest evidence of ITO electromigration. This suggests a roughly proportional relationship between ITO electromigration and device instability.

7.11 References

1 G. Hughes and M.R. Bryce, *Electron-transporting materials for organic electroluminescent and electrophosphorescent devices.* Journal of Materials Chemistry, 15, 94 (2005).

2 I.D. Parker, *Carrier tunneling and device characteristics in polymer light-emitting diodes.* Journal of Applied Physics, 75, 1656 (1994).

3 Cambridge Display Technology Press Release, *CDT Sees Further Rapid Progress In Polymer Lifetime Development*, 13th March 2006.

4 Y. Shi, J. Liu and Y. Yang, *Device performance and polymer morphology in polymer light emitting diodes: The control of thin film morphology and device quantum efficiency.* Journal of Applied Physics, 87, 4254 (2000).

5 Y. Shi, J. Liu and Y. Yang, Organic-light emitting devices, a survey, Springer-Verlag New York, 155 and 177-180 (2004).

6 D.G.J. Sutherland, J.A. Carlisle, P. Elliker, G. Fox, T.W. Hagler, I. Jimenez, H.W. Lee, K. Pakbaz, L.J. Terminello, S.C. Williams, F.J. Himpsel, D.K. Shuh, W.M. Tong, J.J. Jia, T.A. Callcott and D.L. Ederer, *Photo-oxidation of electroluminescent polymers studied by core-level photoabsorption spectroscopy.* Applied Physics Letters, 68, 2046 (1996).

7 B.H. Cumpston, I.D. Parker and K.F. Jensen, *In situ characterization of the oxidative degradation of a polymeric light emitting device.* Journal of Applied Physics, 81, 3716 (1997).

8 T. Zyung and J.J. Kim, *Photodegradation of poly(p - phenylenevinylene) by laser light at the peak wavelength of electroluminescence.* Applied Physics Letters, 67, 3420 (1995).

9 R.E. Gill, P. van de Weijer, C.T.H. Liedenbaum, H.F.M. Schoo, A. Berntsen, J.J.M. Vleggaar and R.J. Visser, *Stability and characterization of large area polymer light-emitting diodes over extended periods.* Optical Materials, 12, 183 (1999).

10 B.H. Cumpston and K.F. Jensen, *Electromigration of aluminum cathodes in polymer-based electroluminescent devices.* Applied Physics Letters, 69, 3941 (1996).

11 M.C. Suh, H.K. Chung, S.Y. Kim, J.H. Kwon and B.D. Chin, *Cathode diffusion and degradation mechanism of polymeric light emitting devices.* Chemical Physics Letters, 413, 205 (2005).

12 J.C. Scott, J.H. Kaufman, P.J. Brock, R. DiPietro, J. Salem and J.A. Goitia, *Degradation and failure of MEH-PPV light-emitting diodes.* Journal of Applied Physics, 79, 2745 (1996).

13 G. Liu, J.B. Kerr and S. Johnson, *Dark spot formation relative to ITO surface roughness for polyfluorene devices.* Synthetic Metals, 144, 1 (2004).

14 S.F. Lim, L. Ke, W. Wang, and S.J. Chua, *Correlation between dark spot growth and pinhole size in organic light-emitting diodes.* Applied Physics Letters, 78, 2116 (2001).

15 K.K. Lin, S.J. Chua, W. Wang and S.F. Lim, *Influence of electrical stress voltage on cathode degradation of organic light-emitting devices.* Journal of Applied Physics, 90, 976 (2001).

16 J. McElvain, H. Antoniadis, M.R. Hueschen, J.N. Miller, D.M. Roitman, J.R. Sheats, and R.L. Moon, *Formation and growth of black spots in organic light-emitting diodes.* Journal of Applied Physics, 80, 6002 (1996).

Chapter Eight

Organic LEDs derived from a blend of MEH-PPV and KTK29 and a brief investigation of device encapsulation

8.1 Introduction

This chapter is divided into two sections. The first is a discussion of characteristics of devices composed of a blend MEH-PPV with KTK29. These devices were among the brightest and most stable of all those discussed in this thesis. The second half provides a brief review of two encapsulation methods which were investigated in an attempt to extend device lifetimes.

8.2 Blends of MEH-PPV with KTK29

The experiments on blended materials were concluded with some investigations into blends of the material KTK29 with MEH-PPV. KTK29 is an electron transport material with the chemical structure shown in Figure 8.1. Like KTK34, the electron transporting ability is derived from an electron deficient 1,3,4 oxadiazol unit. The material also contains a fluorene unit which is represented by three conjoined polygons, and a triphenylamine unit consisting of three benzene rings around a nitrogen atom. KTK29 was synthesised in the Chemistry Department at Durham University from commercially available starting materials.

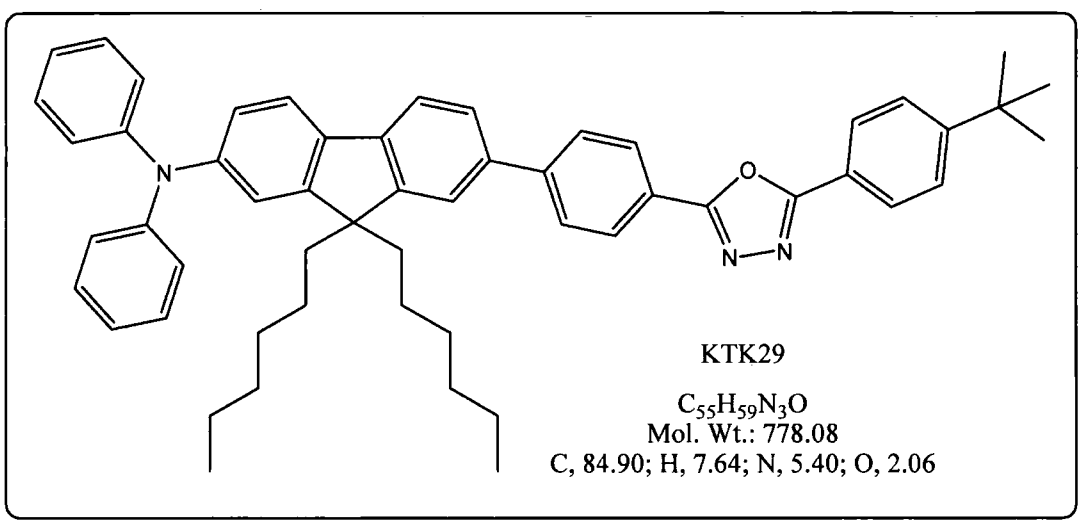

Figure 8.1 Chemical structure of KTK29

The purity of the material was estimated using the elemental analysis technique which showed the proportions of constituent materials to be C: 84.90 %; H: 7.64 %; and N: 5.40 %. Estimated values were: C: 84.68 %; H: 7.66 %; and N: 5.12 %, so the maximum percentage difference was 0.28 %.

The HOMO and LUMO values of KTK29 were estimated, using the molecular modelling method, to be 5.1 eV and 1.9 eV, respectively. An energy diagram, showing these levels together with those of MEH-PPV and PEDOT and the Fermi levels of the electrode materials, is shown in Figure 8.2.

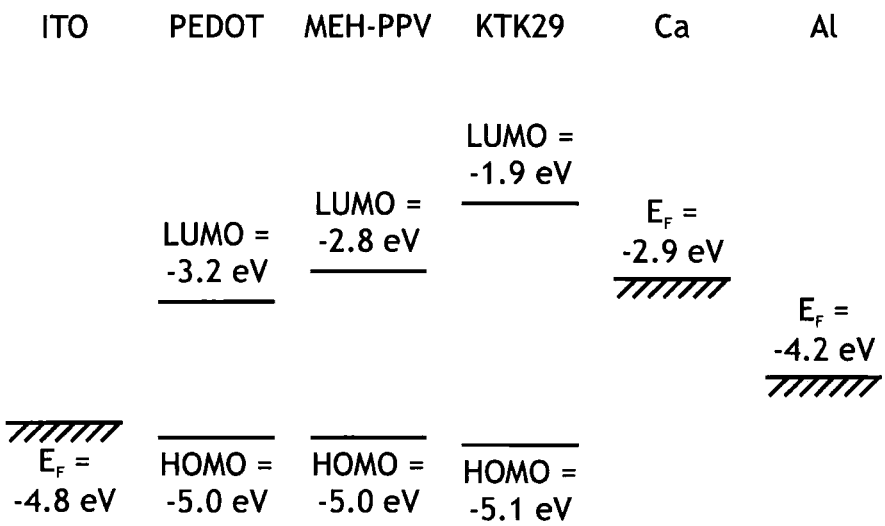

Figure 8.2 Energy level diagram

As the following data reveal, the characteristics are largely similar to those for the blends of MEH-PPV with PDPyDP or KTK34. The MEH-PPV : KTK29 blend is of interest not because it operates fundamentally differently from the other blends, but because it happens to be the most stable blend with the highest light emission. Only the 50 % KTK29 blend devices with calcium cathodes were investigated.

I-V and light-voltage characteristics are given in Figure 8.3, which confirms that the blend devices had a lower turn-on voltage than the pure MEH-PPV devices and more light emission. Of all devices considered in this thesis, the 50 % KTK29 blend emitted the most light, which equated to approximately 500 cd m^{-2} when first operated. A photograph of one such device is shown in Figure 8.4. The QE characteristics, shown in Figure 8.5, reveal that the KTK29 blend devices have marginally lower quantum efficiency than the pure MEH-PPV devices. Again, these data trends are similar to those seen for the KTK34 and the PDPyDP devices, suggesting that the phenomena are largely similar.

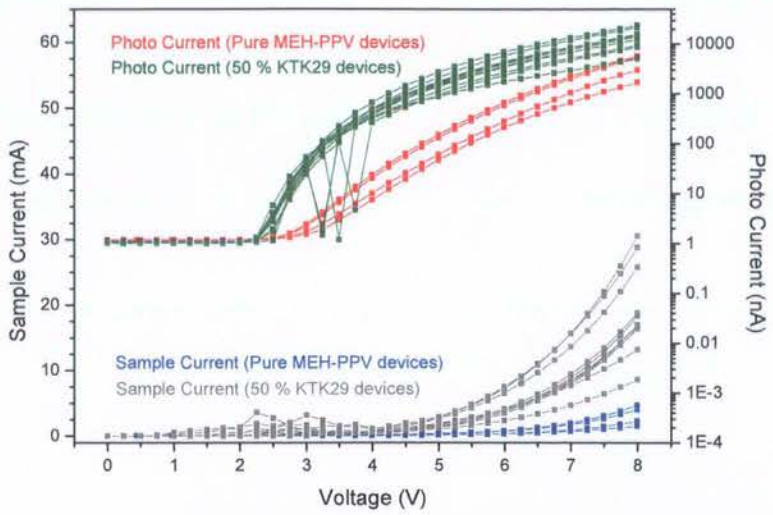

Figure 8.3 I-V and light-voltage characteristics for calcium-cathode devices either with a (50 : 50) blended layer of MEH-PPV : KTK34 or with pure MEH-PPV

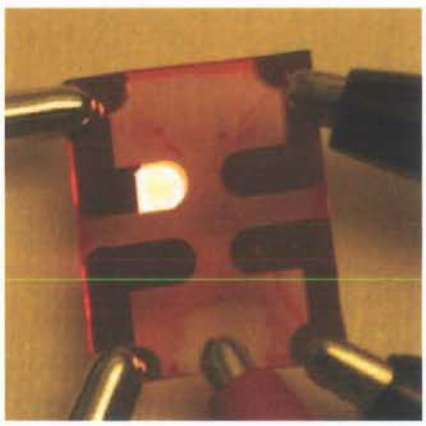

Figure 8.4 Photograph, taken during operation, of a calcium-cathode device with a (50 : 50) blended layer of MEH-PPV : KTK34

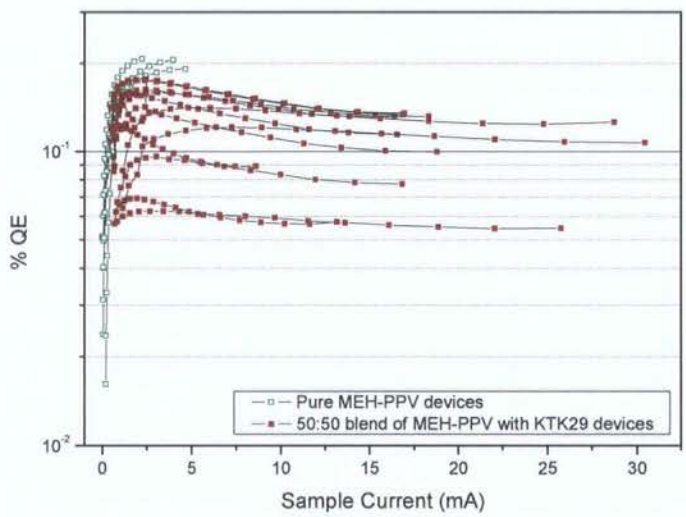

Figure 8.5 QE characteristics for those devices plotted in Figure 8.3

The blended KTK29 devices were also among the most stable of all the devices. The stability characteristics (Figure 8.6) show a comparison of the most stable KTK34 (70 %) blend device with the 50 % KTK29 device. The light emission from the KTK29 blend decayed more slowly and the increase in voltage required to maintain constant current was more gradual.

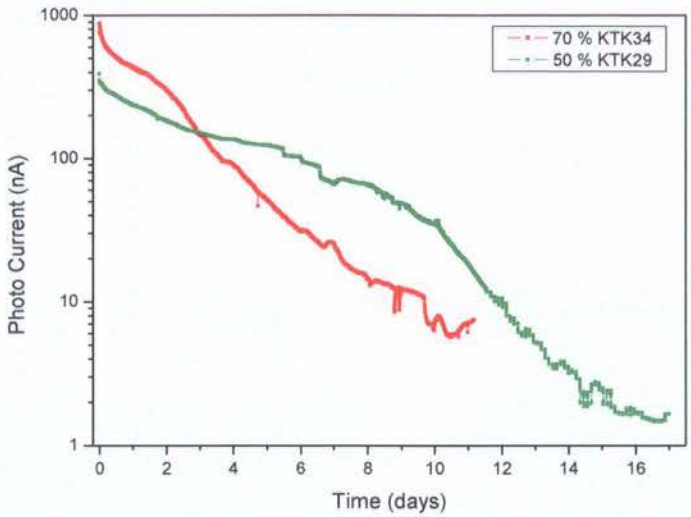

(a)

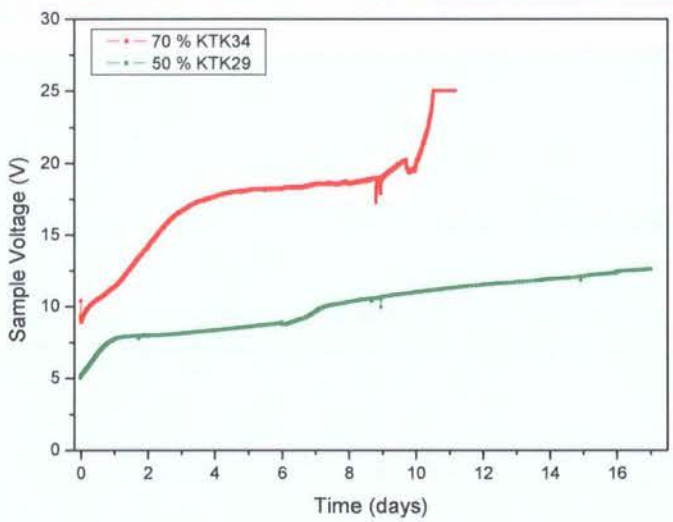

(b)

Figure 8.6 Stability characteristics for a 70 % KTK34 device and a 50 % KTK29 device each with a calcium cathode: (a) photo current against time; and (b) sample voltage against time

The electroluminescent spectrum of a 50 % blend device was analysed at various stages during its degradation while being operated continuously. The electroluminescent spectrum, at six different times, is plotted in Figure 8.7. There was no lateral shift in the

spectrum and the relative height of each peak remained the same with time. As the device degraded, the only change to the spectrum was a reduction in luminance. This reduction occurred in uniform proportions across the whole spectrum. The locations of the main and secondary peaks are influenced by polymer aggregation [1, 2]. As the peaks did not move laterally, the degradation did not change the aggregation of the polymer.

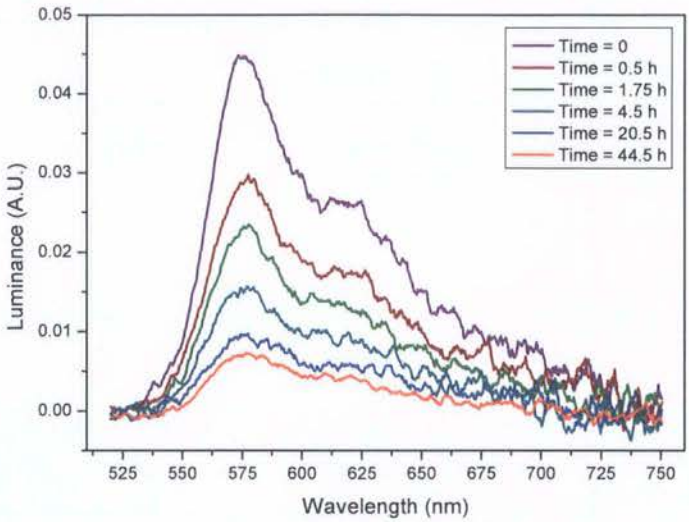

Figure 8.7 Emission spectra of 50 % blend KTK29 blend devices at various stages of degradation while operated continuously

8.3 Encapsulation

As discussed previously (Section 7.8), oxygen and water vapour contribute to several of the common degradation mechanisms, affecting both the polymer blends and the electrodes [3-9].

Attempts were made to investigate the viability of protecting devices from atmospheric oxygen and water vapour using two inert materials. Given the benefits of simple processing and inexpensive manufacture, the encapsulation materials were on the scale of several millimetres diameter to cover the full surface area (5 mm^2) of each device.

The two materials investigated were a two-part silicone-based gel (Wacker Silgel 612A & 612B) and a one-part conformal coating dielectric gel (3-4150), both supplied by Dow Corning, Michigan, U.S.A.. The silicone gel was prepared immediately before use by mixing the two parts in a ratio of 1 : 1.

Encapsulation was carried out immediately following fabrication of the devices and both processes took place in a dry nitrogen glovebox. One batch of devices was encapsulated using silicone and another using dielectric gel. In each case, between 50 and 100 μl of the

liquid encapsulant was applied to the centre of the top (cathode) surface of each device by collecting the material on a needle and allowing it to drop from 5 mm above the device. On impact, the material spread laterally to form a dome with approximate diameter 2.5 mm and maximum height 0.5 mm. Immediately following the application of the encapsulant the device substrate was placed under vacuum which was seen to cause a number of nitrogen bubbles in the silicon to be drawn out of the material. The silicone gel hardened within 20 min. of the two parts being mixed, and the conformal coating hardened after 5 min. on a hot plate at 40 °C. The encapsulation arrangement is shown schematically in Figure 8.8.

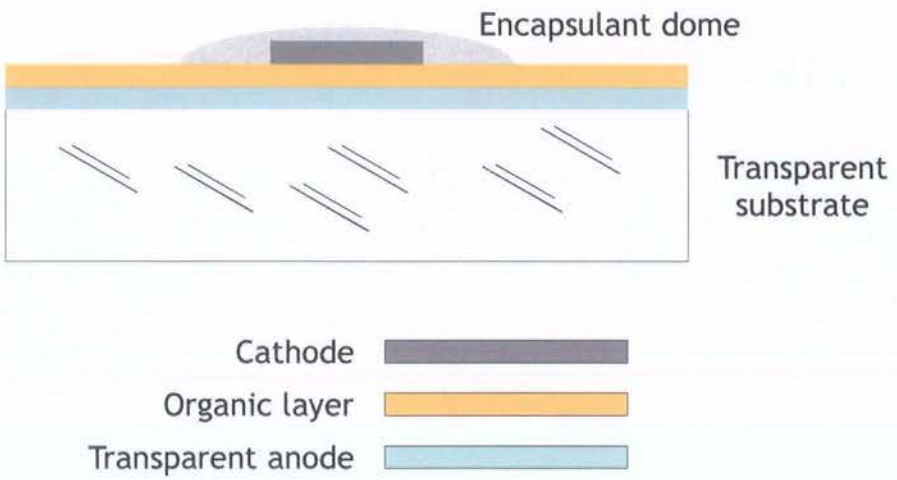

Figure 8.8 Schematic diagram of encapsulation arrangement

As expected neither of the encapsulants affected the I-V or light-voltage characteristics of the devices when measured immediately after fabrication. This confirms that, in the short term, no damage was caused to the polymer or electrodes by the silicone or dielectric gel.

Stability data at a constant current of 0.56 mA for a typical unencapsulated and a typical encapsulated device are shown in Figure 8.9. In both cases the organic layer was a (80 : 20) blend of MEH-PPV and PDPyDP. There was little difference in stability between devices with and without encapsulation. From this there are two possible conclusions. Either (a) the degradation mechanisms were not related to the presence of oxygen and water, or (b) oxygen and water affected the encapsulated devices as much as the unencapsulated ones.

The observed instability may have been caused by a degradation process which did not involve oxygen or water. Alternatively, it is also possible that oxygen and water contributed to the degradation and that the encapsulation methods did not provide

effective protection. For example, oxygen and water vapour might have gained access to the active device areas through the unencapsulated regions of the polymer film, as illustrated in Figure 8.10.

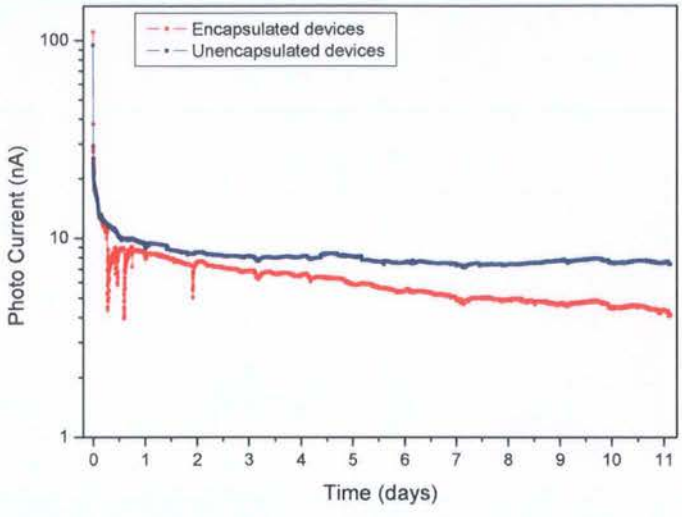

(a)

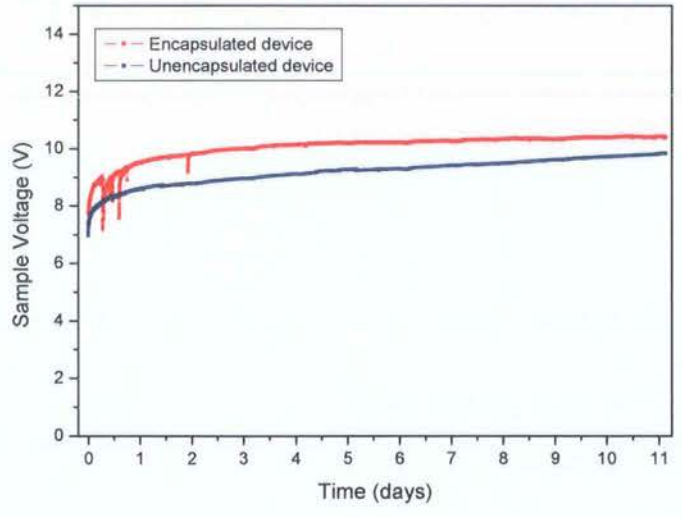

(b)

Figure 8.9 Stability characteristics for devices with and without silicone encapsulant: (a) photo current against time; and (b) sample voltage against time

It is clear that this simple macro approach to encapsulation did not increase device stability. More exact and small scale approaches to encapsulation may have greater benefits by, for example, preventing the opportunity for the ingress of atmospheric content around the sides of the encapsulant. Although, to protect the device against any oxygen emitted from the ITO anode, a different approach would be necessary.

The need for complex encapsulation techniques could be avoided either by developing more stable emissive materials which are not sensitive to atmospheric conditions, or by exploiting the blended layer technique for potential nano-encapsulation of the emissive materials.

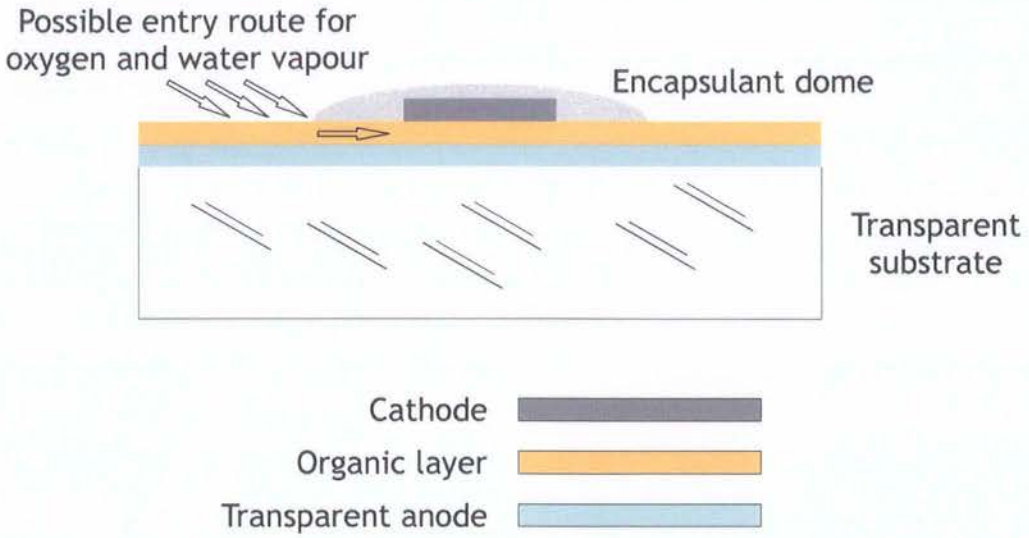

Figure 8.10 Schematic illustration of a possible entry route around encapsulation for oxygen and water vapour

8.4 Conclusion

Of all the blended devices in this thesis, the 50 % KTK29 blends were most stable and emitted the most light. A brief trial of macro-encapsulation techniques has been discussed. The macro-encapsulation techniques did not result in increased stability of the devices. This was in contrast to the increased stability observed in blended material devices that might be explained by the nano-enacpsulation concept.

8.5 References

1 Y. Shi, J. Liu and Y. Yang, *Device performance and polymer morphology in polymer light emitting diodes: The control of thin film morphology and device quantum efficiency.* Journal of Applied Physics, 87, 4254 (2000).

2 J.W. Blatchford, S.W. Jessen, L.B. Lin, T.L. Gustafson, D.K. Fu, H.L. Wang, T.M. Swager, A.G. MacDiarmid and A.J. Epstein, *Photoluminescence in pyridine-based polymers: Role of aggregates.* Physical Review B, 54, 9180 (1996).

3 D.G.J. Sutherland, J.A. Carlisle, P. Elliker, G. Fox, T.W. Hagler, I. Jimenez, H.W. Lee, K. Pakbaz, L.J. Terminello, S.C. Williams, F.J. Himpsel, D.K. Shuh, W.M. Tong, J.J. Jia, T.A. Callcott and D.L. Ederer, *Photo-oxidation of electroluminescent polymers studied by core-level photoabsorption spectroscopy.* Applied Physics Letters, 68, 2046 (1996).

4 B.H. Cumpston, I.D. Parker and K.F. Jensen, *In situ characterization of the oxidative degradation of a polymeric light emitting device.* Journal of Applied Physics, 81, 3716 (1997).

5 B.H. Cumpston and K.F. Jensen, *Electromigration of aluminum cathodes in polymer-based electroluminescent devices.* Applied Physics Letters, 69, 3941 (1996).

6 M.C. Suh, H.K. Chung, S.Y. Kim, J.H. Kwon and B.D. Chin, *Cathode diffusion and degradation mechanism of polymeric light emitting devices.* Chemical Physics Letters, 413, 205 (2005).

7 S.F. Lim, L. Ke, W. Wang and S.J. Chua, *Correlation between dark spot growth and pinhole size in organic light-emitting diodes.* Applied Physics Letters, 78, 2116 (2001).

8 K.K. Lin, S.J. Chua, W. Wang and S.F. Lim, *Influence of electrical stress voltage on cathode degradation of organic light-emitting devices.* Journal of Applied Physics, 90, 976 (2001).

9 J. McElvain, H. Antoniadis, M.R. Hueschen, J.N. Miller, D.M. Roitman, J.R. Sheats and R.L. Moon, *Formation and growth of black spots in organic light-emitting diodes.* Journal of Applied Physics, 80, 6002 (1996).

Chapter Nine

Conclusions

9.1 Conclusions

The purpose of this research was to investigate the characteristics of OLEDs based on blends of a polymer emissive material with small molecule materials. The influences of blends and anode materials on device degradation were considered in particular detail. Limited lifetime is one of the largest barriers to commercialisation of OLEDs for most applications. Another major barrier is the cost of manufacture, which must be minimised if OLEDs are to compete with established display technologies. PLEDs were chosen in this research because of their low manufacturing cost compared to SMOLEDs, and blends were selected both for their low fabrication cost and to minimise the number of interfaces at which degradation mechanisms commonly nucleate.

The variation of device behaviour within a single batch of identically produced devices meant that automated characterisation equipment was necessary to allow batches of devices to be characterised simultaneously. Such equipment was designed and built. The equipment enabled the extent of the variation within batches to be determined and anomalous devices to be identified.

The most widely used anode material, ITO, was shown to have many undesirable properties which influenced the lifetime of devices. The ITO anodes of degraded devices were shown to have undergone electromigration during device operation. The material reformed into craters and spikes which were tall enough to pierce the organic layer. AZO, a less widely used transparent conductor, was investigated as an alternative to ITO, but its high resistance meant that devices with AZO anodes emitted much less light and were no more stable.

By adding an additional layer of PEDOT between the ITO and the organic emissive layer the damage to the anode was less. Few spikes formed and these only occurred at the locations where pin holes were present in the PEDOT. A layer of PEDOT was shown to reduce the roughness and increase the wettability of the anode surface. This resulted in better film contact, better adhesion and fewer pin holes. It also provided a physical barrier which reduced electromigration of ITO. This meant that devices with a PEDOT layer were far more stable than those without.

Blended electroluminescent layers were shown to have a substantial influence on the light output, efficiency and stability of light emission. By blending MEH-PPV with either PDPyDP, KTK34 or KTK29, the number of electrons injected into the device was much

increased. With a blend of the appropriate proportions, the numbers of electrons and holes were balanced, the light emission was increased and the quantum efficiency was maximised. Similar characteristics were obtained in many of the devices with blended films and an aluminium cathode, as were obtained with pure MEH-PPV and a calcium cathode. Calcium was, however, shown to have a detrimental effect on device stability. By using the blended emissive layer with aluminium the need for calcium was eliminated.

The most significant advantage of the blended emissive layers was the reduction in the rate of degradation. This was explained by the concept of nano-encapsulation whereby the small molecule materials enveloped the more vulnerable MEH-PPV. MEH-PPV reacts with oxygen and water vapour which accelerates its degradation. Though the basic macro-encapsulation techniques did not reduce the rate of degradation, the blended devices were the most stable of all those investigated. The devices with the best light emission, efficiency and stability characteristics were those with relatively even proportions of MEH-PPV and small molecule materials. The higher levels of light emission occurred because an even proportion of the two materials resulted in near equal numbers of electrons and holes. The increased stability was explained with reference to the nano-encapsulation concept. Specifically, an even proportion of the two materials was more likely to result in an effective enveloping of the MEH-PPV polymer chains by clusters of the small molecule material.

The 50 % PDPyDP blend device with an aluminium cathode gave a good combination of light output, efficiency and stability of light emission. Compared with the equivalent unblended device the 50 % blend device had 40 times greater light emission, 35 times higher efficiency, and it emitted light for more than 18 days in place of tens of minutes. Of all the blended devices the 50 % KTK29 blends emitted the most light, which equated to over 500 cd m^{-2} when first operated. They were also among the most stable devices as they emitted visible light for two weeks.

In light of the multi-faceted and highly-resourced approaches adopted by commercial OLED developers, it is perhaps over-simple to make direct comparisons between their published data and the data obtained in this research. Nevertheless, for the sake of completeness, data relating to commercially-developed devices are reproduced here. In March 2006, CDT and Sumation published data relating to their red phosphorescent devices [1]. Through accelerated testing of the devices operating at a luminance of 400 cd m^{-2}, they claimed an estimated half-life of 50,000 hours and a maximum efficiency

of 11 cd A^{-1}. By comparison, the best devices presented in this thesis had maximum efficiencies of 0.3 cd A^{-1}. The longest half-life was over 60 hours and the highest luminance value was 500 cd m^{-2} for a device when first operated. This thesis has demonstrated significant improvements in device characteristics obtained almost exclusively as a result of using blended electroluminescent layers. With similar improvements to the other device components (such as electrodes) combined with developments to maximise optical outcoupling and additional measures to reduce the ingress of oxygen and water vapour, the characteristics of such devices would compare more favourably with the characteristics of commercially-developed OLEDs.

For the reasons discussed in this thesis, it is suggested that blended layer polymer light emitting devices have the potential to be used in displays in the future. The fact that they can be produced using the simplest of OLED device architectures means that the will be cheap to produce and will be able to compete on price in the fiercely competitive display market. If the concept of nano-encapsulation, which appears to explain the increased lifetime of blended layer PLEDs, is confirmed and developed further, it is possible that these devices will also be able to compete in terms of lifetime.

9.2 Suggestions for further work

Given that the blend composition and the anode material were seen to influence device stability, further investigation of these two device components may lead to longer device lifetimes.

Rather than physically mix the MEH-PPV with a small molecule, the possibility of incorporating the electron transporting material on the branches of the polymer might be investigated. Lee *et al.* have previously suggested this approach for improving electron transport [2]. Further work might involve the development of similar new materials not only for improved electron transport, but also with the aim of improving device lifetime through integrated nano-encapsulation.

It may be possible to combine the respective benefits of ITO and AZO. The advantage of the AZO was that it did not electromigrate so readily into the polymer layer, while devices with an ITO anode had better I-V and light emission characteristics. Composite anodes formed from ITO covered with a layer of AZO may provide improved stability. An investigation might be undertaken to establish whether a thin layer of AZO on top of ITO would block the electromigration of ITO without significantly reducing the overall

conductivity of the anode. Additionally, an investigation might be made into reducing the roughness of ITO films to decrease the number of spikes which provide nucleation points for defects.

Other common device defects include pin holes in the emissive polymer and PEDOT layers. The number of pin holes may be reduced by heating the polymer films after spin-coating to cause the polymer to re-flow and produce a more uniform film. Research has shown this annealing method to improve the film morphology, the I-V characteristics and the efficiency of blended layer MEH-PPV devices [3]. Further work might be undertaken using this approach to maximise device lifetime.

9.3 References

1 Cambridge Display Technology Press Release, *CDT Sees Further Rapid Progress In Polymer Lifetime Development*, 13th March 2006.

2 Y.-Z. Lee, X. Chen, S.-A. Chen, P.-K. Wei and W.-S. Fann, Journal of the American Chemical Society, 123, 2296 (2001).

3 J.H. Ahn, C. Wang, N.E. Widdowson, C. Pearson, M.R. Bryce and M.C. Petty, *Thermal annealing of blended-layer organic light-emitting diodes.* Journal of Applied Physics, 98, 054508 (2005).

Appendix One: List of publications

1 N.E. Widdowson, C. Pearson, M.C. Petty, C. Wang and M.R. Bryce, *Degradation studies of blended layer polymer light-emitting devices.* Novel Light Sources and Displays, Institute of Physics Congress, Edinburgh, 26th March 2003.

2 N.E. Widdowson, C. Pearson, M.C. Petty, C. Wang and MR Bryce, *Degradation studies of blended layer polymer light emitting devices.* Materials Research Society Spring Meeting, San Francisco, 12th – 16th April 2004.

3 J.H. Ahn, C. Wang, N.E Widdowson, C. Pearson, M.R. Bryce and M.C. Petty, *Thermal annealing of blended-layer organic light-emitting diodes.* Journal of Applied Physics, 98, 054508 (2005).

4 N.E Widdowson, J.H. Ahn, K.T. Kamtekar, C. Wang, C. Pearson, M.R. Bryce and M.C. Petty, *Lifetime studies of blended layer organic light emitting diodes.* Journal of Applied Physics, in preparation.

Appendix Two: Characterisation equipment: instructions for use

OLED characterisation equipment - quick glance instruction sheets

Contents:

1. Introduction

NESTRO is designed to characterise the electrical, light emission and stability characteristics of Organic Light Emitting Devices. The chamber, which provides a controlled environment for sample testing, has a capacity of 24 devices comprising four devices on each of six substrates. There is a range of characterisation functions provided by the software that controls the instrumentation. Those functions which are executed over a short time (seconds or minutes) take place consecutively for each of the 24 devices, while stability tests that can take place over periods of many weeks, are executed simultaneously on six devices (one device on each substrate).

2. Switching on the rig:

- Ensure that the following are switched on:
  - The PC
  - The rotary pump below the bench (this should be left permanently on)
  - Keithley Sourcemeter
  - Agilent DMM
  - Keithley Picoameter
  - NESTRO control box

3. Loading the chamber:

- Close the vacuum supply valve (see Figure 1)
- Open the air admit valve
- Lift off the lid (remove screw fixings if necessary)
- Enter up to six substrates into the sub chambers, starting at sub chamber 1
- Place a rectangular aluminium spacer component onto each substrate
- Replace the lid being aware of alignment pins (and, for lifetime tests, fasten screws)
- Close the air admit valve
- Open the vacuum supply valve

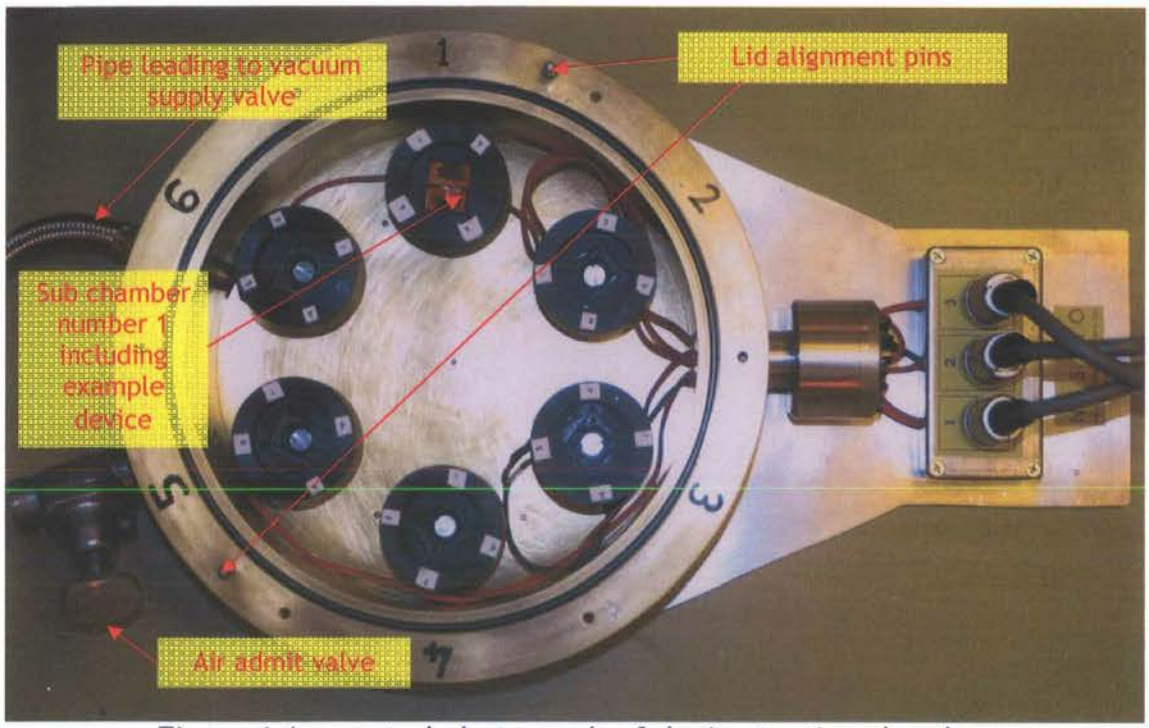

Figure 1 Annotated photograph of device testing chamber

The two main functions provide characterisation of the current-voltage (I-V) behaviour of devices and their stability at constant current. These are introduced on the following pages.

4. Current-voltage (I-V) characterisation

This function will perform a ramping voltage sweep, measuring the sample current and photo current at each step. An estimate of the quantum efficiency at each different voltage value will be made.

1. Open the directory C:\Nestro\NESTRO-IV and select the file NESTRO-IV-8
2. The LabVIEW virtual instrument (Figure 2) will appear (this is the 'IV manager' or 'master' virtual instrument)
3. Enter the input parameters
   - 3.1 Start voltage (V)
   - 3.2 End voltage (V)
   - 3.3 Voltage step (V)
   - 3.4 Delay between steps (s)
   - 3.5 Current limit (mA)
   - 3.6 QE constant = $\frac{\lambda e}{Rhc}$, where λ = peak emission wavelength, e = electronic charge, R = photodiode efficiency, h = Planck's constant, and c = speed of light
   - 3.7 Number of substrates to be characterised ($1 \leq n \leq 6$)
4. Press the arrow button at the left of the task bar to start the function
5. A 'save as' pop up window will appear
6. Insert an appropriate file name and location where prompted and click save
7. A second, 'slave', virtual instrument (screen grab shown in Figure 3) will automatically open
8. The parameters input in the 'master' instrument will appear in the inputs column on the left of the 'slave' instrument
9. As data are acquired they are recorded in a file with the file stem given in step 6
10. Raw data are displayed on the right of the screen and plotted in the centre
11. The 'slave' instrument will run once for each device (four times for each substrate multiplied by the number of substrates)
12. Once the I-V characterisation has run the appropriate number of times both 'master' and 'slave' virtual instruments will stop automatically

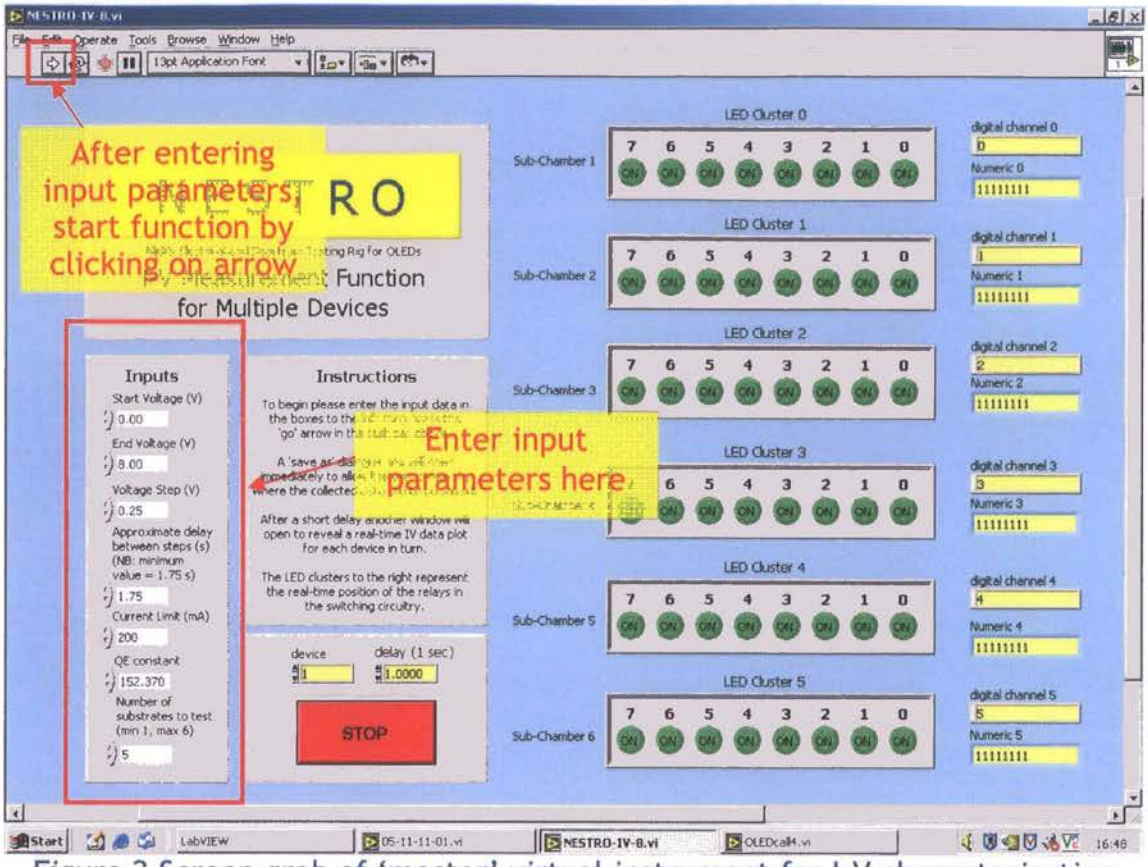

Figure 2 Screen grab of 'master' virtual instrument for I-V characterisation

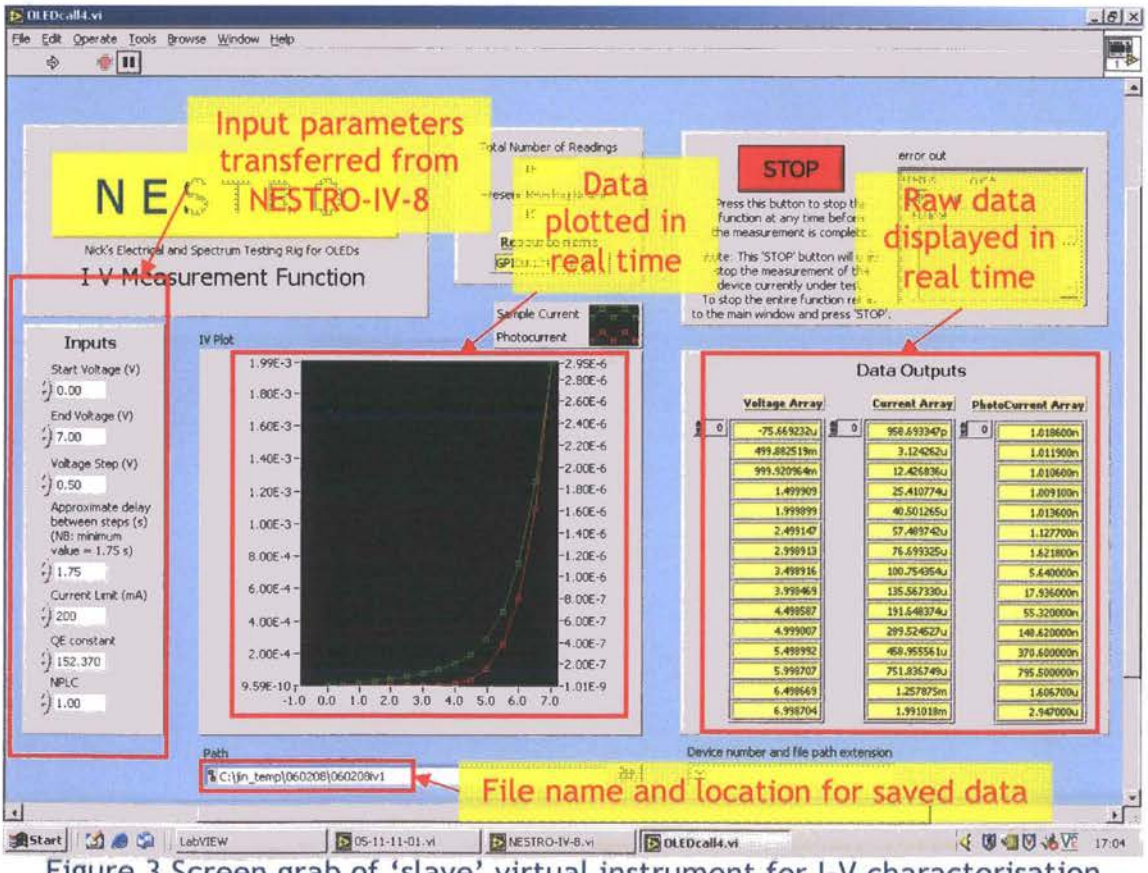

Figure 3 Screen grab of 'slave' virtual instrument for I-V characterisation

5. Constant current stability characterisation

This function will apply a constant current of 0.56 mA to one device on each of the six substrates. At the interval specified by the user the photo current and the voltage necessary to maintain the constant current (independently for each device) will be measured. If less than six substrates are placed into the chamber, results for unoccupied sub-chambers will register noise.

1. Open the directory C:\Nestro\StabilityCC and open the latest version of the file (date order)
2. The LabVIEW virtual instrument (Figure 4) will appear
3. Enter the input parameters
   - 3.1 Voltage limit (V)
   - 3.2 Length of experiment (h)
   - 3.3 Delay between measurements (s)
4. Press the arrow button at the left of the task bar to start the function
5. A pop up window will appear
6. Insert an appropriate file name and location where prompted and click save
7. As data are acquired they are recorded in a file with the file stem given in step 7
8. Data are plotted on the right of the screen: one plot for each sub-chamber
9. The function will stop after the time specified in the length of experiment field (step 3.2) or by clicking the red STOP button at the bottom of the screen

Figure 4 Screen grab of virtual instrument for constant current stability characterisation

Appendix Three: Characterisation equipment software

Copies of four of the software functions used to control the characterisation equipment are supplied on a CD fastened to the inside back cover of this thesis.

The functions require the LabVIEW Run Time Engine (also available on the CD) to be installed before they will open. The functions are likely to show errors if the relevant instruments and switching circuitry are not connected to the PC via GPIB and DIO cards, and if the necessary instrument drivers are not installed.